UNCLASSIFIED

AD 402 314

Reproduced
by the
DEFENSE DOCUMENTATION CENTER
FOR
SCIENTIFIC AND TECHNICAL INFORMATION
CAMERON STATION, ALEXANDRIA, VIRGINIA

UNCLASSIFIED

NOTICE: When government or other drawings, specifications or other data are used for any purpose other than in connection with a definitely related government procurement operation, the U. S. Government thereby incurs no responsibility, nor any obligation whatsoever; and the fact that the Government may have formulated, furnished, or in any way supplied the said drawings, specifications, or other data is not to be regarded by implication or otherwise as in any manner licensing the holder or any other person or corporation, or conveying any rights or permission to manufacture, use or sell any patented invention that may in any way be related thereto.

AD 402 314

61(052)-490

20 December 1962

SECOND TECHNICAL ANNUAL SUMMARY REPORT

ON THE PROPAGATION OF VLF WAVES IN SOLIDS

Dr. W. Bitterlich
Innsbruck, Austria

The research reported in this document has been sponsored by the United States Government.

Zusammenfassung.

Es wurden eingehende theoretische Untersuchungen über die Ausbreitung von VLF-Wellen im homogenen leitenden Medium durchgeführt. Die daraus abgeleiteten Formeln und Diagramme für das elektromagnetische Feld eines magnetischen Dipols und Quadrupols sind in Abhängigkeit von Entfernung, Leitfähigkeit und den Stellungen der Sende- und Empfangsantenne gegeben. Daraus konnte eine Methode zur Leitfähigkeitsbestimmung geologischer Leiter entwickelt werden.

Im experimentellen Teil werden die Messungen der Feldstärke eigener und kommerzieller Sender, so wie die dazu notwendigen Meßgeräte beschrieben.

Die Ergebnisse des Experiments und der Theorie werden eingehend erläutert und mit-einander verglichen.

Summary.

A thorough theoretical study of the propagation of VLF-waves in homogeneous conducting media has been performed. The formulas and diagrams deduced for the electromagnetic fields of a magnetic dipole and quadrupole are given in terms of distance, conductivity, and the positions of the transmitting and receiving aerials. From these, a technique of determining the conductivity of geological conductors could be worked out.

The experimental section gives a description of the measurements of the intensities of our own and of commercial transmitters as well as of the required measuring equipment.

The results of experiment and theory are explained in detail and compared with one another in a special section.

C O N T E NTS

Measurement of the electrical conductivity of rock by means of low-frequency magnetic fields and their propagation

(I) Introduction

The mechanism of the propagation of VLF electromagnetic waves ($\nu < 10$ kcps) in the Earth's interior and on the surface has found little explanation so far. The long range of such waves, in particular when emitted from an underground transmitter, is striking. The mechanism of long-distance propagation presumably is that the transmission aerial emits electromagnetic waves to the Earth's surface. These waves propagate along the surface or in the space between the surface and the ionosphere, penetrate into the ground and are received by the receiving aerial (Fig. 1). Besides by the transmission power and the distance between receiver and transmitter, the field strength at the point of reception is largely dependent on the electrical properties of the soil between the surface and the receiver or transmitter station, which exerts a strong attenuation because of its electrical conductivity. The absorption of electromagnetic energy in this soil is dependent on frequency. Waves of low frequency are damped less than waves of higher frequency. For this reason, the frequency band below 20 kcps (vacuum wavelength greater than 15 km) is particularly suitable for subterranean communication. The positions of the transmitter and the receiver must be

chosen in view of the conductivity of the area in question. But the conductivity of a large region cannot be deduced with the required accuracy from the conductivities of laboratory samples since the grounds are not uniform. Sounding tests in general involve troubles in reproducing uniquely the conditions of contact with the rock. A perfectly integrating method, i.e. one averaging over long distances, is the measurement of conductivity using a variable magnetic field. Its basic idea is as follows: a magnetic coil is fed with an alternating current $I \cdot \exp(i\omega t)$. The magnetic field $\vec{H}$ along its axis is measured at a distance r. The greater the conductivity σ of the medium the greater the eddy losses and the weaker the received field.

(II) Theory. (Prof. Cap, Dr. Hommel)

§1. The field of a magnetic dipole

The calculation of the magnetic intensity of a coil in dissipative media is based on the theory of the Hertzian dipole and on Maxwell's equations. After isolating the time-dependent term $\exp(+i\omega t)$ and introducing the complex dielectric constant $\varepsilon^* = \varepsilon - i\frac{\sigma}{\omega\varepsilon_0}$, where σ is the conductivity as measured in $\text{ohms}^{-1}\text{m}^{-1}$, and when no electrical charge is present, Maswell's equations in the absolute system of units are

$$
(1)\quad
\begin{aligned}
&\operatorname{curl}\vec{H} = \varepsilon^{*}\varepsilon_0 i\omega\vec{E}\\
&\operatorname{curl}\vec{E} = -\mu\mu_0 i\omega\vec{H}\\
&\operatorname{div}\vec{H} = 0\\
&\operatorname{div}\vec{E} = 0
\end{aligned}
\qquad
\begin{aligned}
&\varepsilon_0 = 8.859\cdot10^{-12}\ [\text{amp sec/volts m}]\\
&\mu_0 = 1.256\cdot10^{-6}\ [\text{volts sec/amp m}]
\end{aligned}
$$

Through known transformations one arrives at the Helmholtz equation for $\vec{H}$

$$(2)\quad \Delta\vec{H} + k^{*2}\vec{H} = 0 \text{ with } k^{*2} = \omega^2\varepsilon_0\mu_0\mu\left(\varepsilon - i\frac{\sigma}{\omega\varepsilon_0}\right) = \omega^2\varepsilon_0\mu_0\mu\varepsilon^{*}$$

When referring Eq. (2) particularly to an elementary magnetic dipole at the coordinate origin it is convenient to introduce spherical coordinates. In this case, however, Eq. (2) assumes a form which is very awkward for solving. We therefore introduce the Fitzgerald radiation vector as is usual in the case of magnetic aerials. We write

$$
(3)\quad
\begin{aligned}
\vec{E} &= -\mu\mu_0 i\omega \operatorname{curl}\vec{F}\\
\vec{H} &= \varepsilon^{*}\varepsilon_0\mu\mu_0\omega^2\vec{F} + \operatorname{grad} U
\end{aligned}
$$

The term grad U is to conserve the general validity of the solution through the specialization of $\vec{F}$. Inserting (3) in (1) we fulfill two equations identically. Furthermore, we have

$$(4)\qquad \operatorname{grad} U = \operatorname{curl}\operatorname{curl}\vec{F} - k^{*2}\vec{F}$$

and

$$(5)\qquad k^{*2}\operatorname{div}\vec{F} + \operatorname{div}\operatorname{grad} U = 0$$

after having applied the operator div to Eq. (4). Hence, Eq. (4) does not lead to any new results. With the specialization $\vec{F} = \{F_r, 0, 0\}$, which does <u>not</u> restrict the general validity of the solution, we get from (4)

$$(4\text{-}r)\quad \frac{\partial U}{\partial r} = -k^{*2}F_r - \frac{1}{r^2\sin\vartheta}\frac{\partial}{\partial\vartheta}\sin\vartheta\frac{\partial F_r}{\partial\vartheta} - \frac{1}{r^2\sin^2\vartheta}\frac{\partial^2 F_r}{\partial\varphi^2}$$

$$(4\text{-}\vartheta)\quad \frac{\partial U}{\partial\vartheta} = \frac{\partial^2 F_r}{\partial r\,\partial\vartheta}$$

$$(4\text{-}\varphi)\quad \frac{\partial U}{\partial\varphi} = \frac{\partial^2 F_r}{\partial r\,\partial\varphi}$$

The last two equations can be fulfilled by the substitution

$$(6)\qquad U = \frac{\partial F_r}{\partial r}$$

Inserting (6) and the substitution

$$(7)\qquad F_r = rw \qquad\qquad w = w(r, \vartheta, \varphi)$$

into (4-r), and since

$$(8)\quad \Delta w = \frac{1}{r^2}\frac{\partial}{\partial r}\left(r^2\frac{\partial w}{\partial r}\right) + \frac{1}{r^2\sin\vartheta}\frac{\partial}{\partial\vartheta}\left(\sin\vartheta\frac{\partial w}{\partial\vartheta}\right) + \frac{1}{r^2\sin^2\vartheta}\frac{\partial^2 w}{\partial\varphi^2}$$

we get from (4) the Helmholtz equation

$$(9)\qquad \boxed{\Delta w + k^{*2}w = 0}$$

Then, inserting (7) in (3), we obtain the field strengths

$$(10)\quad E_r = 0;\quad E_\vartheta = -\mu\mu_o i\omega\frac{1}{\sin\vartheta}\frac{\partial w}{\partial\varphi}\ ;\ E_\varphi = \mu\mu_o i\omega\frac{\partial w}{\partial\vartheta}$$

$$(11)\quad H_r = k^{*2}rw + \frac{\partial^2(rw)}{\partial r^2}\ ;\ H_\vartheta = \frac{1}{r}\frac{\partial^2(rw)}{\partial\vartheta\,\partial r}\ ;\ H_\varphi = \frac{1}{r\sin\vartheta}\frac{\partial^2(rw)}{\partial\varphi\,\partial r}$$

This is <u>the most general solution</u> of the electromagnetic field of a <u>magnetic antenna embedded in a conducting medium</u>.

In order to solve (9) we use the known substitution

$$(12)\qquad w(r, \vartheta, \varphi) = P_j^m(\cos\vartheta)\,(a_m\cos m\varphi + b_m\sin m\varphi)\cdot R_1(r)$$

to obtain

$$(13) \qquad R_l'' + \frac{2}{r} R_l' + \left[k^{*2} - \frac{l(l+1)}{r^2}\right] R_l = 0$$

As is well known, the solution of this Bessel type differential equation is

$$(14) \qquad R_l(r) = \frac{1}{\sqrt{r}} Z_{l+\frac{1}{2}}(k^* r)$$

where $Z_{l+\frac{1}{2}}$ is a general cylindrical function. As we are concerned not with standing but with propagating waves we choose Hankel functions for $Z_{l+\frac{1}{2}}$ to obtain

$$(15) \qquad R_l(r) = r^l \left(\frac{d}{rdr}\right)^l \frac{e^{\pm ik^* r}}{r}$$

since Bessel functions with half-integer subscripts can be reduced to $\sin k^* r$ or to $e^{ik^* r}$. Thus we get

$\underline{l = 0}$

$$w = \frac{e^{\pm ik^* r}}{r}$$

This solution produces fields that are independent of the angle ϑ. As it corresponds to a magnetic pole it is not interesting from the physical viewpoint.

$\underline{l = 1}$ (magnetic dipole)

If we use only the asymptotic solution we have

$$(16) \qquad rw(r, \vartheta, \varphi) = \cos\vartheta(a_1\cos\varphi + b_1\sin\varphi)\left(-\frac{e^{-ik^* r}}{r} - ik^* e^{-ik^* r}\right)$$

and obtain

$$(17) \qquad H_r = A\cos\vartheta(\cos\varphi + B\sin\varphi)\left(\frac{2}{r^3} e^{-ik^* r} + \frac{2ik^*}{r^2} e^{-ik^* r}\right)$$

$$(18) \qquad H_\vartheta = -A\sin\vartheta(\cos\varphi + B\sin\varphi)\left(\frac{e^{-ik^* r}}{r^3} + \frac{ik^*}{r^2} e^{-ik^* r} - \frac{k^{*2} e^{-ik^* r}}{r}\right)$$

$$H_\varphi = A\cot g\vartheta(-\sin\varphi + B\cos\varphi)\left(\frac{e^{-ik^*r}}{r^3} + \frac{ik^*}{r^2}e^{-ik^*r} - k^{*2}\frac{e}{r}^{-ik^*r}\right)$$

$H_\varphi = 0$ for $\frac{\partial}{\partial\varphi} = 0$. In (17) and (18) we have then $B = 0$, $\cos\varphi = 1$. We do not calculate the electrical field strength as only $\vec{H}$ is measured. The constant A can be determined by passing to the static limit $k^* \longrightarrow 0$. With $\varphi = 0$ (xz-plane, cf. Fig. 2) we get

$$H_r = A\cos\vartheta\cdot\frac{2}{r^3} \qquad H_\vartheta = -A\sin\vartheta\frac{1}{r^3}$$

From this,

$$A = |\vec{m}| = m$$

and with $\frac{\partial}{\partial\varphi}$ we find the <u>field of a magnetic dipole</u>

(19) $$H_r = m\cos\vartheta\left(\frac{2}{r^3}e^{-ik^*r} + \frac{2ik^*}{r^2}e^{-ik^*r}\right)$$

(20) $$H_\vartheta = -m\sin\vartheta\left(\frac{e^{-ik^*r}}{r^3} + \frac{ik^*}{r^2}e^{-ik^*r} - \frac{k^{*2}e^{-ik^*r}}{r}\right).$$

We will now assume that the magnetic dipole be materialized as an infinitesimal frame antenna inside a hollow sphere of radius R. Let H^i be the field in the hollow sphere and H^a the field in the conducting medium. We have then

(21) $$H^i_\vartheta(R) = H^a_\vartheta(R).$$

For the hollow (air) $\sigma = 0$, and therefore, according to (2), $k_o^2 = \omega^2\varepsilon_o\mu_o\mu\varepsilon$.

From (21) follows

(22) $$m_i\frac{\left(\frac{1}{R^3} + \frac{ik_o}{R^2} - \frac{k_o^2}{R}\right)}{\left(\frac{1}{R^3} + \frac{ik^*}{R^2} - \frac{k^{*2}}{R}\right)}e^{-ik_oR + ik^*R} = m_a.$$

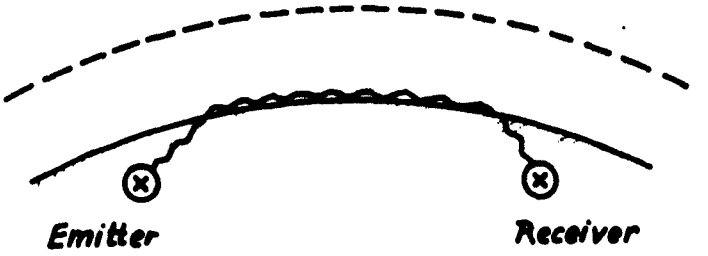

Fig.: 1

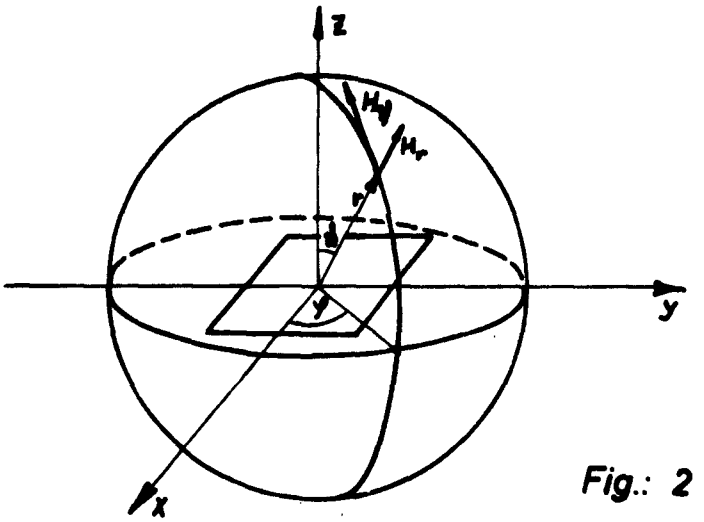

Fig.: 2

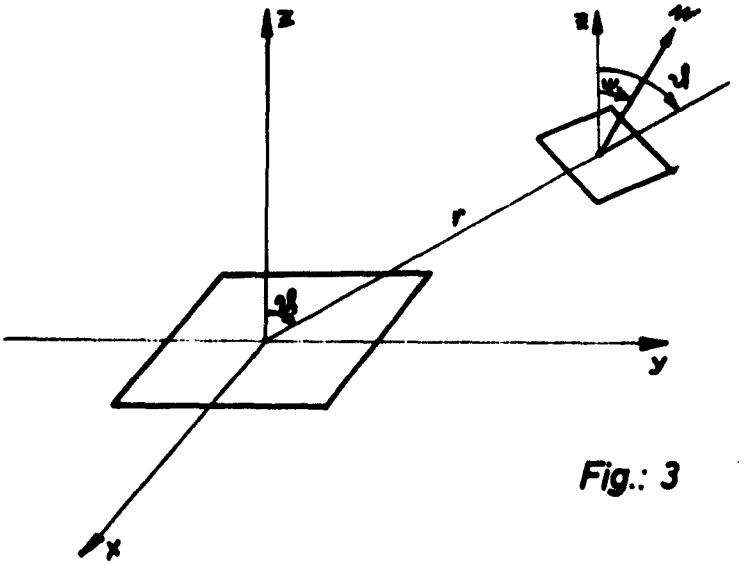

Fig.: 3

The amplitude m_a of the electromagnetic field in the medium thus depends not only on the magnetic moment of the frame antenna but also on the radius R of the hollow sphere (and on k_o and k^*). Therefore, in practice the amplitude m_a will not be calculated from the antenna current etc. but will be determined from one or several absolute measurements of field strength. For m_i we have for an alternating current in vacuo

$$m_i = i\omega\mu_o IFn. \tag{23}$$

F is the frame area, I is the current, n is the number of turns. Through the relations

$F = r^2\pi$, $R = \frac{\varrho}{q} 2r\pi n$ (resistance of coil)

$I = \sqrt{\frac{N}{R}}$, where N denotes the power, Eq. (23) for a given length of wire (given weight of antenna) assumes the form

$$m_i = i\,\omega\mu_o \sqrt{N}\,\frac{a}{\sqrt{\varrho}}\, l^{3/2} \cdot \frac{1}{4\sqrt{\pi}\, n}\,. \tag{24}$$

With power given it is therefore desirable to take few as possible turns (great F) of a thick low-resistivity wire. (Even if l is variable it is desirable to make r as great as possible.)

§2. Theory of the measurement of low-frequency magnetic fields

The magnetic fields in a conducting medium produced by a frame antenna in a hollow space have, according to §§ 1 and 3, the form

$$H_r = H_r(r,\vartheta);\quad H_\vartheta = H_\vartheta(r,\vartheta). \tag{25}$$

When we measure the magnetic field at a point $P(r,\vartheta)$ by means of the voltage induced in a little loop (cf. Fig. 2), then we will find that this voltage depends on the angle ψ formed by the normal $\vec{n}$ to the loop (ferrite antenna, etc.) and the z-axis. As measurement of the fields <u>within</u> the conducting medium is not possible, the measuring loop is placed at a distance r from the transmitter in a hollow space. Let d be the distance between the measuring loop and the wall of the hollow space. The field strength $\vec{H}^s$ at the place of the loop is then

$$H_r^s(r,\vartheta) = m_s \cos\vartheta \left(\frac{2}{r^3} e^{-ik_o r} + \frac{2ik_o}{r^2} e^{-ik_o r} \right)$$

$$H_\vartheta^s(r,\vartheta) = -m_s \sin\vartheta \left(\frac{e^{-ik_o r}}{r^3} + \frac{ik_o}{r^2} e^{-ik_o r} - \frac{k_o^2}{r} e^{-ik_o r} \right)$$

where k_o denotes the values for air. m_s can be found from the boundary condition

$$\frac{H_\vartheta(r-d,\vartheta)}{\sin\vartheta} = -m_a \left(\frac{e^{-ik^*(r-d)}}{(r-d)^3} + \frac{ik^*}{(r-d)^2} e^{-ik^*(r-d)} - \frac{k^{*2}}{(r-d)^2} e^{-ik^*(r-d)} \right) =$$

$$= \frac{H_\vartheta^s(r-d,\vartheta)}{\sin\vartheta} = -m_s \left(\frac{e^{-ik_o(r-d)}}{(r-d)^3} + \frac{ik_o}{(r-d)^2} e^{-ik_o(r-d)} - \frac{k_o^2}{(r-d)^2} e^{-ik_o(r-d)} \right).$$

If measurement is made <u>quite close</u> to the wall ($d \approx 0$) one can use (19) (20) for the formulas. Experiments with 1 kcps showed no difference even when the antenna was 15 m off the wall. For $d \approx 0$ we have thus

$$H_r(r,\vartheta) = \cos\vartheta \cdot f_r(r), \tag{26}$$

$$f_r(r) = m_a \left(\frac{2}{r^3} e^{-ik^* r} + \frac{2ik^*}{r^2} e^{-ik^* r} \right) \tag{27}$$

$$H_\vartheta(r,\vartheta) = -\sin\vartheta \cdot f_\vartheta(r) \tag{28}$$

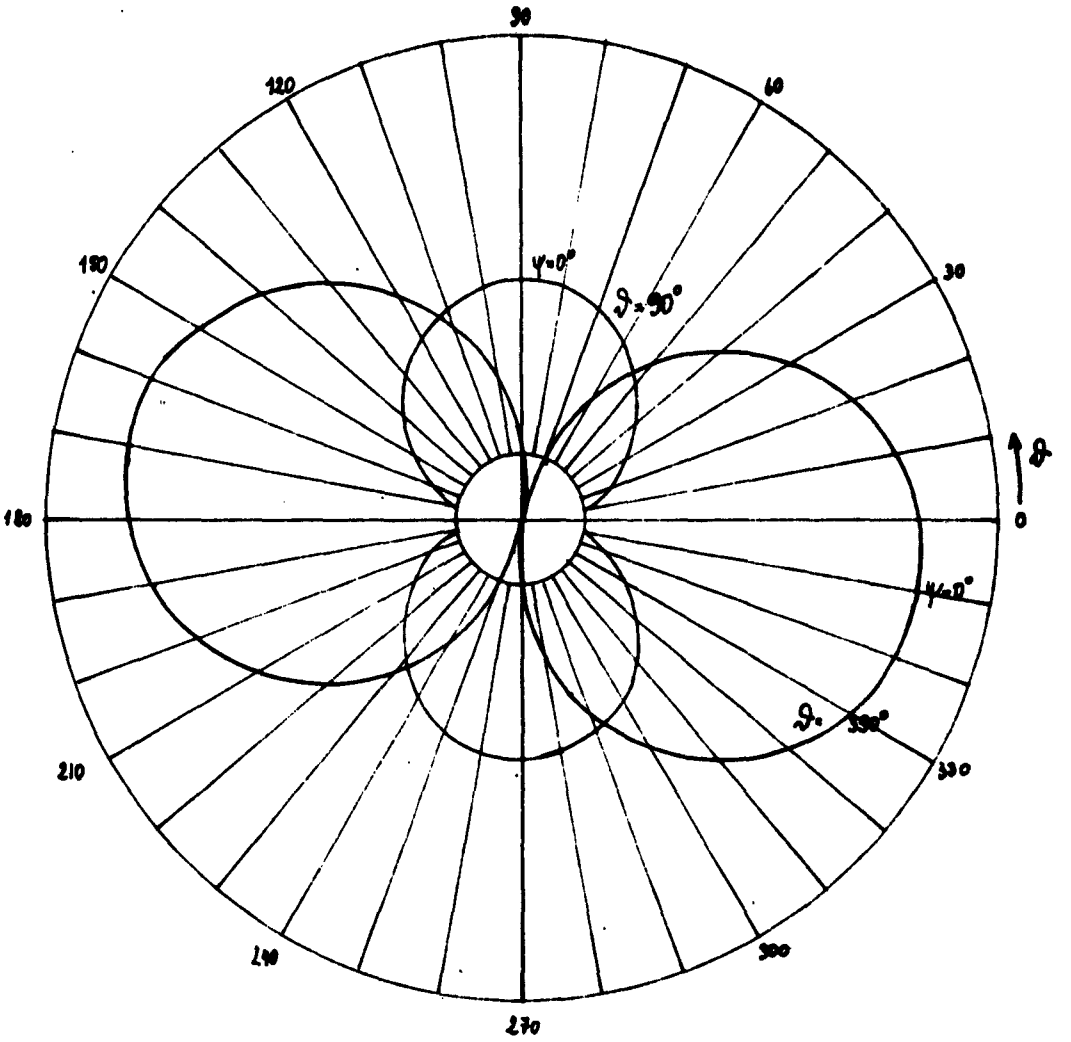

Fig.: 4

$$(29) \qquad f_{\vartheta}(r) = m_a\left(\frac{e^{-ik^*r}}{r^3} + \frac{ik^*}{r^2}e^{-ik^*r} - \frac{k^{*2}}{r}e^{-ik^*r}\right)$$

and consequently

$$(30) \qquad H^{*2} = H_r^2 + H_{\vartheta}^2 = f_r^2\cos^2\vartheta + f_{\vartheta}^2\sin^2\vartheta.$$

The voltage induced in a measuring loop of area f (very small) is given by $(\frac{\partial}{\partial t} = i\omega)$.

$$(31) \qquad |U| = -\mu_o\,\omega|H|f\cos\psi.L$$

With the distance r from the transmitter fixed we have for the measured value $|H|$

$$(32) \quad |H| = \frac{-U(r,\vartheta)}{\mu_o L\omega f\cos\psi} \quad \text{or} \quad U(r,\vartheta,\psi) = A(\omega)\sqrt{f_r^2\cos^2\vartheta + f_{\vartheta}^2\sin^2\vartheta}\cdot\cos\psi.$$

The function $U(r,\vartheta,\psi)$ according to (31) was measured for

(1) ν = 3kcps, r = 316 m, ϑ = 90°, 350°, U = Bcosψ, Fig.4, wherefrom B = 7.55 (90°); B = 12.46 (350°). (The angle ϑ is plotted in the center of the polar graph, the angle ψ at the periphery.) The individual points of the curve correspond to different values of ψ. Measurements were made at ψ = 0°, 30°, 60°, etc. up to 360° (12 readings).

(2) ν = 3kcps, r = 1000 m, Fig. 5

ϑ = 0°, 180°	B = 13.59
ϑ = 30°, 210°	B = 8.09
ϑ = 90°, 270°	B = 7.55
ϑ = 150°, 330°	B = 13.30

(3) ν = 3 kcps, r = 100 m, Fig. 6

ϑ = 0°, 180°	B = 14.244
ϑ = 10°, 190°	B = 13.688
ϑ = 40°, 220°	B = 10.699
ϑ = 70°, 250°	B = 7.646
ϑ = 130°, 310°	B = 8.944
ϑ = 160°, 340°	B = 12.436.

These measurements show that at such distances one is still far from the far field. For the latter, the terms with higher negative powers of r can be omitted. Thus,

$$H_\vartheta = m \sin\vartheta\, k^{*2} \frac{e^{-ik^*r}}{r}, \quad H_r \approx 0. \tag{33}$$

Therefore, $H_\vartheta > H_r$ and $|H| \approx 0$ should hold for $\vartheta = 0^\circ$. But this is not the case, or even $B(0^\circ) > B(90^\circ)$, cf. Fig. 5. However, the measurements were not further evaluated as they were made in different kinds of rock and served only as a first rough check of the theory.

§3. Numerical data

In §2 we defined

$$k^{*2} = \omega^2 \varepsilon_0 \mu_0 \mu \left(\varepsilon - \frac{i\sigma}{\omega \varepsilon_0}\right) \tag{34}$$

where

$$\varepsilon_0 = 8.859 \cdot 10^{-12} \text{ amp sec/volts m} \tag{35}$$

$$\mu_0 = 1.256 \cdot 10^{-6} \text{ volts sec/amp m}, \quad \mu = 1. \tag{36}$$

Splitting $k^* = \omega\sqrt{\varepsilon_0 \mu_0}\ \sqrt{\varepsilon - \frac{i\sigma}{\omega \varepsilon_0}}$ into its real and imaginary parts yields

$$k^* = k_1 - ik_2 \tag{37}$$

$$k_1 = +\sqrt{\frac{\omega^2 \mu_0 \varepsilon \varepsilon_0}{2}} \cdot \sqrt{1 + \sqrt{1 + \left(\frac{\sigma}{\omega \varepsilon_0 \varepsilon}\right)^2}} \tag{38}$$

$$k_2 = +\sqrt{\frac{\omega^2 \mu_0 \varepsilon \varepsilon_0}{2}} \cdot \sqrt{-1 + \sqrt{1 + \left(\frac{\sigma}{\omega \varepsilon_0 \varepsilon}\right)^2}} \tag{39}$$

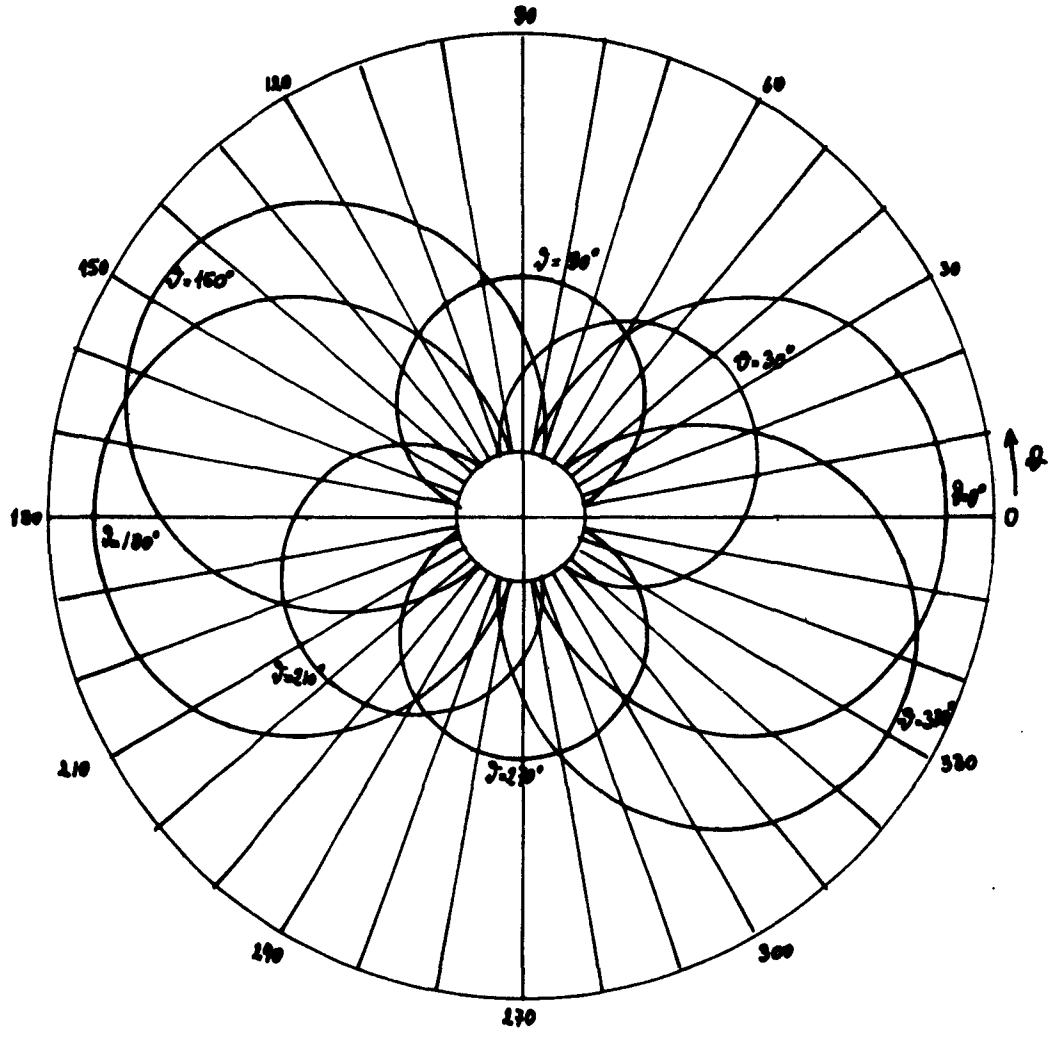

f = 3 kHz ; r = 1000 m

Fig.: 5

We now distinguish two cases.

(1) Displacement current neglected.

For $(\frac{\sigma}{\omega\varepsilon_0\varepsilon})^2 \gg 1$ we can simplify (38) (39): then we get

$$k_1 \approx + \sqrt{\frac{\omega\mu_0\sigma}{2}} \tag{40}$$

$$k_2 \approx + \sqrt{\frac{\omega\mu_0\sigma}{2}} \approx k_1 \tag{41}$$

$$k^* \approx \sqrt{\frac{\omega\mu_0\sigma}{2}}\,(1 - i) = k_3(1 - i). \tag{42}$$

The same expressions can be got when the displacement current is neglected. For $\varepsilon \approx 10$, this leads to the postulate $\frac{\sigma}{\omega} \gg 8\cdot10^{-11}$. From this it follows that when every value $\frac{\sigma}{\nu} > 10^{-8}$ is regarded as relatively great, the range

$\sigma = 10^{-5}$ permits neglection from $\nu < 1$ kcps on

$\sigma = 10^{-4}$ permits neglection from $\nu < 10$ kcps on

$\sigma = 10^{-3}$ permits neglection from $\nu < 100$ kcps on.

As the conductivity is probably around 10^{-4}, and since we always employed frequencies of $\nu < 10$ kcps, this neglection seems to be justified in most of the cases.

(2) Displacement current not neglected.

k_1 and k_2 in this case have to be calculated from (38) (39). Inserting (37) in (26) and (28), and after squaring we get

$$|H_r|^2 = 4m^2\cos^2\vartheta e^{-2k_2 r}\left(\left[\frac{1}{r^3} + \frac{k_2}{r^2}\right]^2 + \frac{k_1^2}{r^4}\right) \tag{43}$$

$$(44)\qquad |H_\vartheta|^2 = m^2 \sin^2\vartheta\, e^{-2k_2 r}\left(\left[\frac{1}{r^3}+\frac{k_2}{r^2}+\frac{k_2^2-k_1^2}{r}\right]^2+\left[\frac{k_1}{r^2}+\frac{2k_1k_2}{r}\right]^2\right).$$

Thus,

$$(45)\qquad |\vec{H}| = me^{-k_2 r}\cdot\left\{4\cos^2\vartheta\left[\frac{1}{r^6}+\frac{2k_2}{r^5}+\frac{k_1^2+k_2^2}{r^4}\right]+\sin^2\vartheta\left[\frac{1}{r^6}+\frac{2k_2}{r^5}+\frac{3k_2^2-k_1^2}{r^4}+\frac{2k_2^3+2k_1^2k_2}{r^3}+\frac{k_2^4+k_1^4+2k_1^2k_2^2}{r^2}\right]\right\}^{1/2}.$$

For the measurements with $\vartheta = 0^\circ$ and 90° (cf. Figs. 4-6) we have

$\underline{\vartheta = 0;}$

$$(46)\qquad H_\vartheta = 0;\ |\vec{H}| = 2me^{-k_2 r}\left\{\frac{1}{r^6}+\frac{2k_2}{r^5}+\frac{k_1^2+k_2^2}{r^4}\right\}^{1/2}.$$

$\underline{\vartheta = 90^\circ;}$

$$(47)\qquad H_r = 0;\ |\vec{H}| = me^{-k_2 r}\left\{\frac{1}{r^6}+\frac{2k_2}{r^5}+\frac{3k_2^2-k_1^2}{r^4}+\frac{2k_2^3+2k_1^2k_2}{r^3}+\frac{k_2^4+k_1^4+2k_1^2k_2^2}{r^2}\right\}^{1/2}.$$

<u>Neglecting the displacement current</u> $\left(k_1 \approx k_2 \sim \sqrt{\frac{\omega\mu_o\sigma}{2}}\right)$,

we obtain with $\alpha = \omega\sigma$

$$(48)\qquad \underline{\vartheta = 0^\circ}\ |\vec{H}| = |H_r| = 2me^{-\sqrt{\frac{\mu_o\alpha}{2}}\,r}\left\{\frac{1}{r^6}+\frac{\sqrt{\frac{\mu_o\alpha}{2}}}{r^5}+\frac{\mu_o\alpha}{r^4}\right\}^{1/2}$$

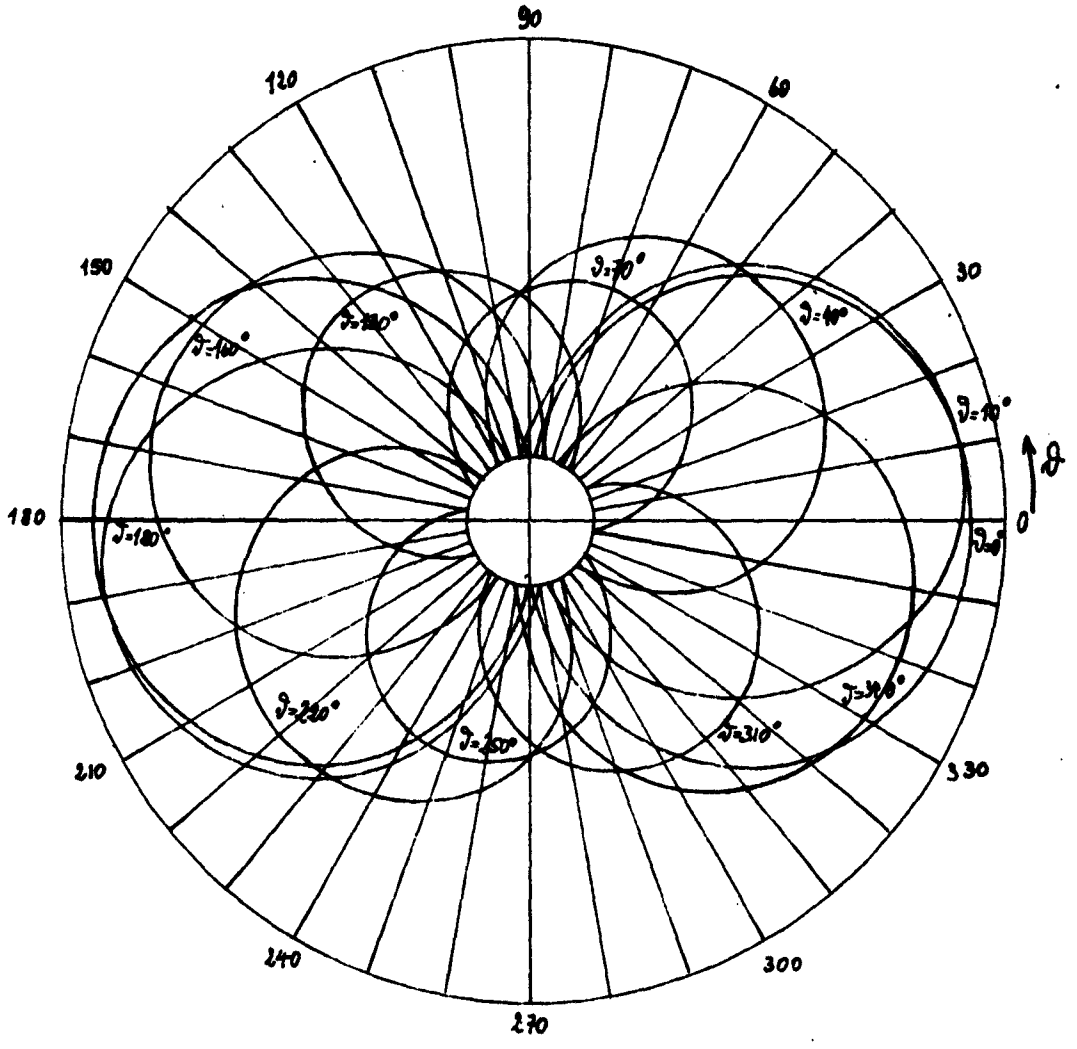

$f = 3\,kHz$; $r = 100\,m$

Fig.: 6

$$(49)\quad \vartheta = 90^\circ \quad |\vec{H}| = |H_\vartheta| = me^{-\sqrt{\frac{\mu_0\alpha}{2}}r}\left\{\frac{1}{r^6} + \frac{2\sqrt{\frac{\mu_0\alpha}{2}}}{r^5} + \frac{\mu_0\alpha}{r^4} + \right.$$

$$\left. + \frac{2\mu_0\alpha\sqrt{\frac{\mu_0\alpha}{2}}}{r^3} + \frac{\mu_0^2\alpha^2}{r^2}\right\}^{1/2}$$

We now define

$$(50)\qquad f(r,\alpha) = e^{-\sqrt{\frac{\mu_0\alpha}{2}}r}\left\{\frac{1}{r^6} + \frac{2\sqrt{\frac{\mu_0\alpha}{2}}}{r^5} + \frac{\mu_0\alpha}{r^4}\right\}^{1/2}$$

and calculate $f(r,\alpha) \sim H_r$ (for $\vartheta = 0^\circ$) as a function of the one variable with the other variable fixed. Fig. 7 shows $f(r;\alpha)$ and Fig. 8 shows $f(\alpha;r)$. Fig. 7a is the same as Fig. 7, but on a larger scale.

We define

$$(51)\quad g(r,\alpha) = e^{-\sqrt{\frac{\mu_0\alpha}{2}}r}\left\{\frac{1}{r^6} + \frac{2\sqrt{\frac{\mu_0\alpha}{2}}}{r^5} + \frac{\mu_0\alpha}{r^4} + \frac{2\mu_0\alpha\sqrt{\frac{\mu_0\alpha}{2}}}{r^3} + \frac{\mu_0^2\alpha^2}{r^2}\right\}^{1/2}$$

and calculate $g(r,\alpha) \sim H_\vartheta$ (for $\vartheta = 90^\circ$) as a function of one variable with the other variable fixed. Fig. 9 shows $g(r;\alpha)$, Fig. 10 shows $g(\alpha;r)$.

Neglecting the displacement current we find from (45) the amount of $|\vec{H}|$ which is

$$(52)\qquad |\vec{H}| = me^{-\sqrt{\frac{\mu_0\alpha}{2}}r}\left\{4\cos^2\vartheta\left[\frac{1}{r^6} + \frac{2\sqrt{\frac{\mu_0\alpha}{2}}}{r^5} + \frac{\mu_0\alpha}{r^4}\right] + \right.$$

$$\left. + \sin^2\vartheta\left[\frac{1}{r^6} + \frac{2\sqrt{\frac{\mu_0\alpha}{2}}}{r^5} + \frac{\mu_0\alpha}{r^4} + \frac{2\mu_0\alpha\sqrt{\frac{\mu_0\alpha}{2}}}{r^3} + \frac{\mu_0^2\alpha^2}{r^2}\right]\right\}^{1/2}$$

Let $h(r,\alpha,\vartheta)$ be the quantity $\frac{|\vec{H}|}{m}$. This function was computed:

Fig. 11 $h(r;\vartheta)$ for $\sigma = 10^{-3}$ and $\sigma = 10^{-4}$ (Tables 1 and 2)

Fig. 12 $h(r;\alpha)$ for $\vartheta = 45^{\circ}$ (Table 3)

Fig. 13 $h(\vartheta;r)$ for $\sigma = 10^{-4}$ (Table 1) and $\sigma = 10^{-3}$ (Table 2)

Fig. 14 $h(\vartheta;\alpha)$ for r = 3160 m (Table 5) and r = 1000 (Table 4)

Fig. 15 $h(\alpha;r)$ for $\vartheta = 45^{\circ}$ (Table 3)

Fig. 16 $h(\alpha;\vartheta)$ for r = 3160 m (Table 5) and r = 1000 m (Table 4)
for $1 < \alpha < 1000$, i.e. for $5 \cdot 10^{-5} < \sigma < 5 \cdot 10^{-2}$

The results of the calculations are compiled in the following tables:

Table 1 Figs. 11, 13 $h(r;\vartheta)$ and $h(\vartheta;r)$, $\sigma = 10^{-4}$

Table 2 Figs. 11, 13 $h(r;\vartheta)$ and $h(\vartheta;r)$, $\sigma = 10^{-3}$

Table 3 Figs. 12, 15 $h(\alpha;r)$ $\vartheta = 45^{\circ}$

Table 4 Figs. 14, 16 $h(\alpha;\vartheta)$ r = 1000 m

Table 5 Figs. 14, 16 $h(\alpha;\vartheta)$ r = 3160 m

Evaluating the formulas

$$(38) \qquad k_1 = + \sqrt{\frac{\omega^2 \mu_0 \varepsilon \varepsilon_0}{2}} \sqrt{1 + \sqrt{1 + \left(\frac{\sigma}{\omega \varepsilon_0 \varepsilon}\right)^2}}$$

$$(39) \qquad k_2 = + \sqrt{\frac{\omega^2 \mu_0 \varepsilon \varepsilon_0}{2}} \sqrt{-1 + \sqrt{1 + \left(\frac{\sigma}{\omega \varepsilon_0 \varepsilon}\right)^2}}$$

$$(42) \qquad k_3 = \sqrt{\frac{\omega \mu_0 \sigma}{2}} \quad \text{(displacement current neglected)}$$

and using the values $\varepsilon_0 = 8.859 \cdot 10^{-12}$, $\mu_0 = 1.256 \cdot 10^{-6}$ for 3000 cps, $\varepsilon = 12.5$ we find

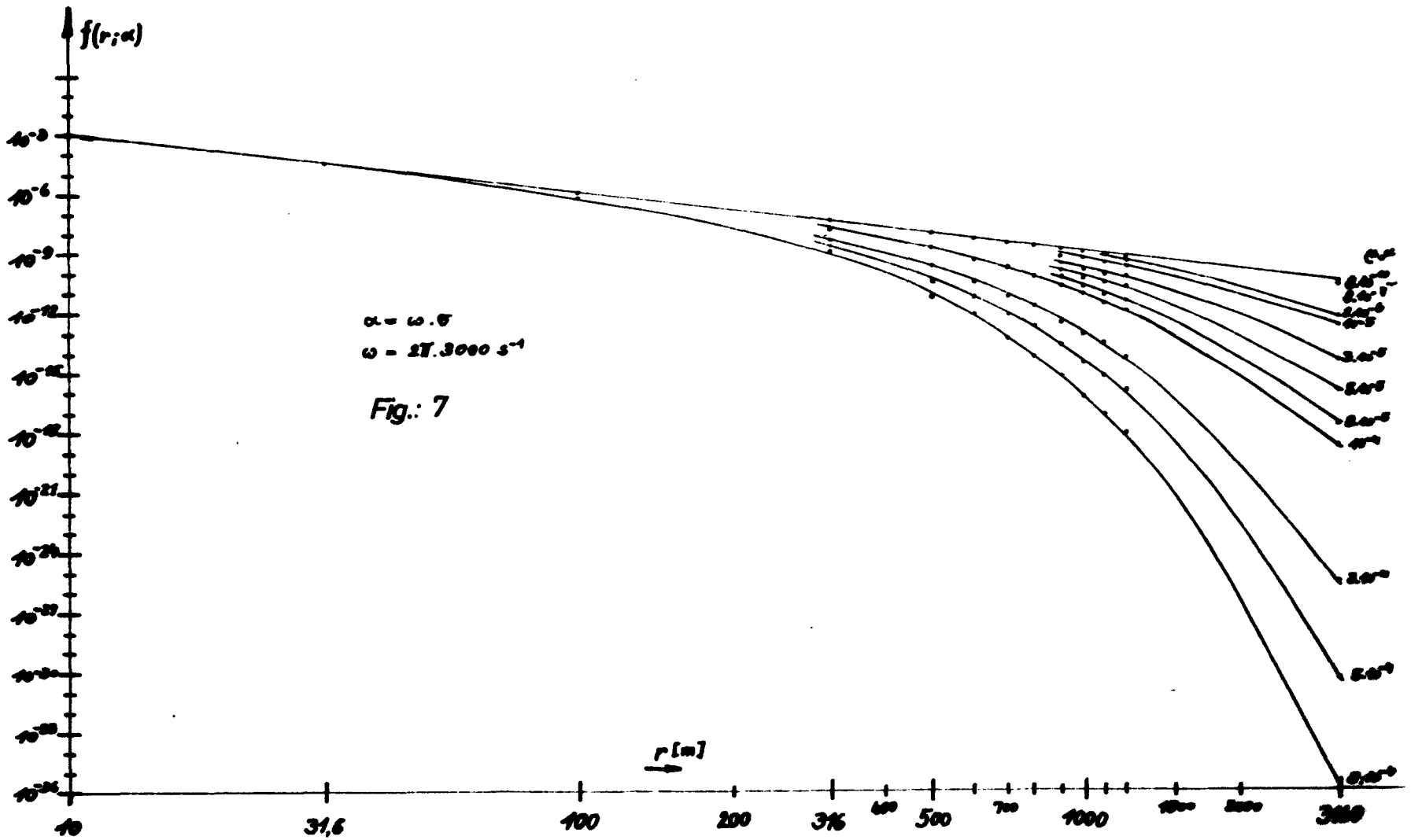

Fig.: 7

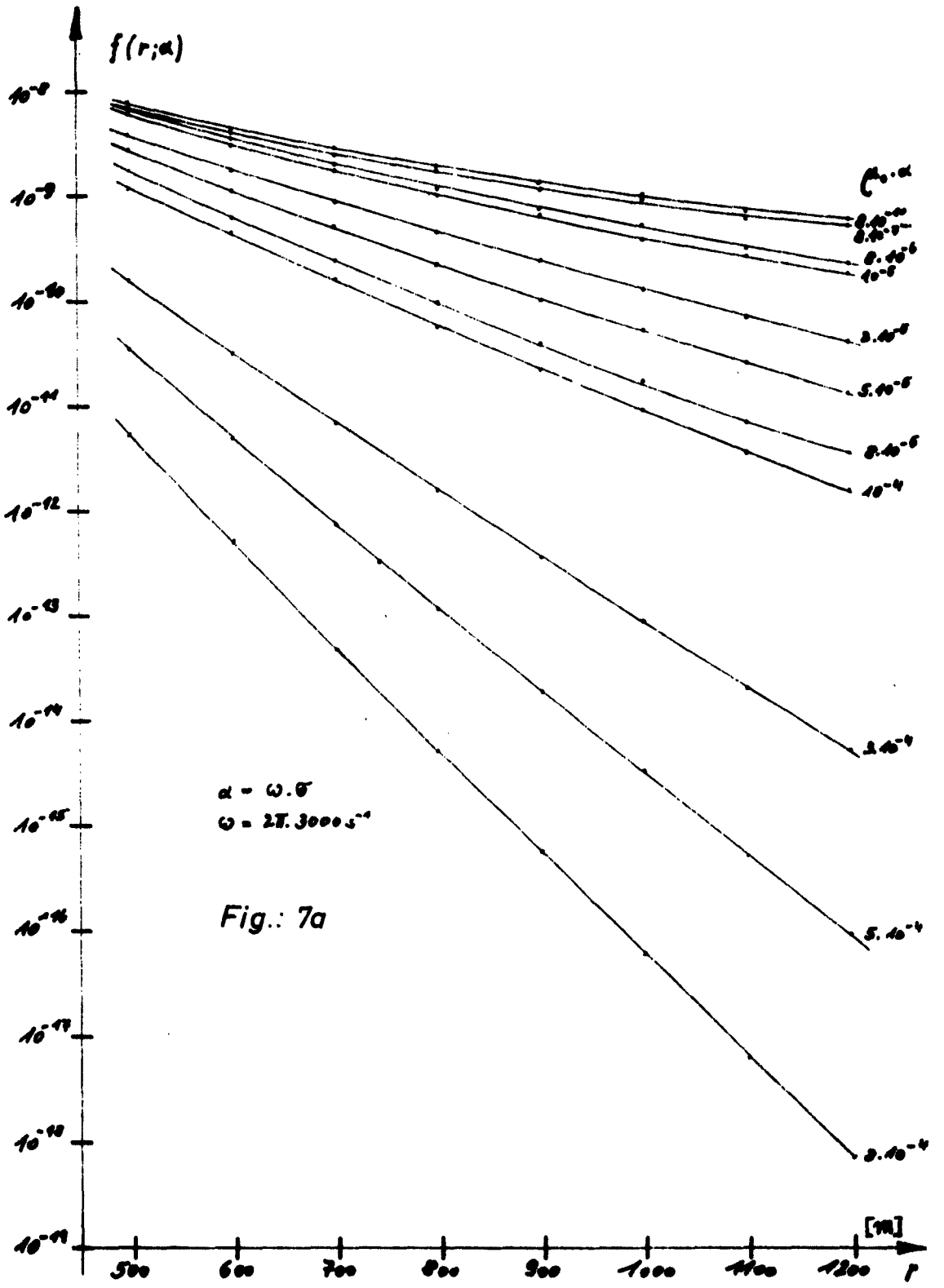
f(r;α)
10⁻⁸
10⁻⁹
10⁻¹⁰
10⁻¹¹
10⁻¹²
10⁻¹³
10⁻¹⁴
10⁻¹⁵
10⁻¹⁶
10⁻¹⁷
10⁻¹⁸
10⁻¹⁹
α = ω.σ
ω = 2π.3000 s⁻¹
10⁻⁴
5.10⁻⁴
2.10⁻³
[nm]
500
600
700
800
900
1000
1100
1200
r

Fig.: 7a

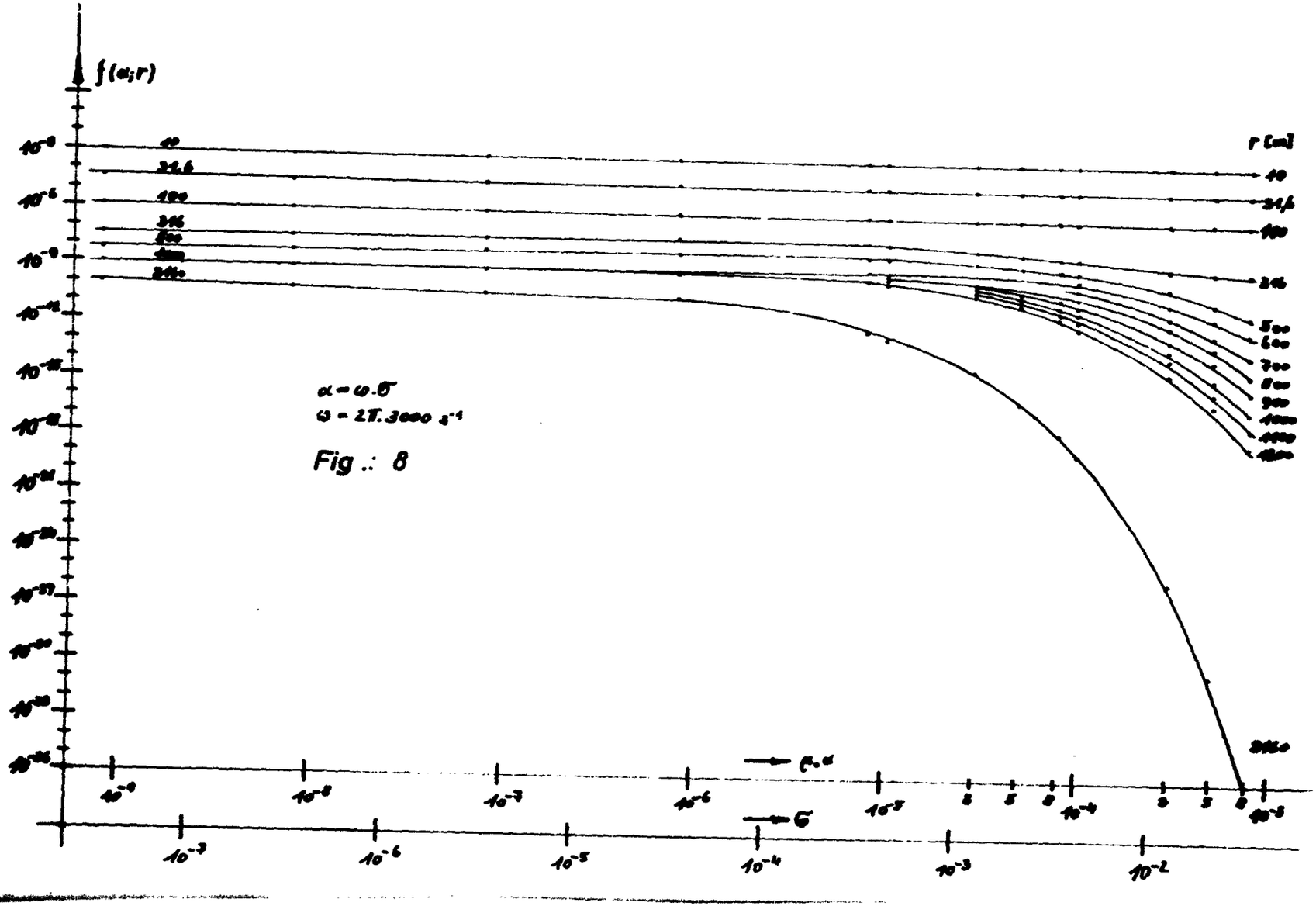

Fig .: 8

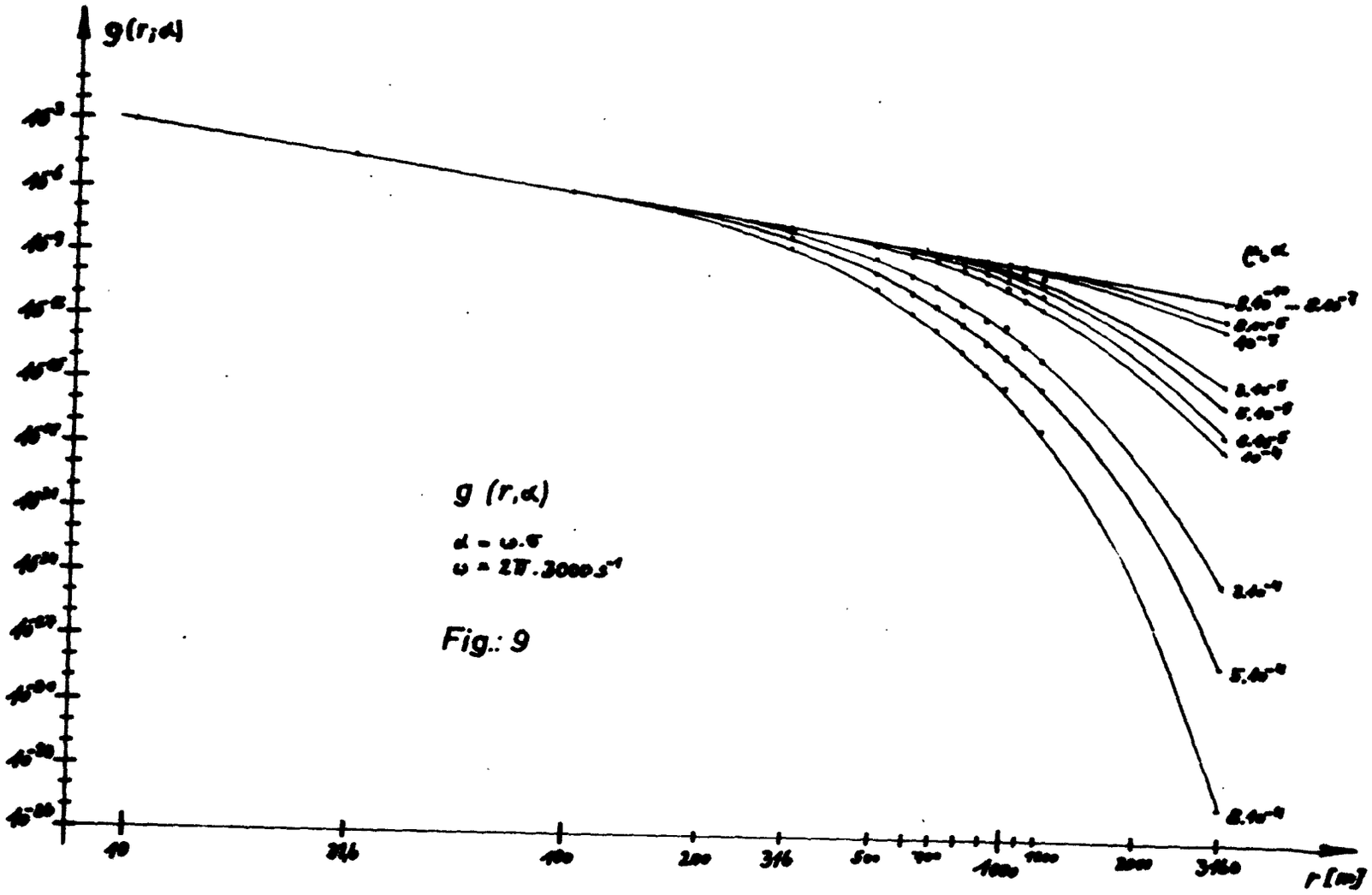

Fig.: 9

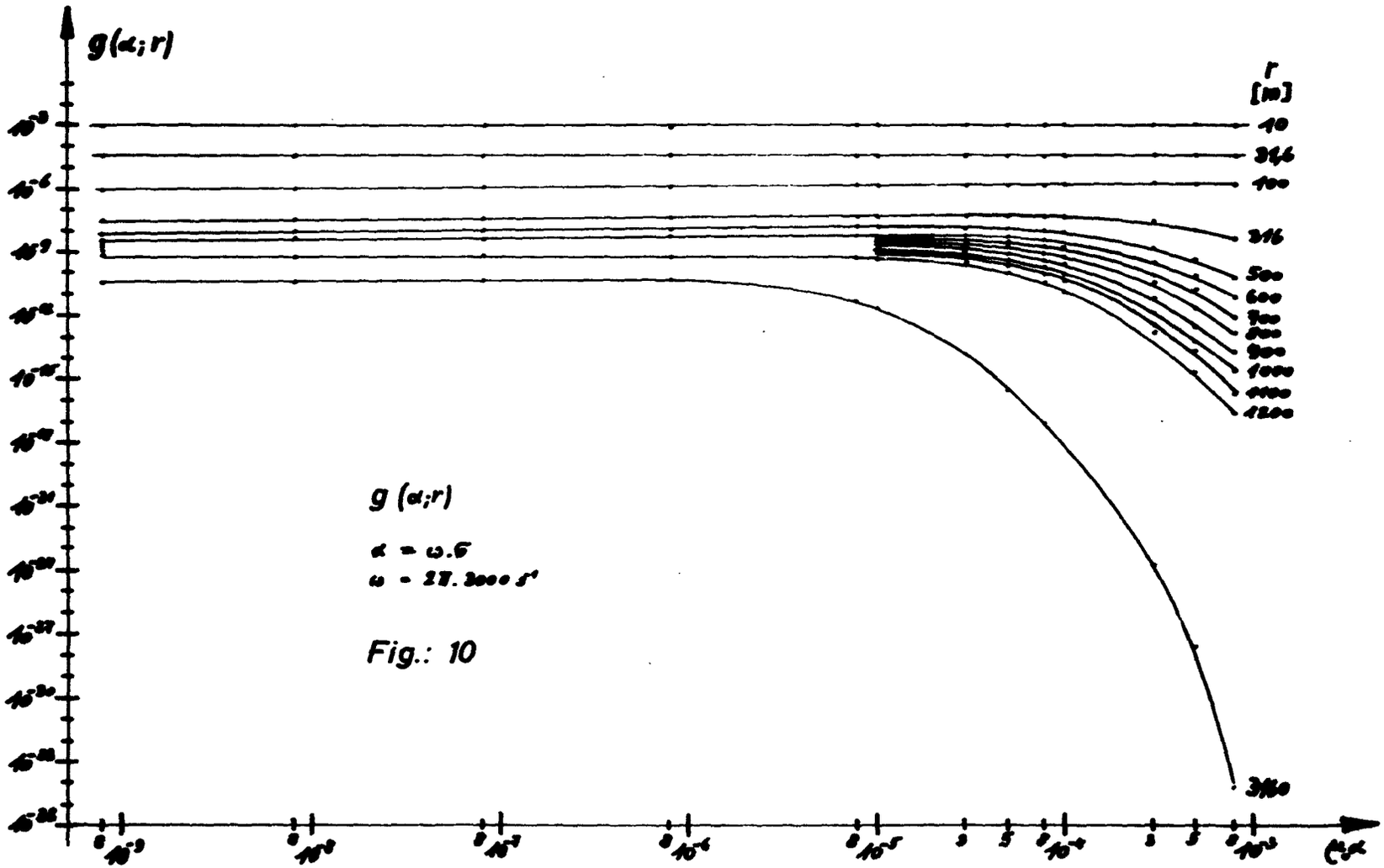
g(α;r)
r
[m]
10
31,6
100
316
500
600
700
800
900
1000
1100
1200
3160
g (α;r)
α = ω.δ
ω = 27.3000 s⁻¹

Fig.: 10

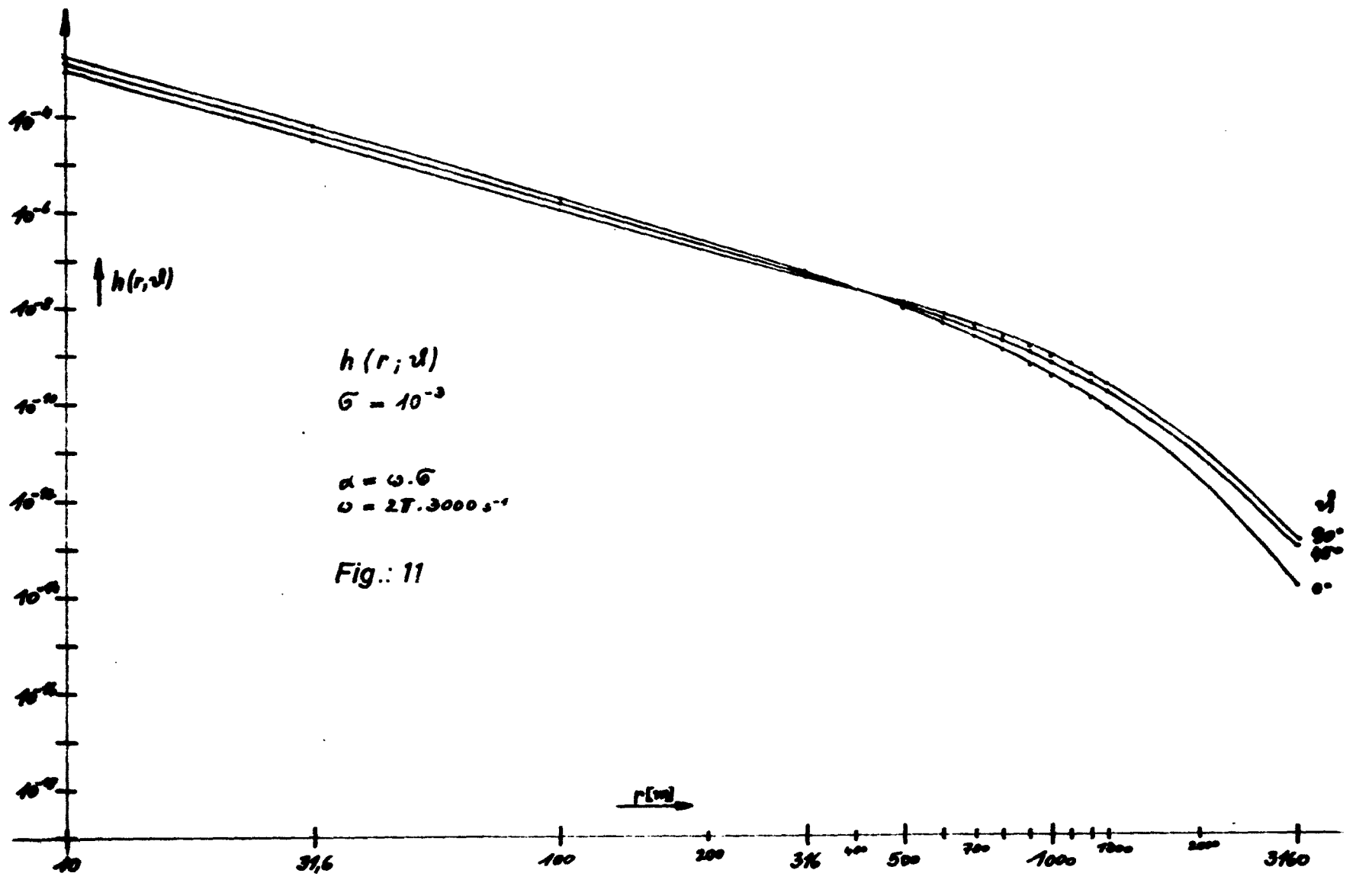

Fig.: 11

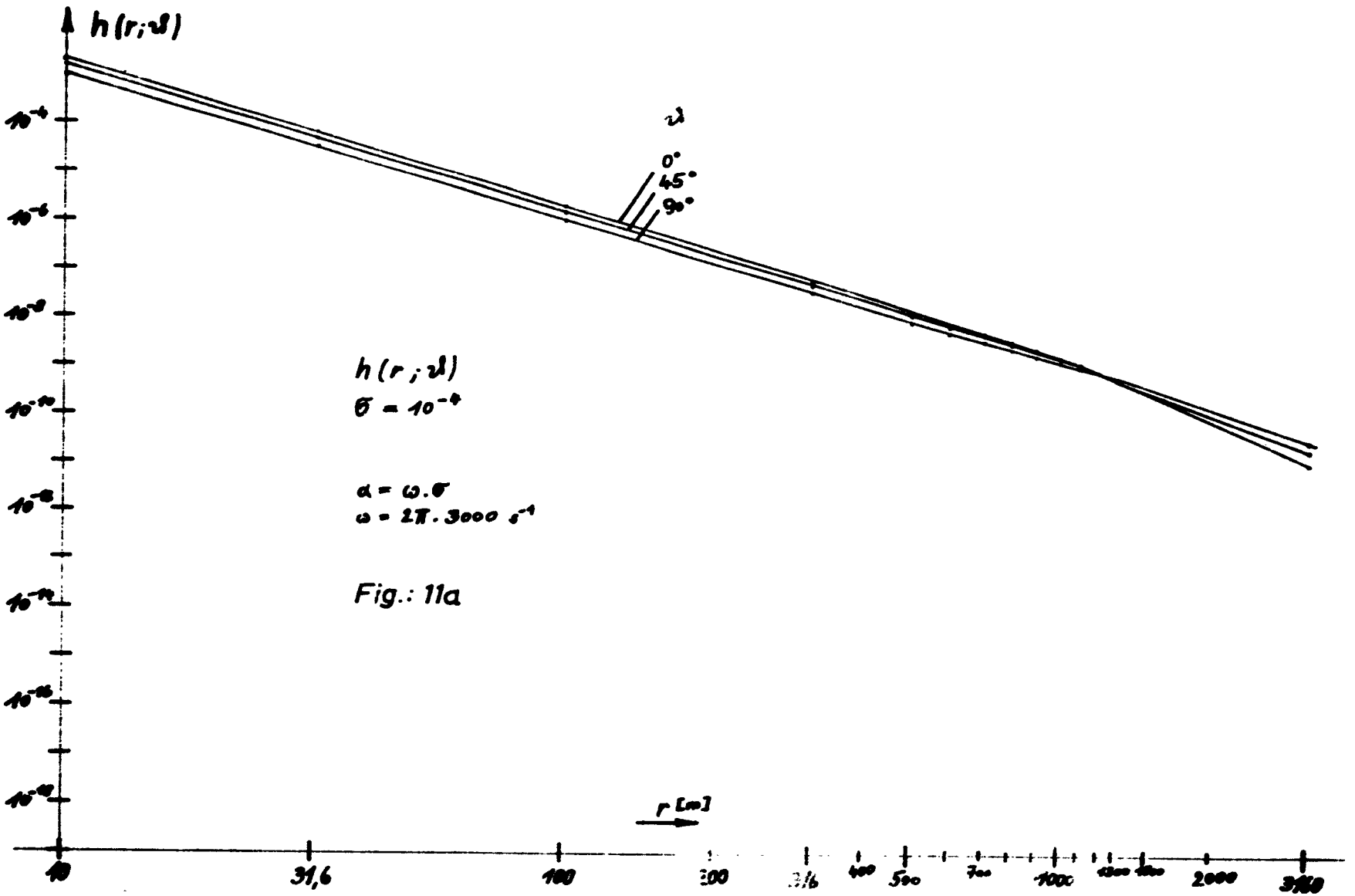
h(r;ϑ)
ϑ
0°
45°
90°
h(r;ϑ)
σ = 10⁻⁴
α = ω·σ
ω = 2π·3000 s⁻¹
r [m]
10
31,6
100
316
400
500
700
1000
2000

Fig.: 11a

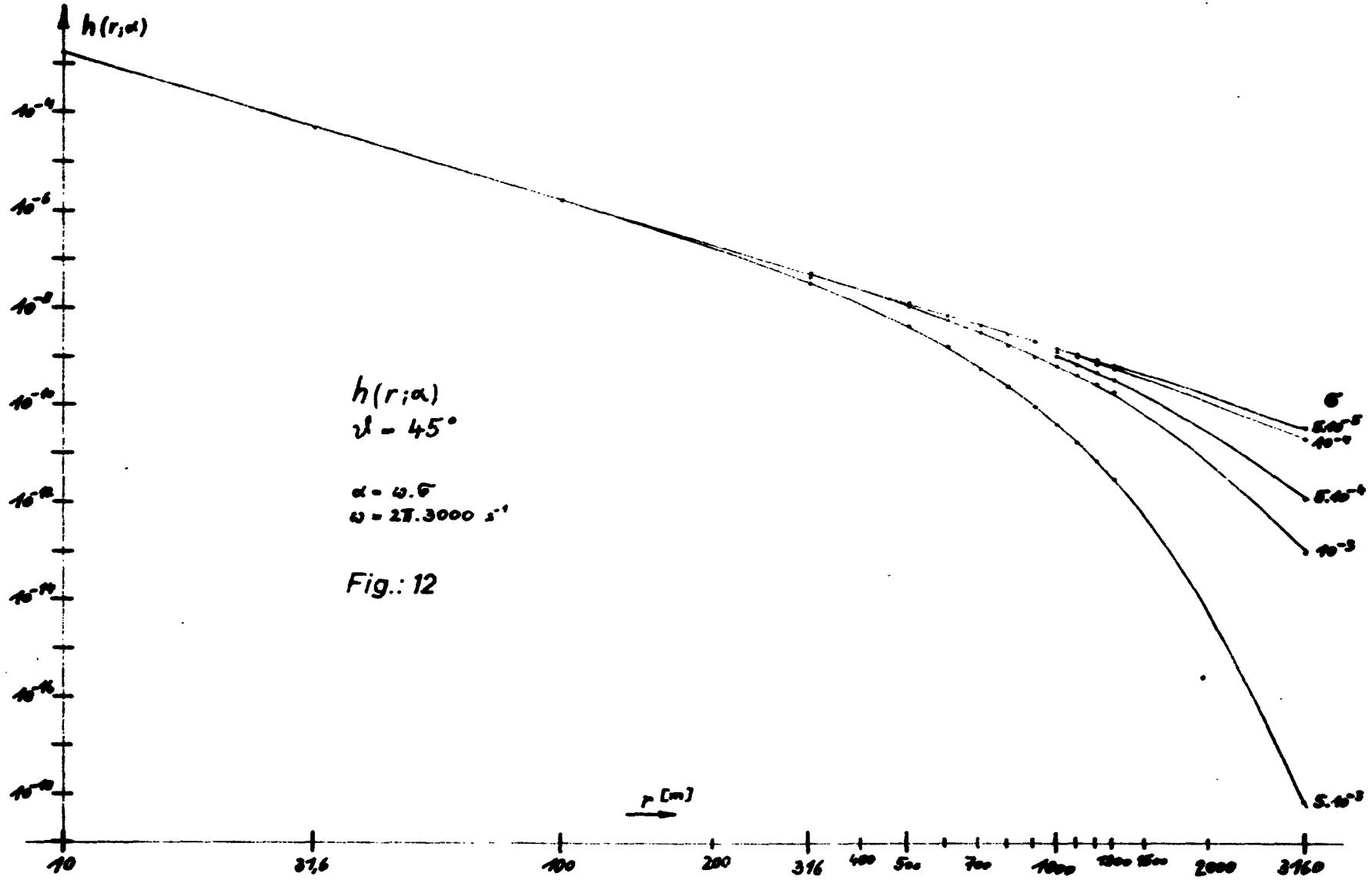
h(r;α)
h(r;α)
ϑ = 45°
α = ω.σ
ω = 2π.3000 s⁻¹
σ
r [m]
10
31,6
100
200
316
400
500
700
1000
1250
1500
2000
3160

Fig.: 12

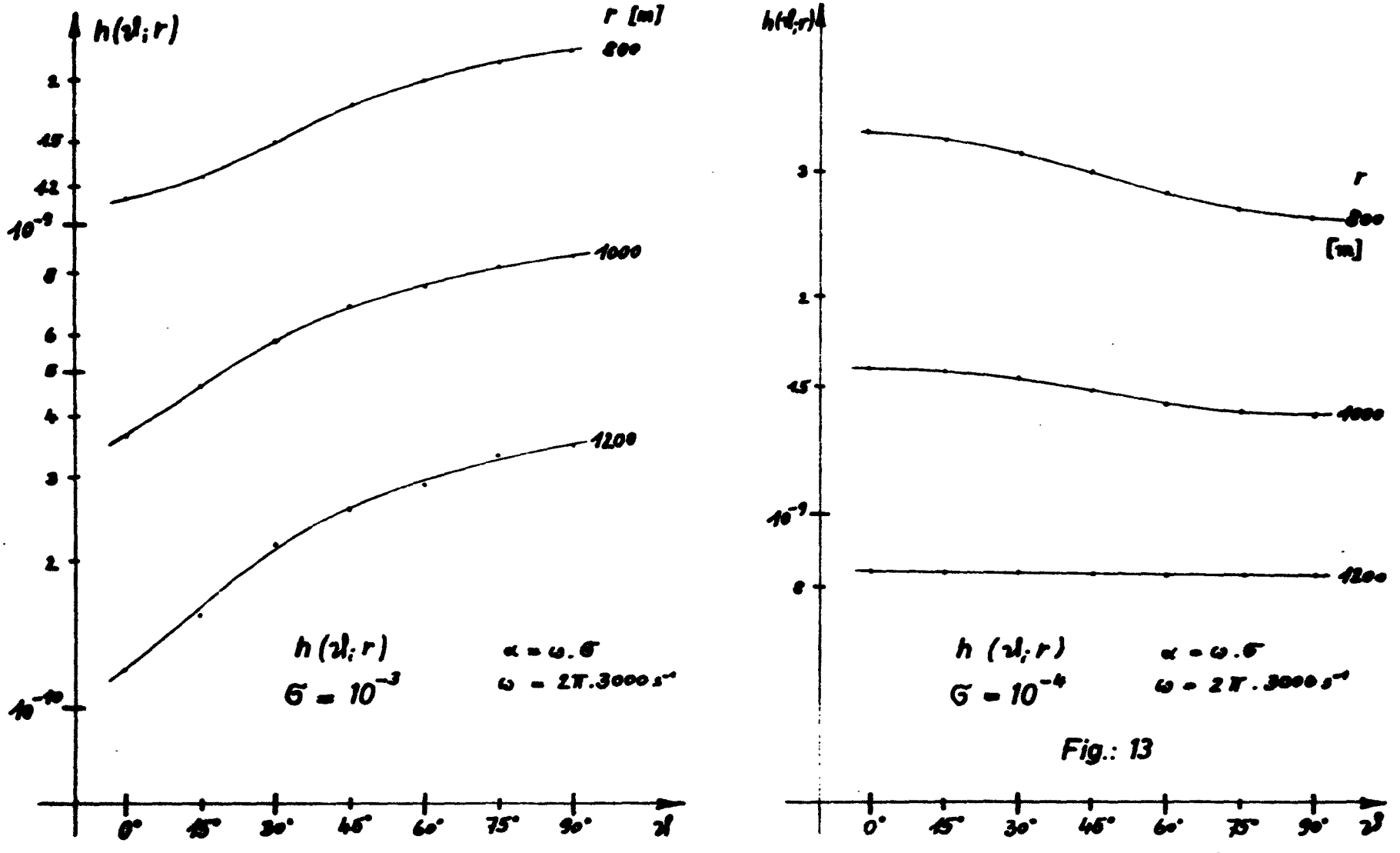
h(ϑ; r)
r [m]
800
1000
1200
h (ϑ; r)
σ = 10⁻³
α = ω . σ
ω = 2π . 3000 s⁻¹
0°
15°
30°
45°
60°
75°
90°
ϑ
h(ϑ; r)
r
[m]
h (ϑ; r)
σ = 10⁻⁴
α = ω . σ
ω = 2π . 3000 s⁻¹

Fig.: 13

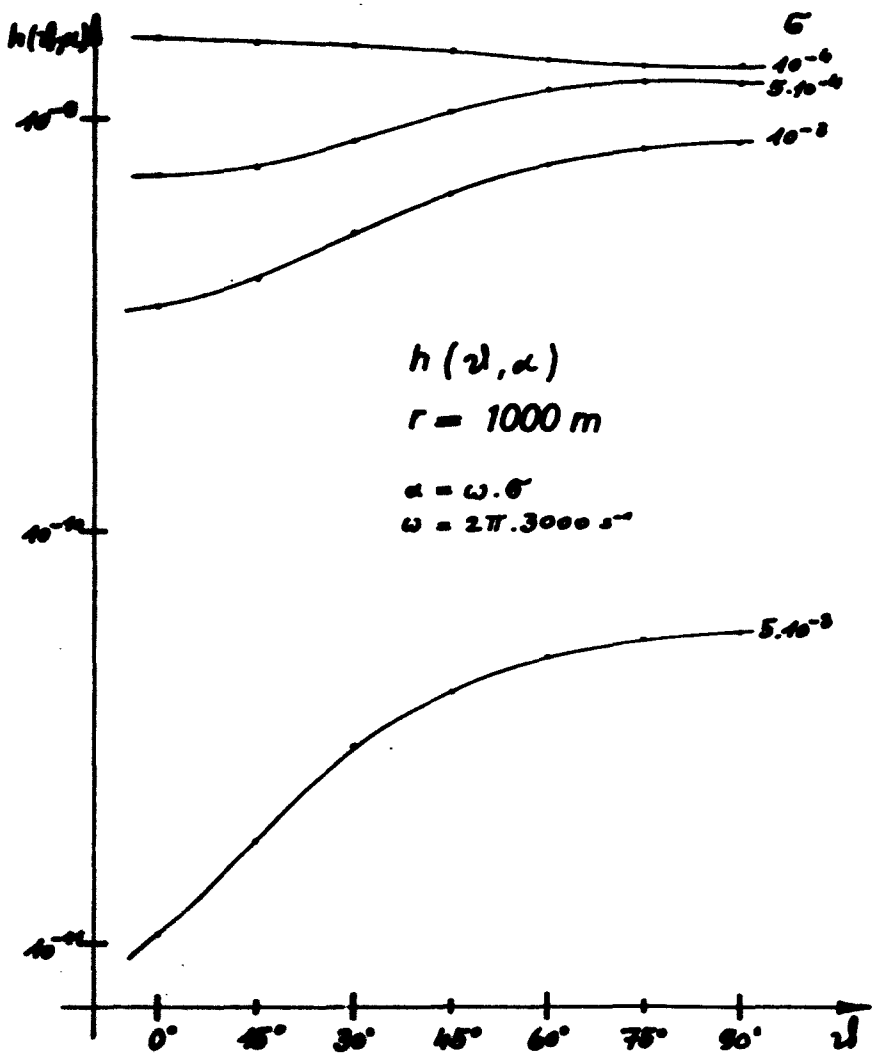
h(ϑ,α)
σ
10⁻⁴
5.10⁻⁴
10⁻³
10⁻⁸
10⁻¹²
10⁻¹⁶
5.10⁻³
h (ϑ, α)
r = 1000 m
α = ω.σ
ω = 2π.3000 s⁻¹
0°
15°
30°
45°
60°
75°
90°
ϑ

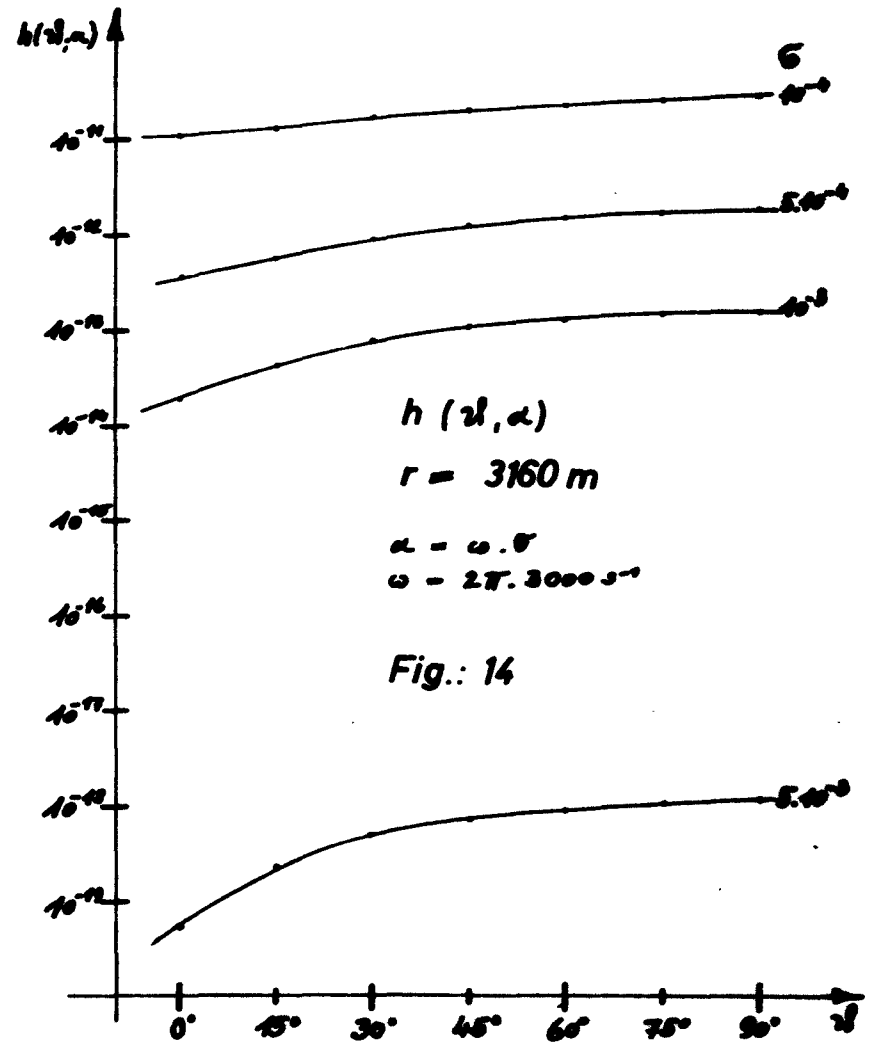
h(ϑ,α)
σ
10⁻⁴
5.10⁻⁴
10⁻³
10⁻¹¹
10⁻¹²
10⁻¹³
10⁻¹⁴
10⁻¹⁵
10⁻¹⁶
10⁻¹⁷
10⁻¹⁸
10⁻¹⁹
5.10⁻³
h (ϑ, α)
r = 3160 m
α = ω.σ
ω = 2π.3000 s⁻¹
0°
15°
30°
45°
60°
75°
90°
ϑ

Fig.: 14

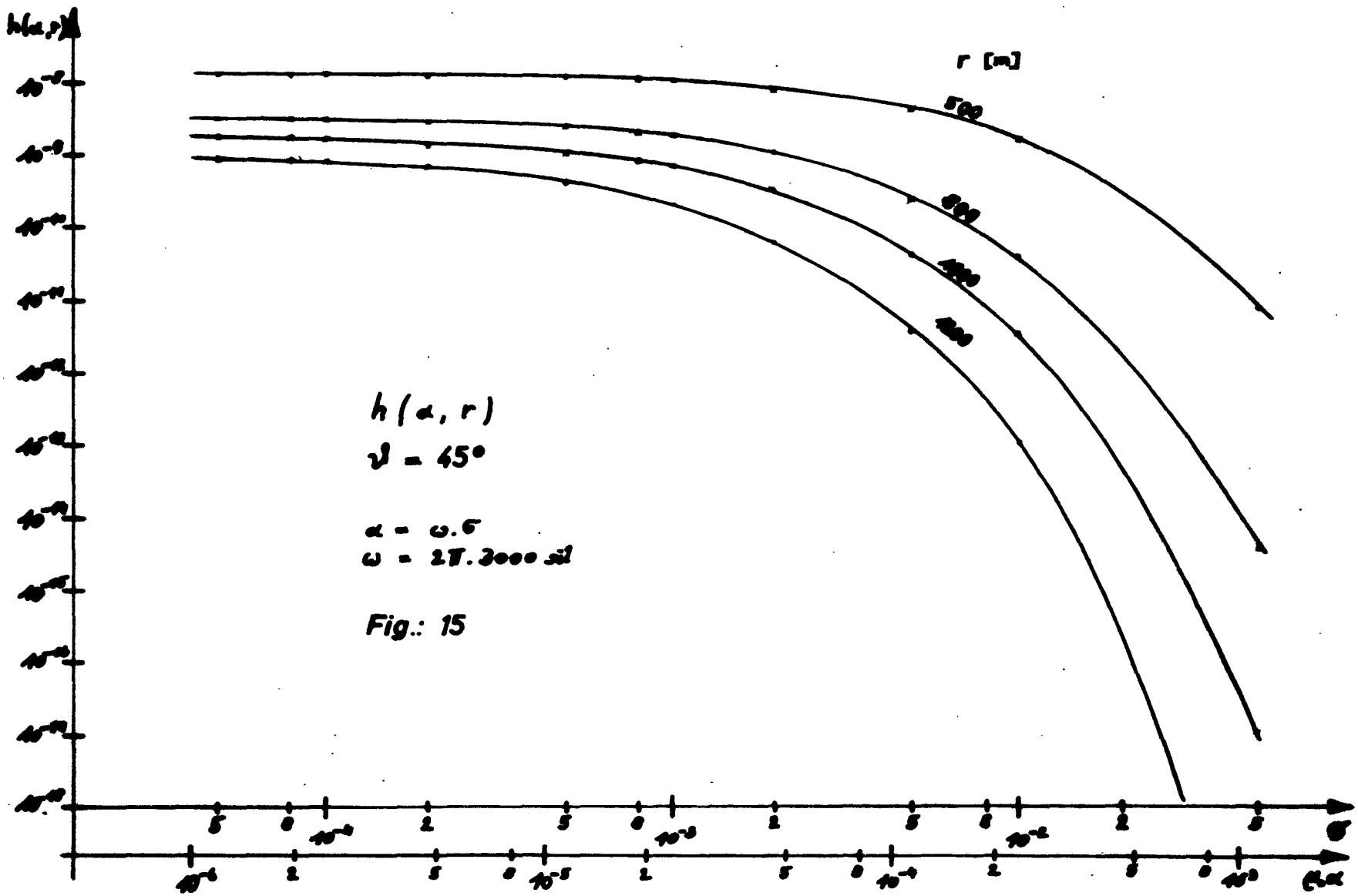

Fig.: 15

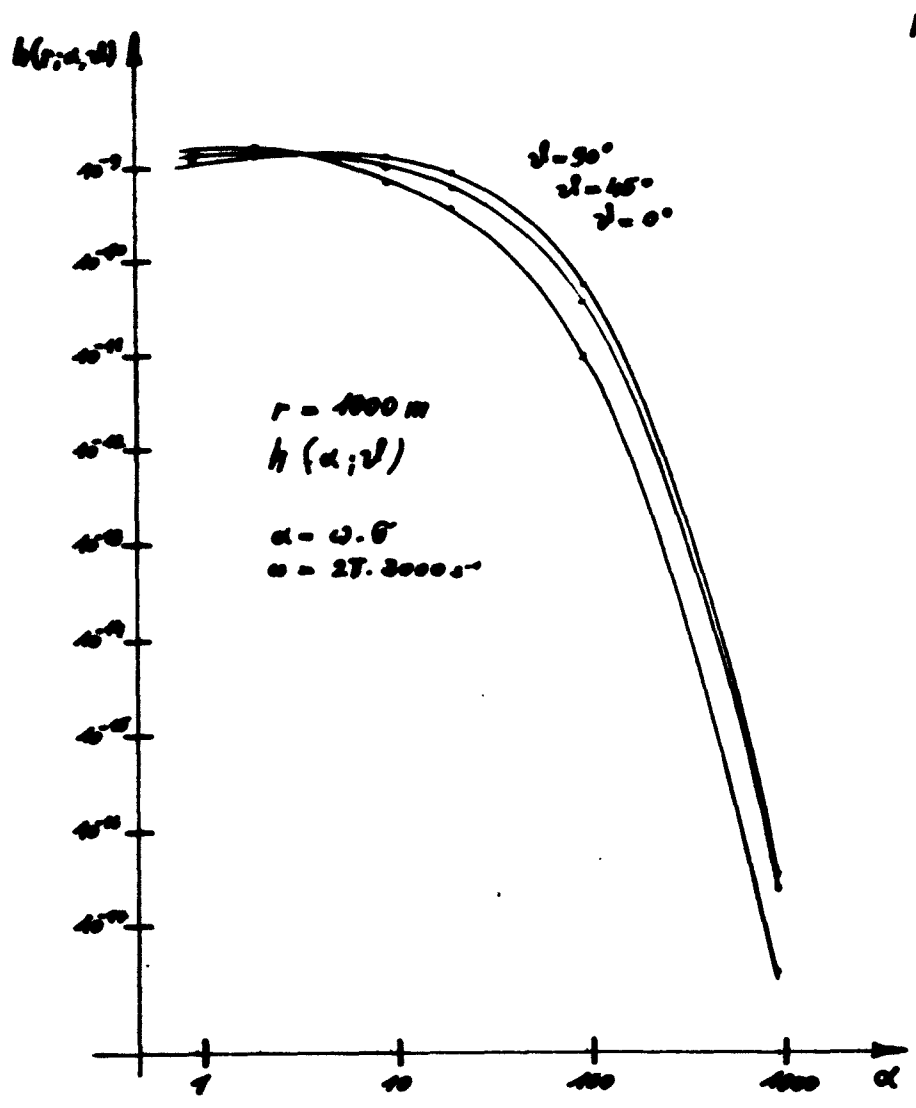
h(r;α,ϑ)
ϑ = 90°
ϑ = 45°
ϑ = 0°
r = 1000 m
h (α;ϑ)
α = ω.θ
ω = 2π.3000 s⁻¹
1
10
100
1000
α

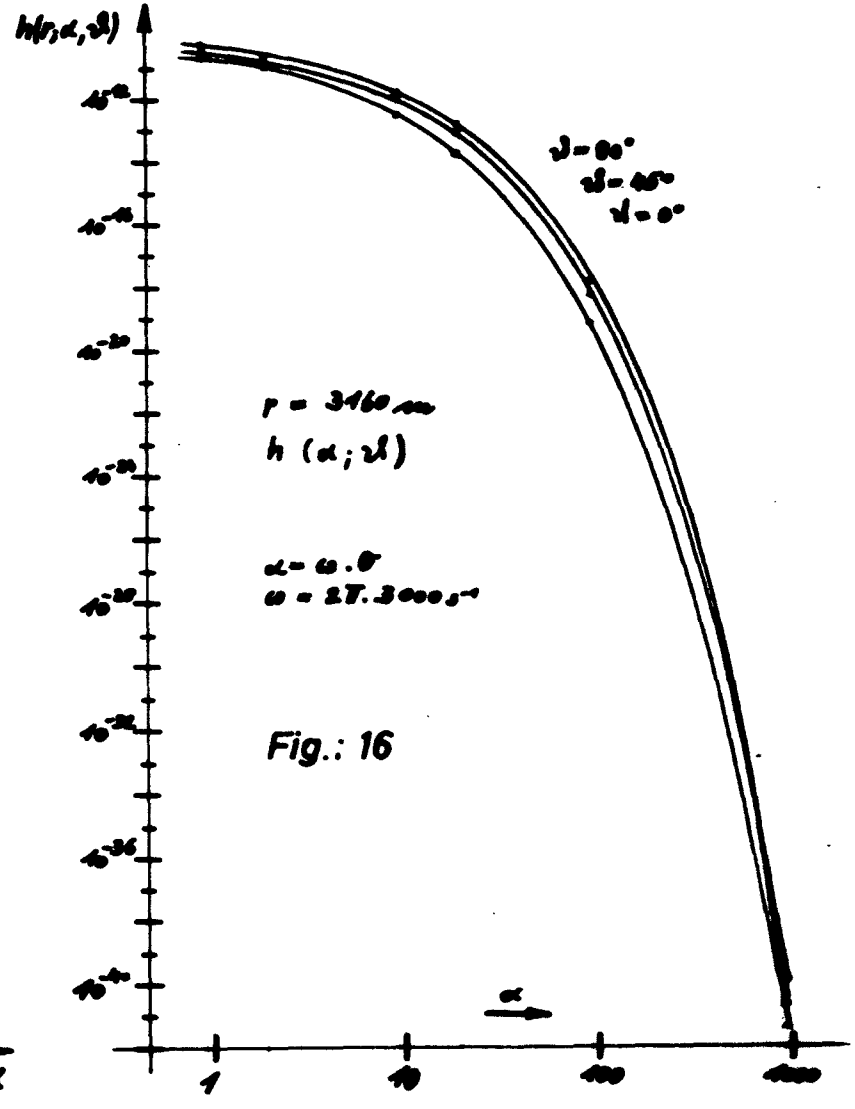
h(r;α,ϑ)
ϑ = 90°
ϑ = 45°
ϑ = 0°
r = 3160 m
h (α;ϑ)
α = ω.θ
ω = 2π.3000 s⁻¹
α
1
10
100
1000

Fig.: 16

Tab. 1 $h(r,\varphi)$ $\sigma = 10^{-4}$

r[m] / φ	0°	45°	90°
10	$2{,}00\cdot10^{-5}$	$1{,}58\cdot10^{-5}$	$9{,}98\cdot10^{-4}$
31,6	$6{,}33\cdot10^{-5}$	$5{,}01\cdot10^{-5}$	$3{,}17\cdot10^{-5}$
100	$2{,}00\cdot10^{-6}$	$1{,}58\cdot10^{-6}$	$1{,}00\cdot10^{-6}$
316	$6{,}24\cdot10^{-8}$	$5{,}00\cdot10^{-8}$	$3{,}29\cdot10^{-8}$
500	$1{,}52\cdot10^{-8}$	$1{,}25\cdot10^{-8}$	$8{,}92\cdot10^{-9}$
600	$8{,}59\cdot10^{-9}$	$7{,}18\cdot10^{-8}$	$5{,}41\cdot10^{-9}$
700	$5{,}24\cdot10^{-9}$	$4{,}52\cdot10^{-9}$	$3{,}65\cdot10^{-9}$
800	$3{,}39\cdot10^{-9}$	$2{,}98\cdot10^{-9}$	$2{,}49\cdot10^{-9}$
900	$2{,}29\cdot10^{-9}$	$2{,}05\cdot10^{-9}$	$1{,}82\cdot10^{-9}$
1000	$1{,}60\cdot10^{-9}$	$1{,}48\cdot10^{-9}$	$1{,}37\cdot10^{-9}$
1100	$1{,}14\cdot10^{-9}$	$1{,}09\cdot10^{-9}$	$1{,}05\cdot10^{-9}$
1200	$8{,}42\cdot10^{-10}$	$8{,}28\cdot10^{-10}$	$8{,}25\cdot10^{-10}$
1250	$7{,}23\cdot10^{-10}$	$7{,}24\cdot10^{-10}$	$7{,}40\cdot10^{-10}$
1300	$6{,}26\cdot10^{-10}$	$6{,}38\cdot10^{-10}$	$6{,}64\cdot10^{-10}$
3160	$1{,}14\cdot10^{-11}$	$2{,}14\cdot10^{-11}$	$2{,}8\cdot10^{-11}$

Tab. 2 $h(r,\varphi)$ $\sigma = 10^{-3}$

0°	45°	90°
$2{,}00\cdot10^{-5}$	$1{,}58\cdot10^{-5}$	$1{,}0\cdot10^{-3}$
$6{,}34\cdot10^{-5}$	$5{,}01\cdot10^{-5}$	$3{,}17\cdot10^{-5}$
$2{,}00\cdot10^{-6}$	$1{,}57\cdot10^{-6}$	$1{,}04\cdot10^{-6}$
$5{,}03\cdot10^{-8}$	$4{,}69\cdot10^{-8}$	$4{,}31\cdot10^{-8}$
$9{,}22\cdot10^{-9}$	$1{,}03\cdot10^{-8}$	$1{,}16\cdot10^{-8}$
$4{,}36\cdot10^{-9}$	$5{,}50\cdot10^{-9}$	$6{,}50\cdot10^{-9}$
$2{,}19\cdot10^{-9}$	$3{,}26\cdot10^{-9}$	$4{,}07\cdot10^{-9}$
$1{,}16\cdot10^{-9}$	$1{,}81\cdot10^{-9}$	$2{,}28\cdot10^{-9}$
$6{,}36\cdot10^{-10}$	$1{,}08\cdot10^{-9}$	$1{,}40\cdot10^{-9}$
$3{,}60\cdot10^{-10}$	$6{,}79\cdot10^{-10}$	$8{,}81\cdot10^{-10}$
$2{,}09\cdot10^{-10}$	$4{,}22\cdot10^{-10}$	$5{,}60\cdot10^{-10}$
$1{,}23\cdot10^{-10}$	$2{,}68\cdot10^{-10}$	$3{,}59\cdot10^{-10}$
$9{,}50\cdot10^{-10}$	$2{,}14\cdot10^{-10}$	$2{,}90\cdot10^{-10}$
$7{,}39\cdot10^{-11}$	$1{,}73\cdot10^{-10}$	$2{,}34\cdot10^{-10}$
$1{,}94\cdot10^{-14}$	$1{,}06\cdot10^{-13}$	$1{,}50\cdot10^{-13}$

r[m] / φ	15°	30°	60°	75°
800	$3{,}12\cdot10^{-9}$	$2{,}99\cdot10^{-9}$	$2{,}61\cdot10^{-9}$	$2{,}46\cdot10^{-9}$
1000	$1{,}57\cdot10^{-9}$	$1{,}53\cdot10^{-9}$	$1{,}42\cdot10^{-9}$	$1{,}38\cdot10^{-9}$
1200	$8{,}30\cdot10^{-10}$	$8{,}29\cdot10^{-10}$	$8{,}27\cdot10^{-10}$	$8{,}26\cdot10^{-10}$

15°	30°	60°	75°
$1{,}26\cdot10^{-9}$	$1{,}51\cdot10^{-9}$	$2{,}00\cdot10^{-9}$	$2{,}21\cdot10^{-9}$
$2{,}98\cdot10^{-10}$	$4{,}66\cdot10^{-10}$	$7{,}54\cdot10^{-10}$	$8{,}35\cdot10^{-10}$
$1{,}49\cdot10^{-10}$	$2{,}25\cdot10^{-10}$	$2{,}79\cdot10^{-10}$	$3{,}38\cdot10^{-10}$

Tab. 4 $h(\alpha,\varphi)$ $r = 1000$ m

σ / φ	0°	15°	30°	45°	60°	75°	90°
$5\cdot10^{-5}$	$1{,}61\cdot10^{-9}$			$1{,}53\cdot10^{-9}$			$1{,}10\cdot10^{-9}$
10^{-4}	$1{,}58\cdot10^{-9}$	$1{,}57\cdot10^{-9}$	$1{,}53\cdot10^{-9}$	$1{,}48\cdot10^{-9}$	$1{,}42\cdot10^{-9}$	$1{,}38\cdot10^{-9}$	$1{,}36\cdot10^{-9}$
$5\cdot10^{-4}$	$7{,}38\cdot10^{-10}$	$7{,}58\cdot10^{-10}$	$9{,}025\cdot10^{-10}$	$1{,}05\cdot10^{-9}$	$1{,}17\cdot10^{-9}$	$1{,}25\cdot10^{-9}$	$1{,}29\cdot10^{-9}$
10^{-3}	$3{,}60\cdot10^{-10}$	$4{,}15\cdot10^{-10}$	$5{,}42\cdot10^{-10}$	$6{,}73\cdot10^{-10}$	$7{,}82\cdot10^{-10}$	$8{,}52\cdot10^{-10}$	$8{,}80\cdot10^{-10}$
$5\cdot10^{-3}$	$1{,}07\cdot10^{-11}$	$1{,}80\cdot10^{-11}$	$3{,}02\cdot10^{-11}$	$4{,}18\cdot10^{-11}$	$5{,}00\cdot10^{-11}$	$5{,}55\cdot10^{-11}$	$5{,}82\cdot10^{-11}$
$5\cdot10^{-2}$	$2{,}89\cdot10^{-18}$			$2{,}49\cdot10^{-17}$			$3{,}40\cdot10^{-17}$

Tab. 5 $h(\alpha,\varphi)$ $r = 3160$ r

σ / φ	0°	15°	30°	45°	60°	75°	90°
$5\cdot10^{-5}$	$2{,}66\cdot10^{-11}$			$3{,}35\cdot10^{-11}$			$4{,}11\cdot10^{-11}$
10^{-4}	$1{,}15\cdot10^{-11}$	$1{,}28\cdot10^{-11}$	$1{,}71\cdot10^{-11}$	$2{,}11\cdot10^{-11}$	$2{,}49\cdot10^{-11}$	$2{,}72\cdot10^{-11}$	$2{,}74\cdot10^{-11}$
$5\cdot10^{-4}$	$3{,}48\cdot10^{-13}$	$5{,}74\cdot10^{-13}$	$9{,}60\cdot10^{-13}$	$1{,}32\cdot10^{-12}$	$1{,}60\cdot10^{-12}$	$1{,}77\cdot10^{-12}$	$1{,}90\cdot10^{-12}$
10^{-3}	$1{,}94\cdot10^{-14}$	$4{,}26\cdot10^{-14}$	$7{,}62\cdot10^{-14}$	$1{,}06\cdot10^{-13}$	$1{,}28\cdot10^{-13}$	$1{,}45\cdot10^{-13}$	$1{,}49\cdot10^{-13}$
$5\cdot10^{-3}$	$6{,}55\cdot10^{-20}$	$2{,}39\cdot10^{-19}$	$5{,}25\cdot10^{-19}$	$7{,}98\cdot10^{-19}$	$9{,}11\cdot10^{-19}$	$1{,}02\cdot10^{-18}$	$1{,}13\cdot10^{-18}$
$5\cdot10^{-2}$	$5{,}27\cdot10^{-42}$			$1{,}50\cdot10^{-40}$			$2{,}12\cdot10^{-41}$

Table 6

for $\nu = 3$kops

σ	k_1	k_2	k_3	$\alpha = \omega\sigma$
10^{-6}	$2.26224 \cdot 10^{-4}$	$0.49644 \cdot 10^{-4}$	$1.0858 \cdot 10^{-4}$	0.0189
10^{-5}	$3.81753 \cdot 10^{-4}$	$3.09487 \cdot 10^{-4}$	$3.44 \cdot 10^{-4}$	0.189
$5 \cdot 10^{-5}$	$7.83929 \cdot 10^{-4}$	$7.52509 \cdot 10^{-4}$	$7.695 \cdot 10^{-4}$	0.942
10^{-4}	$1.098 \cdot 10^{-3}$	$1.075 \cdot 10^{-3}$	$1.0858 \cdot 10^{-3}$	1.89
$5 \cdot 10^{-4}$	$2.435 \cdot 10^{-3}$	$2.419 \cdot 10^{-3}$	$2.43 \cdot 10^{-3}$	9.42
10^{-3}	$3.441 \cdot 10^{-3}$	$3.434 \cdot 10^{-3}$	$3.44 \cdot 10^{-3}$	18.85
$5 \cdot 10^{-3}$	$7.682 \cdot 10^{-3}$	$7.682 \cdot 10^{-3}$	$7.69 \cdot 10^{-3}$	94.2
$5 \cdot 10^{-2}$	$2.430 \cdot 10^{-2}$	$2.430 \cdot 10^{-2}$	$2.43 \cdot 10^{-2}$	$9.42 \cdot 10^{2}$

It is easy to see (cf. p.11) that the displacement current at a frequency of 3000 cps can be neglected only for conductivities greater than 10^{-4}.

Further calculation gives

Table 7

10^5 cps, $\varepsilon = 11.5$		
$\sigma = 10^{-3}$	$k_1 = 7.1263 \cdot 10^{-3}$	$k_2 = 5.5455 \cdot 10^{-4}$
$\sigma = 10^{-4}$	$k_1 = 8.4934 \cdot 10^{-3}$	$k_2 = 4.6482 \cdot 10^{-3}$
$\sigma = 10^{-3}$	$k_1 = 2.0510 \cdot 10^{-2}$	$k_2 = 1.9240 \cdot 10^{-2}$
10^4 cps, $\varepsilon = 12.5$		
$\sigma = 10^{-3}$	$k_1 = 8.6546 \cdot 10^{-4}$	$k_2 = 4.5681 \cdot 10^{-4}$
$\sigma = 10^{-4}$	$k_1 = 2.0556 \cdot 10^{-3}$	$k_2 = 1.9197 \cdot 10^{-3}$
$\sigma = 10^{-3}$	$k_1 = 6.3037 \cdot 10^{-3}$	$k_2 = 6.2607 \cdot 10^{-3}$
10^2 cps, $\varepsilon = 14.5$		
$\sigma = 10^{-5}$	$k_1 = 6.3071 \cdot 10^{-5}$	$k_2 = 6.1140 \cdot 10^{-5}$
$\sigma = 10^{-4}$	$k_1 = 1.9874 \cdot 10^{-4}$	$k_2 = 1.9858 \cdot 10^{-4}$
$\sigma = 10^{-3}$	$k_1 = 6.2824 \cdot 10^{-4}$	$k_2 = 6.2819 \cdot 10^{-4}$

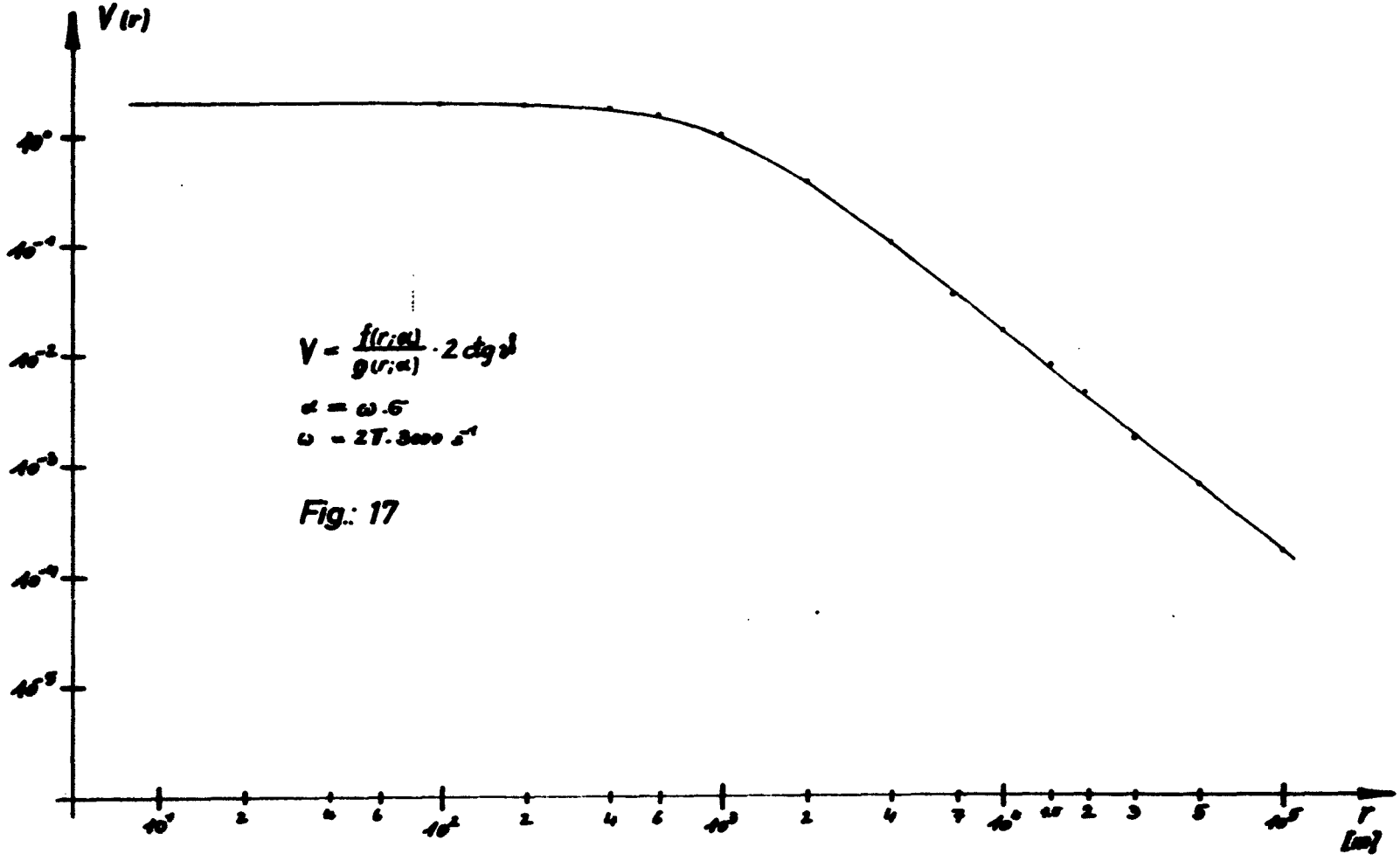
V (r)
$V = \frac{f(r;\alpha)}{g(r;\alpha)} \cdot 2\,\mathrm{ctg}\,\vartheta$
$\alpha = \omega \cdot \delta$
$\omega = 27.3000\ s^{-1}$
r [m]

Fig.: 17

Tab. 3 $h(\alpha;r)$ $= 45^{\circ}$

r [m] \ σ	$5\cdot10^{-5}$	$8\cdot10^{-5}$	10^{-4}	$2\cdot10^{-4}$	$5\cdot10^{-4}$	$8\cdot10^{-4}$	$\cdot10^{-3}$	$2\cdot10^{-3}$	$5\cdot10^{-3}$	10^{-2}	$5\cdot10^{-2}$
10	$1,58\cdot10^{-3}$		$1,58\cdot10^{-3}$		$1,58\cdot10^{-3}$		$1,58\cdot10^{-3}$		$1,58\cdot10^{-3}$		
31,6	$5,01\cdot10^{-5}$		$5,01\cdot10^{-5}$		$5,01\cdot10^{-5}$		$5,01\cdot10^{-5}$		$4,99\cdot10^{-5}$		
100	$1,58\cdot10^{-6}$		$1,58\cdot10^{-6}$		$1,58\cdot10^{-6}$		$1,57\cdot10^{-6}$		$1,53\cdot10^{-6}$		
316	$5,00\cdot10^{-8}$		$4,98\cdot10^{-8}$		$4,90\cdot10^{-8}$		$4,69\cdot10^{-8}$		$3,33\cdot10^{-8}$		
500	$1,27\cdot10^{-8}$	$1,25\cdot10^{-8}$	$1,25\cdot10^{-8}$	$1,22\cdot10^{-8}$	$1,16\cdot10^{-8}$	$1,09\cdot10^{-8}$	$1,03\cdot10^{-8}$	$8,15\cdot10^{-9}$	$4,34\cdot10^{-9}$	$1,60\cdot10^{-9}$	$7,91\cdot10^{-12}$
600	$7,21\cdot10^{-9}$		$7,16\cdot10^{-9}$		$6,43\cdot10^{-9}$		$5,50\cdot10^{-9}$		$1,61\cdot10^{-9}$		
700	$4,52\cdot10^{-9}$		$4,48\cdot10^{-9}$		$3,84\cdot10^{-9}$		$3,26\cdot10^{-9}$		$6,23\cdot10^{-10}$		
800	$3,03\cdot10^{-9}$	$2,99\cdot10^{-9}$	$2,96\cdot10^{-9}$	$2,82\cdot10^{-9}$	$2,31\cdot10^{-9}$	$2,13\cdot10^{-9}$	$1,81\cdot10^{-9}$		$2,48\cdot10^{-10}$	$3,79\cdot10^{-11}$	$3,62\cdot10^{-15}$
900	$2,12\cdot10^{-9}$		$2,05\cdot10^{-9}$		$1,57\cdot10^{-9}$		$1,08\cdot10^{-9}$		$1,01\cdot10^{-10}$		
1000	$1,53\cdot10^{-9}$	$1,50\cdot10^{-9}$	$1,48\cdot10^{-9}$	$1,34\cdot10^{-9}$	$1,05\cdot10^{-9}$	$8,04\cdot10^{-10}$	$6,79\cdot10^{-10}$	$2,98\cdot10^{-10}$	$4,14\cdot10^{-11}$	$3,32\cdot10^{-12}$	$1,06\cdot10^{-17}$
1100	$1,14\cdot10^{-9}$		$1,09\cdot10^{-9}$		$7,15\cdot10^{-10}$		$4,22\cdot10^{-10}$		$1,73\cdot10^{-11}$		
1200	$8,72\cdot10^{-10}$	$8,40\cdot10^{-10}$	$8,28\cdot10^{-10}$	$6,78\cdot10^{-10}$	$4,95\cdot10^{-10}$	$3,39\cdot10^{-10}$	$2,68\cdot10^{-10}$	$9,10\cdot10^{-11}$	$7,29\cdot10^{-12}$	$3,12\cdot10^{-13}$	$1,33\cdot10^{-19}$
1250	$7,69\cdot10^{-10}$		$7,24\cdot10^{-10}$		$4,15\cdot10^{-10}$		$2,14\cdot10^{-10}$		$4,75\cdot10^{-12}$		
1300	$6,81\cdot10^{-10}$		$6,38\cdot10^{-10}$		$3,51\cdot10^{-10}$		$1,73\cdot10^{-10}$		$3,10\cdot10^{-12}$		
3160	$3,33\cdot10^{-11}$		$2,14\cdot10^{-11}$		$1,32\cdot10^{-12}$		$1,06\cdot10^{-13}$		$7,47\cdot10^{-19}$		

This shows that the quantities determinant for the propagation are highly dependent on the frequency.

Neglecting the displacement current we now calculate the ratio $\frac{|H_r|}{|H_\vartheta|}$ as this is independent of the constant A involved in the measurement. Considering the angular dependence we find from (48) and (49) with (42) the expression

$$(53)\quad \frac{|H_r|}{|H_\vartheta|} = 2\cot\vartheta \frac{\left\{\frac{1}{r^6} + \frac{2k_3}{r^5} + \frac{2k_3^2}{r^4}\right\}^{1/2}}{\left\{\frac{1}{r^6} + \frac{2k_3}{r^5} + \frac{2k_3^2}{r^4} + \frac{4k_3^3}{r^3} + \frac{4k_3^4}{r^2}\right\}^{1/2}} = V(r)$$

Fig. 17 was plotted with $\vartheta = 45^\circ$, $k_3 = 7.695 \cdot 10^{-4}$, i.e. $\sigma = 5 \cdot 10^{-5}$, $\nu = 3$ kcps. We can see that at distances of about 1 km we are by far not in the wave field. The inequality $|H_\vartheta| > |H_r|$ does not yet indicate the wave field; only $|H_\vartheta| \gg |H_r|$ does. The distance r_f from which on $|H_\vartheta|$ is greater than $|H_r|$ can be computed from the condition $f(r_f,\alpha) = g(r_f,\alpha)$. A preliminary estimate of the equation for r_f gives

$$(54)\qquad r_f = \frac{1670}{\sqrt{\omega\sigma}} \qquad [m]$$

which, however, we do not claim to be correct.

On the other hand we can, keeping r fixed, search for an optimum $\omega\sigma$-product at which $|H_\vartheta|$ has a maximum. From $\partial H_\vartheta / \partial(\omega\mu_0\sigma) = 0$ we find the rough estimate

$$(55)\qquad \omega\sigma = \frac{(2140)^2}{r^2}$$

Also these considerations are intended to be continued on a larger scale next year.

§ 4. The magnetic quadrupole

The field of a magnetic dipole was dealt with in §2. The intensity of this field tends to infinity with $r \to 0$, which corresponds to the ideal representation of a circular coil by a dipole. The formulas given are therefore not valid for small values of r. To estimate up to what distances the dipole formulas are applicable one can calculate either the magnetic field of an a.c. circular coil or the quadrupole term 1 = 2.

For the vector potential of a suitably arranged circular coil there is only a φ-component

$$A_\varphi = \frac{1}{4\pi} \int_0^{2\pi} \frac{I a \cos\bar{\varphi} d\bar{\varphi}}{R} e^{-ik^*R} \qquad \Delta\varphi = \bar{\varphi}, \text{ where}$$

$$R^2 = r^2 + a^2 - 2ar \cos\bar{\varphi}\sin\vartheta$$

This corresponds to the Biot-Savart formula extended to non-static processes.

H_r can be calculated from $H_r = \text{curl}_r A_\varphi =$

$$H_r = -\frac{1}{r \sin\vartheta} \frac{\partial}{\partial\vartheta} (A_\varphi \sin\vartheta) = -\frac{1}{r} \frac{\partial A_\varphi}{\partial\vartheta} - \frac{1}{r} \frac{A_\varphi}{\tan\vartheta}$$

The field on the axis is obtained by taking ϑ equal to zero. In this case, A_φ and $\tan\vartheta$ vanish simultaneously. Passing to the limit one gets

$$H_r = -\frac{2}{r} \frac{\partial A_\varphi}{\partial\vartheta} = -\frac{2}{r} \frac{Ia}{4\pi} \int_0^{2\pi} \frac{\partial}{\partial\vartheta} \frac{e^{-ik^*R}}{R} \cos\bar{\varphi} d\bar{\varphi} =$$

$$= -\frac{Ia}{2r} \int_0^{2\pi} \left(\frac{ar}{R^3} + \frac{ik^*ar}{R^2}\right) e^{-ik^*R} \cos^2\bar{\varphi} d\bar{\varphi}$$

$$H_r = -\frac{Ia^2}{2}\left(\frac{1}{R^3} + \frac{ik^*}{R^2}\right) e^{-ik^*R} \text{ with } R^2 = a^2 + r^2 \text{ and } \vartheta = 0$$

In unfavorable cases of large k*-values, the deviation of the dipole formula from the above exact formula for a radius of a = 1 m is less than 10% for r = 3 m and less than 2% for r = 10 m. It can therefore be neglected.

Eqs. (11), (12), (15) (with m = 0, l = 2) lead to the quadrupole term

$$(56) \qquad H_r(r,\vartheta) = 6a_o\left(\frac{3}{2}\cos^2\vartheta - \frac{1}{2}\right) e^{-ik^*r}\left\{-\frac{k^{*2}}{r^2} + \frac{3ik^*}{r^3} + \frac{3}{r^4}\right\}$$

$$(57) \qquad H_\vartheta = a_o\frac{3}{2}\sin 2\vartheta\, e^{-ik^*r}\left\{-\frac{ik^{*3}}{r} - \frac{3k^{*2}}{r^2} + \frac{6ik^*}{r^3} + \frac{6}{r^4}\right\}$$

The absolute value, considering $k^* = k_1 - ik_2$, is

$$(58) \qquad |H_r|^2 = 36a_o^2\left(\frac{3}{2}\cos^2\vartheta - \frac{1}{2}\right)^2 e^{-2k_2r} \cdot \left\{\frac{k_1^4 + k_2^4 + 2k_1^2k_2^2}{r^4} + \right.$$
$$\left. + \frac{6k_2(k_1^2 + k_2^2)}{r^5} + \frac{3k_1^2 + 14k_2^2}{r^6} + \frac{18k_2}{r^7} + \frac{9}{r^8}\right\}$$

$$(59) \qquad |H_\vartheta|^2 = a_o^2 \cdot \frac{9}{4}\sin^2 2\vartheta\, e^{-2k_2r} \cdot \left\{\frac{k_1^6 + 3k_1^4k_2^2 + 3k_1^2k_2^4 + k_2^6}{r^2} + \right.$$
$$+ \frac{6k_1^4k_2 + 12k_1^2k_2^3 + 6k_2^5}{r^3} + \frac{-3k_1^4 + 18k_1^2k_2^2 + 21k_2^4}{r^4} +$$
$$\left. + \frac{72k_1^2k_2 + 24k_2^3}{r^5} + \frac{72k_1^2}{r^6} + \frac{-72k_2}{r^7} + \frac{36}{r^8}\right\}$$

The effect of these terms on the magnitude of the total field $|\vec{H}|$ will be thoroughly investigated in the near future.

§5. The effect of the cavity

This section is devoted to a short examination of the effect of the cavity, in which the magnetic coil is usually placed for measurements in the conducting medium, on the accuracy of measurement. The electrical and magnetic variable fields produced by the magnetic coil in the cavity which is assumed to be spherical with the radius $r = r_0$ give rise to displacement and conduction currents in the outer medium according to the conductivity of the latter. These currents induce secondary fields in the cavity and influence the effective dipole moment. The primary vector potential a_{1p} is therefore superimposed by a secondary potential a_{1s} which must not have any singularities in the cavity as is required by the physical circumstances.

Therefore, to describe the fields in the cavity, one has to consult the complete solution of the equation $k^{*2} a_1 + \Delta a_1 = 0$.

$$a_{1I} = \text{const.} \sqrt{\frac{\pi}{2k_I^* r}}\, H^{(2)}_{1/2}(k_I^* r) + \text{const.} \sqrt{\frac{\pi}{2k_I^* r}}\, I_{1/2}(k_I^* r)$$

where k_I^* is the wave number of the medium in the cavity ($\sim$ vacuum).

The secondary fields are represented by the half-integer Bessel functions which are regular at zero. If the magnetic dipole is aligned in the direction of the z-axis then we have symmetry with regard to the spherical coordinate φ. In this case, the two components of a_{1I} which are necessary for a complete description of the fields are, after the sines and cosines have been inserted, as follows:

$$\alpha_{1I_r} = \left(A_1 \frac{e^{-ik_I^* r}}{r} + B \frac{\sin k_I^* r}{k_I^* r}\right) \cos\vartheta$$

$$\alpha_{1I_\varphi} = -\left(A_1 \frac{e^{-ik_I^* r}}{r} + B \frac{\sin k_I^* r}{k_I^* r}\right) \sin\vartheta$$

As before, the vector potential α_{1II} follows the Hankel funotion

$$\alpha_{1II_r} = C \cdot \frac{e^{-ik_{II}^* r}}{r} \cos\vartheta$$

$$\alpha_{1II} = C \cdot \frac{e^{-ik_{II}^* r}}{r} \sin\vartheta$$

where k_{II} is the wave number of the conducting medium. The two constants B and C are determined by the condition that E_φ and H_ϑ be continuous:

E_φ: $\quad \text{curl}\, \alpha_{1I}|_{r=r_o} = \text{curl}\, \alpha_{1II}|_{r=r_o}$

H_ϑ: $\quad \left(r \frac{\partial}{\partial r} + 1\right) \text{curl}\, \alpha_{1II}|_{r=r_o} = \left(r \frac{\partial}{\partial r} + 1\right) \text{curl}\, \alpha_{1II}|_{r=r_o}$

The last equation follows from the Maxwell equation $\text{curl}\, \xi = -\mu\mu_o i\omega \mathfrak{H}$. Substitution leads to

$$B = \frac{1}{E}\left(C(1/r_o + ik_{II}^*) e^{-ik_{II}^* r_o} - A_1 (1/r_o + ik_I^*) e^{-ik_I^* r_o}\right)$$

with $E = \dfrac{\sin k_I^* r_o}{k_I^* r_o} - \cos k_I^* r_o$

Thus

$$A_1 e^{-ik_I^* r_o} \left(k_I^{*2} r_o^2 - ik_I^* r_o - 1 - (1 + ik_I^* r_o) \frac{r}{E} \frac{\partial E}{\partial r}\Big|_{r=r_o}\right) =$$

$$= C e^{-ik_{II}^* r_o} \left(k_{II}^{*2} r_o^2 - ik_{II}^* r_o - 1 - (1 + ik_{II}^* r_o) \frac{r}{E} \frac{\partial E}{\partial r}\Big|_{r=r_o}\right)$$

In the range of frequencies considered ($\nu < 15$ kcps), $k_I^* = \omega\sqrt{\varepsilon_o \mu_o} < 10^{-4}$. Consequently, $k_I^* r_o$ for $r_o < 3$ m is less than $3 \cdot 10^{-4} \ll 1$.

For $\frac{r}{E}\frac{\partial E}{\partial r}\Big|_{r=r_o}$, the limit

$$\lim_{r_o \to 0} \frac{r}{E}\frac{\partial E}{\partial r}\Big|_{r=r_o} = -1 + k_I^* r_o \sin k_I^* r_o / (\sin k_I^* r_o / k_I^* r_o - \cos k_I^* r_o)_{r_o \to 0} = 2$$

is therefore a good approximation. Thus ($k_I \ll 1$)

$$C = A_1 \frac{3}{3 + 3ik_I^* r_o - k_{II}^{*2} r_o^2} e^{ik_{II}^* r_o}$$

For $r_o = 3$ meters, and for medium conductivities and frequencies, C is by less than 1% greater than A. This means that the virtual increment in antenna current caused by the cavity can be neglected in regard of the formula (8) for a homogeneous conductive medium.

§6. The transformer and other plans for further theoretical work

As the displacement current can be neglected already in the present measurements, the transmitter and receiver aerials can be regarded as an open transformer. This is even more justified at still lower frequencies (< 3 kcps). However, the lack of time made it impossible to perform more exact calculations in this respect and to compare them with the results obtained so far. The calculations made until now were based only on the Hertzian dipole. The electrical dipole has not been considered

at all. The following considerations were decisive:

(a) As was shown in the first final report, a greater emissive power at a given power and VLF-waves can be reached with a magnetic antenna.

(b) The losses in a conducting medium are lower when magnetic fields (instead of electric fields) occur in the r and ϑ directions.

The <u>following plans</u> are made for further <u>theoretical work</u>:

(1) transformer concept

(2) evaluation of the formulas with k_1, k_2 (displacement current not neglected)

(3) study of the Ohmian losses as depending on the kind of excitation of electromagnetic fields in a conducting medium (b)

(4) further studies on magnetic antennas (a)

(5) consideration of terms of higher order in the expansion (cf. $\S_8$)

(6) problems of wave propagation in inhomogeneous media

(7) surface waves (modes)

(8) continuation of the considerations of the end of §3.

§ 7 Plane Boundary Layer Waves

We study the well known problem of the propagation of plane waves along the interface between two media with different electric properties. We shall take the interface to divide the earth and the air space and place the x-y plane of a Cartesian coordinate system in this interface, the positive z-axis pointing upwards. The waves are considered to propagate along the x-axis. Maxwell's equations read as follows:

$$\text{curl } \vec{H} = \varepsilon\varepsilon_0 \frac{\partial \vec{E}}{\partial t} + \sigma\vec{E} \tag{60}$$

$$\text{curl } \vec{E} = -\mu\mu_0 \frac{\partial \vec{H}}{\partial t} \tag{61}$$

From the foregoing, we assume $\vec{H}$ to have the form

$$\vec{H} = H_y = f(z)e^{i\omega(t - \frac{x}{v})} \tag{62}$$

Substitution in Maxwell's equations leads us to put

$$\begin{aligned} E_x &= g(z)e^{i\omega(t - \frac{x}{v})} \\ E_z &= h(z)e^{i\omega(t - \frac{x}{v})} \end{aligned} \tag{63}$$

Inserting this into Maxwell's equations, we obtain

$$-\frac{dt}{dz} e^{i\omega(t - \frac{x}{v})} = \varepsilon\varepsilon_0 g(z) i\omega e^{i\omega(t - \frac{x}{v})} + \sigma g(z) e^{i\omega(t - \frac{x}{v})}$$

$$-\frac{i\omega}{v} f(z) e^{i\omega(t - \frac{x}{v})} = \varepsilon\varepsilon_0 h(z) i\omega e^{i\omega(t - \frac{x}{v})} + \sigma h(z) e^{i\omega(t - \frac{x}{v})}$$

After cancelling $e^{i\omega(t - \frac{x}{v})}$, there remains

$$g = \frac{-\frac{dt}{dz}}{\varepsilon\varepsilon_0 i\omega + \sigma} \tag{64}$$

$$h = \frac{-\frac{i\omega}{v} f}{\varepsilon\varepsilon_0 i\omega + \sigma} \tag{65}$$

Using (60, 61), we arrive at an equation containing g, f, and h. Substituting (64) and (65) into this equation, we obtain

$$\left[(\varepsilon\varepsilon_0 i\omega + \sigma)\mu\mu_0 i\omega + \frac{\omega^2}{v^2}\right] f = \frac{d^2 f}{dz^2} \tag{66}$$

We now make use of the relation

$$\varepsilon_0\mu_0 = \frac{1}{c_0^2} \tag{67}$$

which specifies the velocity of light in empty space.
So we have

$$\left[\omega^2\left(\frac{1}{v^2} - \frac{\varepsilon\mu}{c_0^2}\right) + \frac{i\omega\mu\sigma}{\varepsilon_0 c_0^2}\right] f = \frac{d^2 f}{dz^2} \tag{68}$$

This has the solution

$$\vec{H} = \vec{A}\, e^{\pm \varrho z} \tag{69}$$

where

$$\varrho^2 = \frac{\omega}{v^2} - \frac{\varepsilon\mu}{c_0^2}\omega^2 + \frac{i\omega\mu\sigma}{\varepsilon_0 c_0^2} \tag{70}$$

This solution holds for both the air and the earth space. We are bound to choose the sign of ϱ in such a manner that the amplitude decreases both with growing z (air space) and with negative z ($z < 1$, earth space). Hence ϱ will be negative for the air space and positive for the earth space.

We now distinguish between ϱ for the air and the earth space

by the index $_L$ for the air and the index $_E$ for the earth space, respectively. We shall, however, for the moment ignore the fact that for practical purposes the conductivity of the air is zero. Hence, by a rearrangement of terms, we obtain

$$\varrho_L^2 - \frac{\omega^2}{v^2} = -\frac{\varepsilon_L \mu_L}{c_o^2}\omega^2 + \frac{i\omega\mu_L\sigma_L}{\varepsilon_o c_o^2}$$

$$\varrho_E^2 - \frac{\omega^2}{v^2} = -\frac{\varepsilon_E \mu_E}{c_o^2}\omega^2 + \frac{i\omega\mu_E\sigma_L}{\varepsilon_o c_o^2}$$

$$\frac{\omega^2}{v^2} - \varrho_L^2 = \frac{\varepsilon_L \mu_L}{c_o^2}\omega^2 - \frac{i\omega\mu_L\sigma_L}{\varepsilon_o c_o^2}$$

$$\frac{\omega^2}{v^2} - \varrho_E^2 = \frac{\varepsilon_E \mu_E}{c_o^2}\omega^2 - \frac{i\omega\mu_E\sigma_L}{\varepsilon_o c_o^2}$$

In these two relationships we have made use of the condition that the tangential components of the E- and H-vector (with respect to the X-Y plane) must be continuous on both sides of the interface. As this condition holds independently of time, the phase velocities of both the terrestrial and the air wave must be the same. Hence

$$v_L = v_E$$

Likewise, this boundary condition, when applied to the amplitudes, gives for $z = 0$

$$H_{yL} = H_{yE}$$

$$A_L = A_E.$$

The longitudinal component E_x (with respect to the direction of propagation) is then

$$E_x = g(z)e^{i\omega(t - \frac{x}{v})} = -\frac{\frac{dt}{dz}}{(\varepsilon\varepsilon_o i\omega + \sigma)} e^{i\omega(t - \frac{x}{v})}$$

Calculating $\frac{dt}{dz}$, we find, considering that the sign of the exponent is positive for the earth space

$$\frac{dt}{dz} = +\varrho_E A e^{\varrho_E z}$$

and this for E_{xE}

$$E_{xE} = \frac{-\varrho_E A e^{\varrho_E z}}{\varepsilon\varepsilon_o i\omega + \sigma_E} e^{i\omega(t - \frac{x}{v})}$$

As for $\vec{H}$, the boundary condition for the tangential components gives for $z = 0$

$$\frac{\varrho_L A e^{i\omega(t - \frac{x}{v})}}{\varepsilon_L\varepsilon_o i\omega + \sigma_L} = -\frac{\varrho_E A e^{i\omega(t - \frac{x}{v})}}{\varepsilon_E\varepsilon_o i\omega + \sigma_E}$$

$$\frac{\varrho_L}{\varepsilon_L\varepsilon_o i\omega + \sigma_L} = -\frac{\varrho_E}{\varepsilon_E\varepsilon_o i\omega + \sigma_E}$$

So we obtain

$$\varrho_E = \varrho_L \frac{\varepsilon_E\varepsilon_o i\omega + \sigma_E}{\varepsilon_L\varepsilon_o i\omega + \sigma_L}$$

We are now capable of eliminating ϱ_L and we obtain

$$(71) \qquad \varrho_E = +\sqrt{\frac{b_E - b_L}{q^2 - 1}}$$

The plus sign of the root holds because ϱ must be positive for $z < 0$. Inserting the formula for ϱ_E^2 we obtain

$$(72) \qquad v = +\omega \cdot \sqrt{\frac{q^2 - 1}{b_E q^2 - b_L}}$$

Now we are in a position to calculate the numerical values of the different constants involved. We use the formulas accounting for the fact that $\sigma_L = 0$:

$$b_L = \frac{\varepsilon_L \mu_L}{c_o^2} \omega^2 \tag{73}$$

$$b_E = \frac{\varepsilon_L \mu_E}{c_o^2} \omega^2 - \frac{i\omega \mu_E \sigma_E}{\varepsilon_o c_o^2} \tag{74}$$

$$q^2 = \left(\frac{\varepsilon_L \varepsilon_o i\omega}{\varepsilon_E \varepsilon_o i\omega + \sigma E} \right)^2 \tag{75}$$

We shall use the following numerical values for the parameters:

$\varepsilon_o = 8.86 \cdot 10^{-12}$ $\qquad$ $c_o = 3 \cdot 10^8$ [ms^{-1}]

$\varepsilon_L = 1$ $\qquad$ $\mu_L = 1$

$\varepsilon_E = 10$ $\qquad$ $\mu_E = 1$

$\sigma_E = 5 \cdot 10^{-3}$

and the three angular frequencies

$$\omega_1 = 2\pi \cdot 10^3; \qquad \omega_2 = 2\pi \cdot 10^4; \qquad \omega_3 = 2\pi \cdot 10^5$$

corresppnding to 1, 10, and 100 kc. We shall calculate every parameter for the three frequencies, using one column for each value.

	ω_1	ω_2	ω_3
b_L	$4.4 \cdot 10^{-10}$	$4.4 \cdot 10^{-8}$	$4.4 \cdot 10^{-6}$
b_E	$4.4 \cdot 10^{-9} - i3.94 \cdot 10^{-5}$	$4.4 \cdot 10^{-7} - i3.94 \cdot 10^{-4}$	$4.4 \cdot 10^{-5} - i3.94 \cdot 10^{-3}$
q^2	$-1.23 \cdot 10^{-10} + i2.72 \cdot 10^{-14}$	$-1.23 \cdot 10^{-8} + i2.72 \cdot 10^{-11}$	$-1.23 \cdot 10^{-6} + i2.72 \cdot 10^{-8}$

In calculating the root for v we are forced to neglect the second term under the root sign, because it is smaller by ten orders of magnitude compared to the first one. Hence it is far below the accuracy of a slide rule. Moreover, considering the representation of complex numbers in the complex plane,

it is at once evident that the complex numbers in question deviate from the real axis so little that for practical purposes they can be regarded as real numbers. We must not forget, however, that this approximation is valid only if it is not to be expected that in further mathematical operations the imaginary part will be multiplied by a factor which is large enough to restore approximate equality between the two parts of a complex number. Hence we were not allowed to apply this reasoning to the earlier steps of our development.

Accordingly, we shall calculate v from the approximative formula

$$v = \omega \sqrt{A + iB} \quad , \qquad B \approx 0$$

we obtained

	ω_1	ω_2	ω_3
$v\left[ms^{-1}\right]$	$2.99 \cdot 10^8$	$2.99 \cdot 10^8$	$2.99 \cdot 10^8$

This result, e.g. that the phase velocity within the accuracy of slide rule computations, is equal for all three frequencies, and moreover equal to the velocity of light in empty space, permits to simplify the formula for ϱ_E.

We obtain

$$\varrho_E(\omega_1) = 4.45 \cdot 10^{-3} + i\ 4.44 \cdot 10^{-3}$$

$$\varrho_E(\omega_2) = 1.4 \cdot 10^{-2} + i\ 1.405 \cdot 10^{-2}$$

$$\varrho_E(\omega_3) = 4.43 \cdot 10^{-2} + i\ 4.45 \cdot 10^{-2}$$

From these values of ϱ_E we take only the real part which represents the exponent of the amplitude damping term, and

calculate the depth of penetration, e.g. the distance through which the original amplitude drops to 1/e (37%). For this it is required that the exponent in the expression

$$A = A_o e^{+\varrho z} \quad ; \qquad z < 0$$

is equal to unity, hence

$$\varrho z = 1$$

$$z = \frac{1}{\varrho}$$

So we obtain the penetration depth of boundary layer waves

$Z(\omega_1) = 218$ m for $\omega_1 = 2\pi \cdot 10^3$, $\varepsilon_E = 10$, $\sigma_E = 5 \cdot 10^{-3}$

$Z(\omega_2) = 71.5$m, for $\omega_2 = 2\pi \cdot 10^4$

$Z(\omega_3) = 22.6$m for $\omega_2 = 2\pi \cdot 10^5$

This calculation was made only to check our ideas and experimental results. We know very well that considerable work has been done in the US concerning the propagation of such waves along a curved interface. We will attach this problem in the next future. Furthermore the penetration of vertically inciding plane waves will be considered.

§ 8. Comparison between experiment and theory

Before comparing the measured results with our calculations we shall calculate the wavelength. Neglecting the displacement current we have according to (42)

$$k_3 = \frac{2\pi}{\lambda} = \sqrt{\frac{\mu_0 \omega \sigma}{2}} .$$

Therefrom with $\nu = 3$ kcps we get

(76) $$\lambda = 8180 \text{ m}$$

in rock, whereas the wavelength in vacuo is 100,000 m.
All the measurements were made at distances of less than 1500 m because more powerful transmitter was not yet available. Thus, the measurements were made in the near field ($r < \lambda$). Let r be given, ϑ and φ be known. If the field strength is measured then from Figs. 11 - 16 one can read that conductivity which had to be substituted into the theoretical formulas to yield a correct description of the measured values. When this conductivity approximately agrees with the measured one, we can assume that our theory describes the experiments correctly. We shall now determine the effect of the frequency and of the distance on the accuracy of the measurement of conductivity. From the expansion of the radical and of the exponential function for small values of ω, σ, and r in Eq. (50)

$$f(r,\alpha) = \frac{1}{r^3}\left(1 + r\sqrt{\frac{\omega\mu_0\sigma}{2}} - \ldots\ldots\right)\left(1 - r\sqrt{\frac{\omega\mu_0\sigma}{2}} + \ldots\ldots\right)$$

one can see the opposed variations of radical and exponential.

$f(r,\alpha)$ is therefore practically independent of σ at short distances and low frequencies (horizontal course of the curves in Fig. 8). As conductivity is dependent on frequency which usually is predetermined by the aim of the measurement, we can choose freely only the quantity r. The following minimum distances should be observed for a sufficiently accurate measurement:

For $\omega\mu_0\sigma > 2.5\cdot10^{-4}$ $r > 500$ m

$\omega\mu_0\sigma > 8\cdot10^{-5}$ $r > 800$ m

$\omega\mu_0\sigma > 8\cdot10^{-6}$ $r > 1200$ m

$\omega\mu_0\sigma > 2.5\cdot10^{-7}$ $r > 3000$ m

If the measuring frequency for instance is 3 kcps, measurements in the region of conductivities around 10^{-3} are sensible only from about 800 m on. Greater distances must be chosen for lower conductivities.

The practical measuring arrangement consists of a magnetic coil and an a.c. power supply on the transmitter side, and a magnetometer whose sensitivity has to meet high requirements because of the rapid decrease of the field strength at longer distances. The magnetic field probe (a highly inductive coil on high-permeability ferrite cores) is connected to an amplifier which transforms the weak signals to a value convenient for reading. In contrast to the usual measuring and amplifying arrangements, the sensitivity of the magnetometer is determined not by the natural noise of the probe or of the amplifier but by the atmospherics which come from discharges in the air, thunderstorms, and similar static processes and which produce

considerably strong magnetic fields in the VLF range (Ref. 2). However, they have a broad frequency spectrum so that their effect can be reduced by selective amplifiers. The sensitivity is therefore determined by the selectivity of the amplifier whose 40-db band width should not be above 100 cps.

Until now, the measurements have been made with a 30-cps band width amplifier on a frequency of 3 kcps in the area of the mines at Schwaz, St. Gertraudi, and Lafatsch. The results are as follows:

Measurement 20-11-62, Schwaz (details, e.g. ψ. in the experimental part) (ε presumably 12.5). The voltage U measured was represented as $U = B \cos \psi$, according to (32), and B was calculated.

r = 580 m	$\vartheta = 0^\circ$	B = 16.9 $\pm$ 1.5	[mv]
r = 760 m	$\vartheta = 0^\circ$	B = 12.3 $\pm$ 1.7	[mv]
r = 870 m	$\vartheta = 8^\circ$	B = 12.3 $\pm$ 3.7	[mv]
r = 1040 m	$\vartheta = 10^\circ$	B = 6 $\pm$ 4	[mv]

Measurements 27-11-62, St. Gertraudi

r [m]	ϑ [°]	B [mv]
110	30	42.64 $\pm$ 0.40
(corresponds to $\lvert H \rvert = 79.6 \cdot 10^{-6}$ or $\lvert B \rvert = 100 \cdot 10^{-12}$ [Wb m^{-2}])		
150	18	17.88 $\pm$ 0.80
200	11	8.28 $\pm$ 0.30
240	7.5	4.93 $\pm$ 0.70
290	5.5	2.83 $\pm$ 0.70
340	4	1.66 $\pm$ 0.20
390	3	1.33 $\pm$ 0.70
440	2	0.679 $\pm$ 0.14
490	1	0.611 $\pm$ 0.05
540	0.5	0.564 $\pm$ 0.09
590	0	0.395 $\pm$ 0.03

640	-0.5	0.307 ± 0.02
690	-0.5	0.2503 ± 0.02
710	-0.5	0.2148 ± 0.01
820	-0.5	0.1306 ± 0.01

A second measurement at St. Gertraudi (transmitting antenna turned through 45°) gave

r [m]	ϑ [°]	B [mv]
70	0	95
150	27	32.7
240	37	15.2
340	41	11.87
490	44	0
640	45	1.785
820	45	0.7499

Both series of measurements are plotted in Fig. 19. Let us first consider the Schwaz measurements. First, the mean value of B was determined from the measured voltage U, according to (32).

For $\vartheta = 0°$ where $H_\vartheta = 0$, using (32), i.e. $B = A(\omega) \cdot |H|$, we obtain according to (52) (50) (46)

(77) $$B = A\ 2m\ f(r,\alpha) = C \cdot f(r,\alpha)$$

f can be taken from Fig. 7a (calculation see later)

580 m $\vartheta = 0°$ B = 16.9 $f = 2 \cdot 10^{-9}$ for $\sigma = 5 \cdot 10^{-5}$, thus $C_1 = 8.45 \cdot 10^9$

$f = 6 \cdot 10^{-9}$ for $\sigma = 10^{-5}$, thus $C_1 = 2.83 \cdot 10^9$

760 m $\vartheta = 0°$ B = 12.3 $f = 6 \cdot 10^{-10}$ for $\sigma = 5 \cdot 10^{-5}$, thus $C_2 = 2.05 \cdot 10^{10}$

$f = 3 \cdot 10^{-9}$ for $\sigma = 10^{-5}$, thus $C_2 = 4.10 \cdot 10^9$

For $\sigma = 5 \cdot 10^{-5}$ the error in C is $C_1 - C_2 = -12 \cdot 10^9$ and

for $\sigma = 10^{-5}$ the error in C is $C_1 - C_2 = -1.3 \cdot 10^9$

This first rough estimate shows that σ is of the order of 10^{-5}. But for such conductivities at 3 kcps distances of at least 3 km are required.

To perform reliable measurements of the conductivity and to be able to verify the theoretical opinions about the propagation of VLF waves, a more powerful transmitter on a lower frequency is necessary.

A similar picture is put forward by the measurements at St. Gertraudi

	B	$f(r,\alpha)$ for $\sigma=5\cdot10^{-5}$ from Fig. 7a	relevant C	$f(r,\alpha)$ for $\sigma=10^{-5}$ from Fig. 7a
490 m	0.611	$4\cdot10^{-9}$	$0.153\cdot10^9$	$8\cdot10^{-9}$
590 m	0.395	$2\cdot10^{-9}$	$0.197\cdot10^9$	$6\cdot10^{-9}$
690 m	0.250	$9\cdot10^{-10}$	$0.250\cdot10^9$	$4\cdot10^{-9}$
820 m	0.131	$3\cdot10^{-10}$	$0.435\cdot10^9$	$2\cdot10^{-9}$
			$\Delta C = 0.282\cdot10^9$	$\Delta C=0.0109\cdot10^9$

As C increases with the distance at $\sigma = 5\cdot10^{-5}$, the value $5\cdot10^{-5}$ is obviously too great. At $\sigma = 10^{-5}$, C first decreases, and then increases somewhat. But this increase might be due to inaccurate reading. This behavior of C leads to the conclusion that $5\cdot10^{-5} > \sigma > 10^{-5}$ in the Schwaz measurements.

A more systematic investigation of the results of the measurements gave the same picture. We define

$$C(r,\alpha) = \frac{B(r,\vartheta)}{h(r,\vartheta,\alpha)} \tag{78}$$

$B(r,\vartheta)$ is the quantity

$$B = \frac{U(r,\vartheta,\psi)}{\cos\psi} \tag{79}$$

calculated from Eq. (32) and from the measured $U(r,\vartheta,\psi)$.

$\overline{C}(\alpha)$ is the average over the $C(r,\alpha)$ with α fixed.

Measurement Schwaz (we have 1 v = $2.32\cdot10^{-12}$ [Weber.m^{-2}], cf. experimental part)

r[m]	B [mv]	B[Weber.m^{-2}]$\cdot10^{12}$	h according to (52)	C(r,α)	$\overline{C}$ h[Weber m^{-2}]10^{12}
580	85	0.2	$1.024\cdot10^{-8}$	$83.0\cdot10^{8}$	0.1464
760	36	0.083	$4.776\cdot10^{-9}$	$75.4\cdot10^{8}$	0.0684
870	16	0.035	$3.01377\cdot10^{-9}$	$53.1\cdot10^{8}$	0.0430
1040	6	0.014	$1.7477\cdot10^{-9}$	$34.35\cdot10^{8}$	0.0250

Mean value $\overline{C}(\alpha) = 61.67\cdot10^{8}$, deviation $C_{max} - C_{min} = 48\cdot10^{8}$.

The calculations performed with $\alpha = 0.0189$ ($\sigma = 10^{-6}$) showed, as was expected, that $\overline{C}$ was quite insensitive. It is therefore not possible to draw an unambigous conclusion about $\omega\sigma = \alpha$. According to Fig. 18 it can be assumed that the conductivity $\sigma = 10^{-6}$ is too small. The values of $\overline{C}(\alpha)h(r,\alpha)$[Weber m^{-2}] are plotted in Fig. 18 together with the results for B [Weber.m^{-2}] for $\alpha = 0.0189$ ($\sigma = 10^{-6}\Omega^{-1}\,m^{-1}$). The quadrupole terms are being studied in detail.

Measurement St. Gertraudi

r[m]	B [v]	B[Weber m^{-2}].10^{12}	h according to (52)	C(r,α)	$\overline{C}$ h [Weber m^{-2}].10^{12}
110	42.64 ± 0.40	98.9	$1.355\cdot10^{-6}$	$3.14\cdot10^{7}$	115
150	17.88 ± 0.80	41.5	$5.71\cdot10^{-7}$	$3.13\cdot10^{7}$	48.25

200	8.28 ± 0.30	19.2	$2.46 \cdot 10^{-7}$	$3.37 \cdot 10^{7}$	20.9
240	4.93 ± 0.70	11.44	$1.435 \cdot 10^{-7}$	$3.44 \cdot 10^{7}$	12.8
290	2.83 ± 0.70	6.57	$8.19 \cdot 10^{-8}$	$3.46 \cdot 10^{7}$	6.95
340	1.66 ± 0.20	3.85	$5.075 \cdot 10^{-8}$	$3.26 \cdot 10^{7}$	4.29
390	1.33 ± 0.70	3.09	$3.37 \cdot 10^{-8}$	$3.49 \cdot 10^{7}$	2.85
440	0.679 ± 0.14	1.574	$3.245 \cdot 10^{-8}$	$2.89 \cdot 10^{7}$	2.76
490	0.611 ± 0.05	1.416	$1.6984 \cdot 10^{-8}$	$3.59 \cdot 10^{7}$	1.45
540	0.564 ± 0.09	1.307	$1.267 \cdot 10^{-8}$	$4.45 \cdot 10^{7}$	1.075
590	0.395 ± 0.03	0.916	$0.872 \cdot 10^{-8}$	$4.06 \cdot 10^{7}$	0.82
640	0.307 ± 0.02	0.711	$0.7612 \cdot 10^{-8}$	$4.03 \cdot 10^{7}$	0.645
690	0.2503 ± 0.02	0.581	$0.6066 \cdot 10^{-8}$	$4.12 \cdot 10^{7}$	0.515
710	0.2148 ± 0.01	0.496	$0.557 \cdot 10^{-8}$	$3.81 \cdot 10^{7}$	0.47
820	0.1306 ± 0.01	0.306	$0.3612 \cdot 10^{-8}$	$3.62 \cdot 10^{7}$	0.301

Mean value $\overline{C}(\alpha) = 3.65 \cdot 10^{7}$. Deviation $C_{max} - C_{min} = 1.56 \cdot 10^{7}$

The calculations made with $\alpha = 0.0942$ ($\sigma = 5 \cdot 10^{-6}$) gave the above table. The deviation was greater for other α:

α	1.89	0.942	0.189	0.0189
$\overline{C}(\alpha)$	$3.93 \cdot 10^{7}$	$3.74 \cdot 10^{7}$	$3.66 \cdot 10^{7}$	$3.61 \cdot 10^{7}$
$C_{max}-C_{min}$	$1.71 \cdot 10^{7}$	$1.63 \cdot 10^{7}$	$1.57 \cdot 10^{7}$	$1.56 \cdot 10^{7}$

Agreement of experiment and theory for $\sigma < 5 \cdot 10^{-6}$ is quite good as shows Fig. 19.

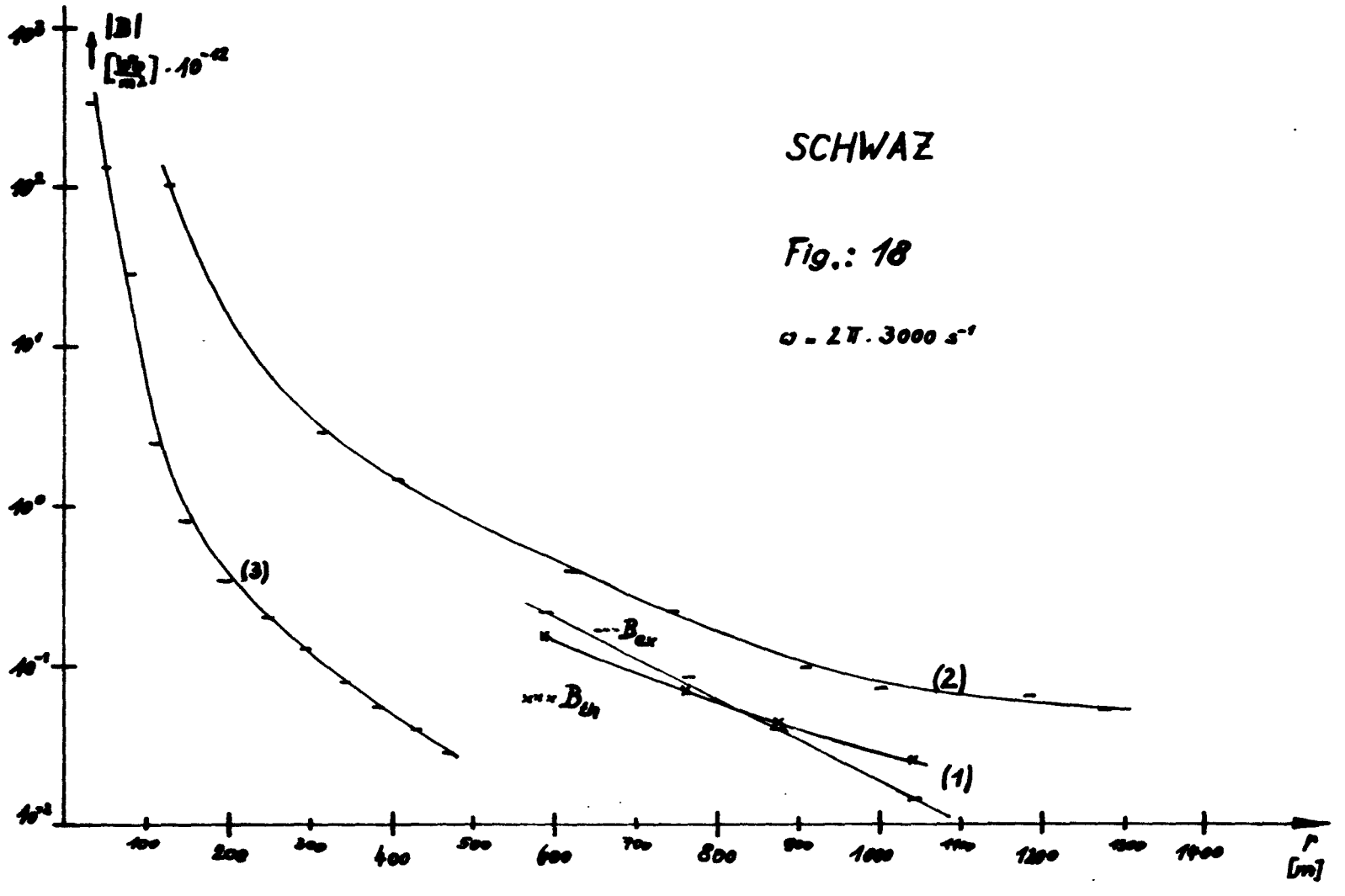

SCHWAZ

Fig.: 18

$\omega = 2\pi \cdot 3000\ s^{-1}$

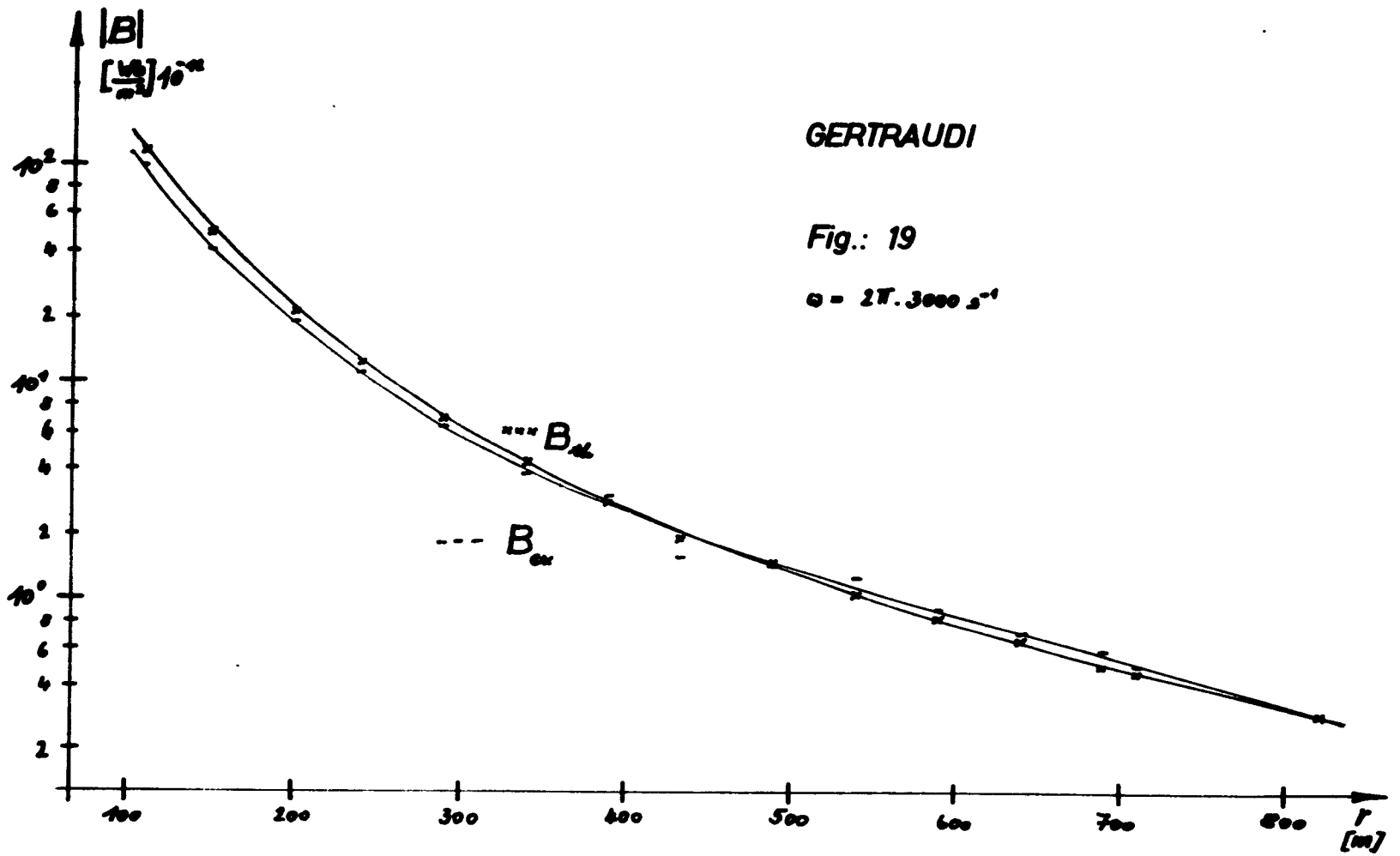

GERTRAUDI

Fig.: 19

$\omega = 2\pi \cdot 3000\ s^{-1}$

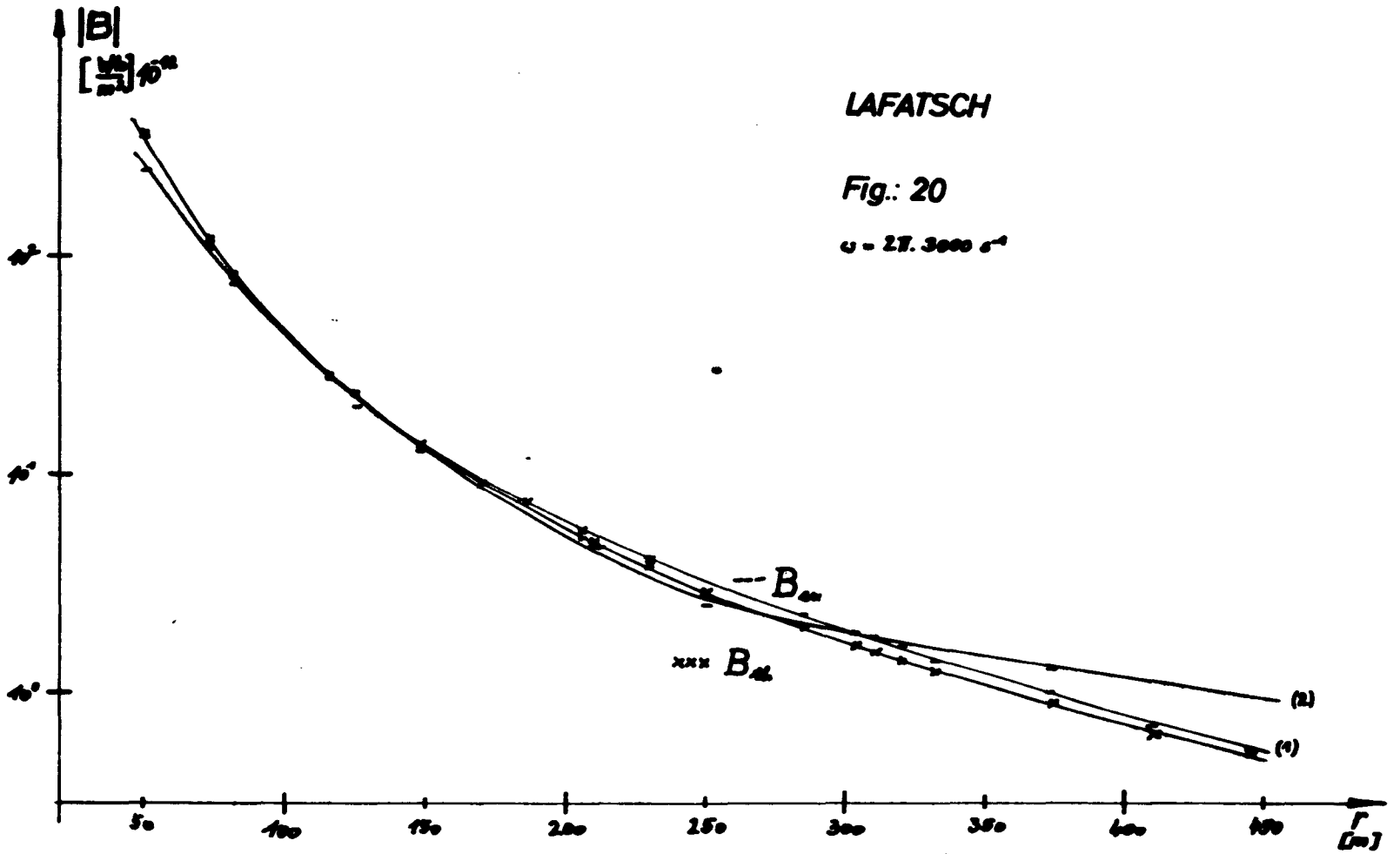
|B|
LAFATSCH
Fig.: 20
ω = 27. 3000 s⁻¹
B_ex
B_ab
(2)
(1)
r [m]

Measurement St. Gertraudi (antenna turned)

r [m]	B [v]	h according to (52) for $\sigma = 10^{-5}$	$C(r,\alpha)$
70	95	$5.885 \cdot 10^{-6}$	$1.615 \cdot 10^{7}$
150	32.65	$5.443 \cdot 10^{-7}$	$5.999 \cdot 10^{7}$
240	15.2	$1.233 \cdot 10^{-7}$	$12.320 \cdot 10^{7}$
340	11.87	$4.290 \cdot 10^{-8}$	$2.699 \cdot 10^{8}$
490	?	$1.404 \cdot 10^{-8}$	-
640	1.785	$6.022 \cdot 10^{-9}$	$2.965 \cdot 10^{8}$
820	0.745	$2.859 \cdot 10^{-9}$	$2.625 \cdot 10^{8}$

The calculations performed with $\sigma = 10^{-5}$ yielded $\overline{C}(\sigma = 10^{-5}) = 7.77 \cdot 10^{7}$. The $\overline{C}$ values obtained with the turned antenna are about twice as large as those obtained with the antenna not turned. This and the wide deviations of the $C(r,\alpha)$ in the case of the turned antenna are indicative of a systematic error or of considerable inhomogeneities of the conductivity. For this reason these measurements were not further evaluated.

Measurement Lafatsch

According to the geological conditions (ore layer) a higher conductivity should occur. The measurements at $\vartheta = 0^{\circ}$, $\varphi = 0^{\circ}$ gave

series I	r [m]	B [wb m^{-2}] 10^{12}	B [Weber m^{-2}] calculated
	82	77	83.3
	116	28	29.3
	125	20	24.0
	170	7.7	9.28
	186	7	7.45
	210	4.6	4.90
	230	4.1	3.82
	304	1.9	1.64
	332	1.4	1.25
	374	1.0	0.895
	410	0.7	0.67
	445	0.55	0.53

series II	50	250	368
	73	110	119
	148	12	14.3
	204	4.5	5.4
	212	4.2	4.83
	250	2.5	2.84
	285	2.3	1.98
	310	1.8	1.55
	321	1.6	1.38
	373	1.3	0.89

The results are compiled in Fig. 20 ($\overline{C} = 4.63 \cdot 10^7$, $\alpha = 0.0942$, $\sigma = 5 \cdot 10^{-6}$ in series I and $\overline{C} = 4.577 \cdot 10^7$, $\alpha = 0.189$, $\sigma = 10^{-5}$ in series II). On the whole they show a good agreement between theory and experiment. In the future it will be studied if the present deviations go back to the neglection of the displacement current, to an improper choice of σ, to the neglection of the quadrupole terms, or to other causes.

III. Experimental part

§ 1. Summary

The measurements on the propagation of low-frequency electromagnetic waves through rock were continued on a larger scale in 1962. On the basis of the results given in the 1961 annual report an attempt was made to improve these results by improving the measuring equipment. The experiments were made in the following mines: Schwaz tetrahedrite mine, St. Gertraudi baryta mining, Lafatsch lead and zinc mining (all in the Tyrol). The measurements in the Hall salt mine are still incomplete at present. New conditions arise in this area as compared to the others since the conductivity of the salt-bearing bed is very high. The content in water is some 4%. The large inhomogeneities observed have not yet been studied theoretically. Besides measurements with the test transmitter, the signals from known long-wave transmitters were recorded underground. In particular the transmitters NAA and GBR were observed and measured over a longer period. The results of the first probing work in this area brought a special working team into operation which is to register the field strength above and under the surface, the signal-to-noise ratio, rapid and slow seasonal fluctuations, etc. Particularly suitable measuring locations with a mountain cover of ~~some~~ 1000 m were found in the Schwaz mining range.

§ 2. Design and construction of the transmitter station

For the measurements of underground propagation, a portable all-transistor transmitter was designed which in spite of its light weight and small volume has a power output of about 50 watts. Larger accumulators of 66 Ah guarantee a 10-hrs operation at full power. The transmitter itself consists of a stabilized RC generator which produces the required frequency, the electronic code automatic switch (Fig. 23), and the power amplifier (circuit diagram see Fig. 22). The power stage is in essential a strong low-frequency amplifier. The antenna matching is different from the usual LF wiring. The best matching of antenna and amplifier in each individual case can be adjusted with the aid of several tappings at the secondary winding of the output transformer. Each transmitting antenna is tuned to series resonance by means of mica switch capacitors. In this case only their ohmic resistance appears which usually can be kept low. To determine the power output the antenna current for a known impedance of the aerial is measured by means of a current transformer. As is clear from the theoretical formulas for the field strength of a magnetic dipole, the value of this current alone is enough for the exact calculation. In the case of resonance a voltage boost of up to 800 volts may occur although the impedance of the transmitter aerial is of the order of 10 ohms. On the one hand this furnishes a good insulation of the antenna and on

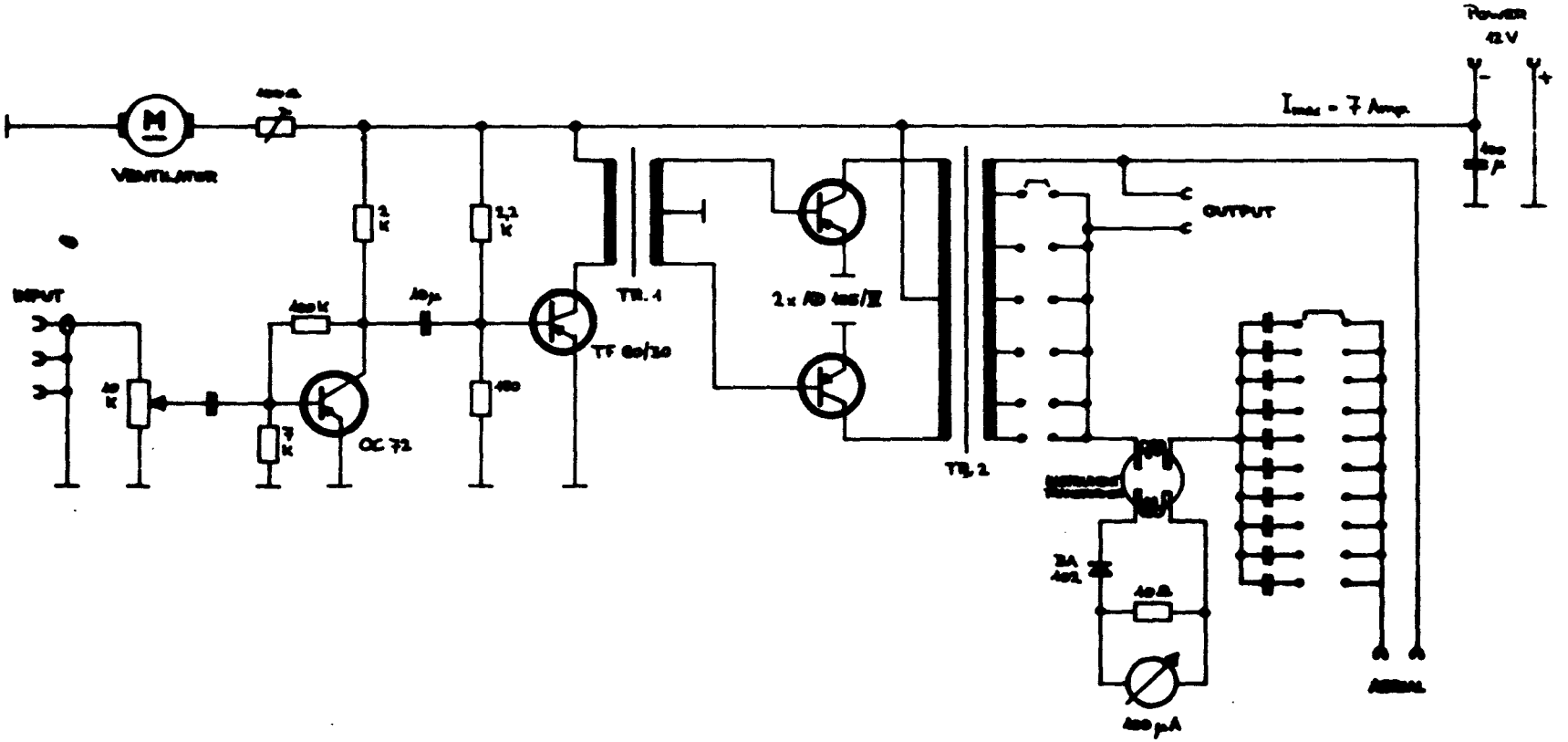

TRANSMITTER
50 W

Fig. 22

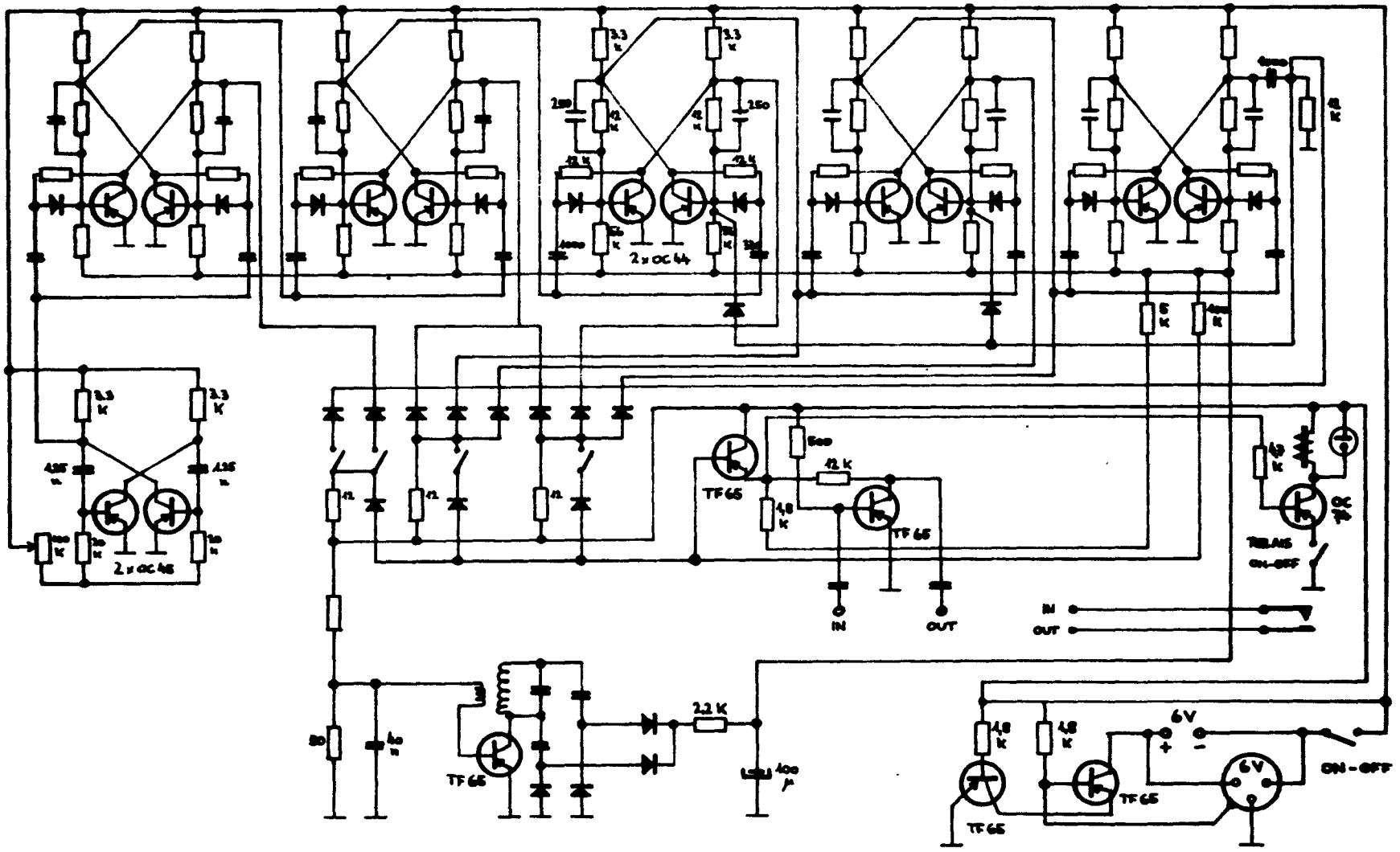

AUTOMATIC MORSE CODE SWITCH

NOW PRODUCING • • — — — • •

Fig. 23

the other very powerful capacitor decades. The cooling plates necessary for the thermal stabilization of the output stage transistors were reduced to a minimum to provide small geometrical dimensions. The required cooling was performed by a controllable blower. Fig. I shows the complete transmitter station.

As for the transmitter antennas, the way taken last year is being continued. The aerials are all large air-core coils. For the purpose of installing the transmitter station at the different places of the mine, aerials of small dimensions and light weight were designed, as e.g. SA IV, SA V, SA VI. For the long-distance measurements, however, the frame dimensions were larger so that their easy portability had to be abandoned. Such aerials were mounted in exhausted mines or in suited galleries. In the Schwaz mine, for instance, a rotary frame of 17 m^2 was installed for long-term measurements. Technical data of the transmitter aerials:

SA IV	100 turns Cu 1 mm R = 1 ohm, L = 23 mH rigid frame	diameter 1m
SA V	60 turns Cu 1 mm R = 5 ohms, L = 11 mH rigid frame	diameter 1.5 m
SA VI	60 turns of stranded wire = 2.5 mm^2 R = 2.1 ohms, L = 15 mH	diameter about 1.5 m area 1.4 m^2

To be able to forward these aerials with their relatively large diameters also through narrow tunnels, the wire turns

were fused into flexible plastic tube which is set up on a special frame only at the required place. This is shown in Fig. II.

SA VII 36 turns of stranded wire 0.75 mm^2, area of aerial 17 m^2, R = 13.5 ohms, L = 12 mH.
Rectangular shape.

The field produced by this antenna is sufficient to make measurements at distances of up to 1.2 km possible. A detection at even longer distances is also possible. Fig. IV shows the aerial SA VII as installed in the Schwaz mine.

§ 3. The receiver station

The portable all-transistor receiver (Fig. III) consists of four units:
removable receiving aerial
selective receiver
millivoltmeter
audio amplifier.
Also the receiving aerials are built as magnetic antennas only. Three different designs were employed.
The receiving aerial IV consists of five ferrite rods, 20 mm in diameter and 65 cm long, which are arranged along the edges of a prism with a regular pentagon as the base plane. An approximately 15 cm long cross-coil winding of 1600 turns is in the middle of each rod. The optimum edge length of the pentagon was calculated to be 15 cm. It depends on the

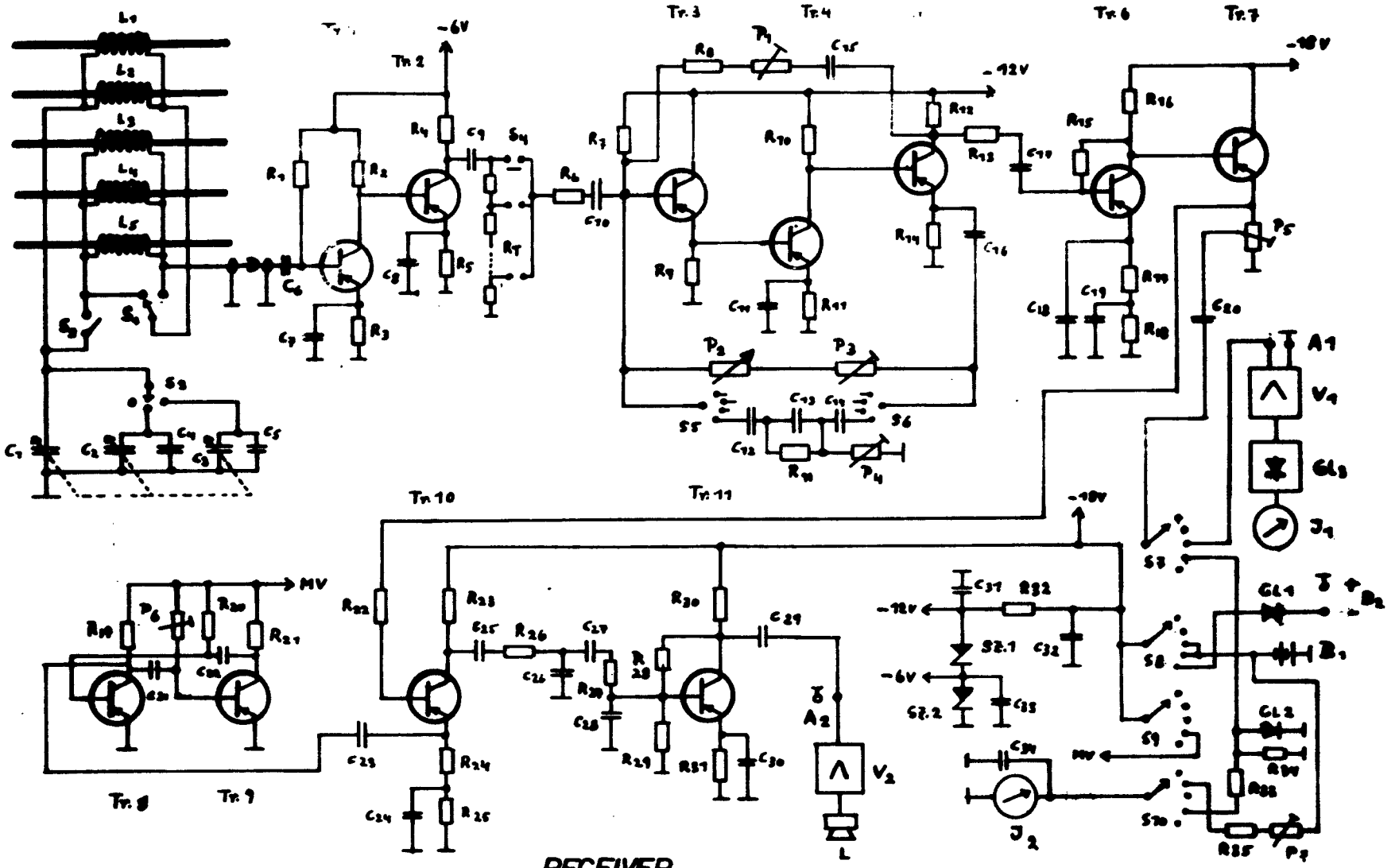
Tr. 1
Tr. 2
Tr. 3
Tr. 4
Tr. 6
Tr. 7
Tr. 8
Tr. 9
Tr. 10
Tr. 11
-6V
-12V
-18V
MV
L1
L2
L3
L4
L5
S1
S2
S3
S4
S5
S6
S7
S8
S9
S10
S11
S12
S13
S14
S15
S16
S17
S18
S19
S20
S21
S22
S23
S24
S25
S26
S27
S28
S29
S30
S31
S32
S33
S34
S35
S36
S37
S38
S39
S40
S41
S42
S43
S44
S45
S46
S47
S48
S49
S50
S51
S52
S53
S54
S55
S56
S57
S58
S59
S60
S61
S62
S63
S64
S65
S66
S67
S68
S69
S70
S71
S72
S73
S74
S75
S76
S77
S78
S79
S80
S81
S82
S83
S84
S85
S86
S87
S88
S89
S90
S91
S92
S93
S94
S95
S96
S97
S98
S99
S100
S101
S102
S103
S104
S105
S106
S107
S108
S109
S110
S111
S112
S113
S114
S115
S116
S117
S118
S119
S120
S121
S122
S123
S124
S125
S126
S127
S128
S129
S130
S131
S132
S133
S134
S135
S136
S137
S138
S139
S140
S141
S142
S143
S144
S145
S146
S147
S148
S149
S150
S151
S152
S153
S154
S155
S156
S157
S158
S159
S160
S161
S162
S163
S164
S165
S166
S167
S168
S169
S170
S171
S172
S173
S174
S175
S176
S177
S178
S179
S180
S181
S182
S183
S184
S185
S186
S187
S188
S189
S190
S191
S192
S193
S194
S195
S196
S197
S198
S199
S200
S201
S202
S203
S204
S205
S206
S207
S208
S209
S210
S211
S212
S213
S214
S215
S216
S217
S218
S219
S220
S221
S222
S223
S224
S225
S226
S227
S228
S229
S230
S231
S232
S233
S234
S235
S236
S237
S238
S239
S240
S241
S242
S243
S244
S245
S246
S247
S248
S249
S250
S251
S252
S253
S254
S255
S256
S257
S258
S259
S260
S261
S262
S263
S264
S265
S266
S267
S268
S269
S270
S271
S272
S273
S274
S275
S276
S277
S278
S279
S280
S281
S282
S283
S284
S285
S286
S287
S288
S289
S290
S291
S292
S293
S294
S295
S296
S297
S298
S299
S300
S301
S302
S303
S304
S305
S306
S307
S308
S309
S310
S311
S312
S313
S314
S315
S316
S317
S318
S319
S320
S321
S322
S323
S324
S325
S326
S327
S328
S329
S330
S331
S332
S333
S334
S335
S336
S337
S338
S339
S340
S341
S342
S343
S344
S345
S346
S347
S348
S349
S350
S351
S352
S353
S354
S355
S356
S357
S358
S359
S360
S361
S362
S363
S364
S365
S366
S367
S368
S369
S370
S371
S372
S373
S374
S375
S376
S377
S378
S379
S380
S381
S382
S383
S384
S385
S386
S387
S388
S389
S390
S391
S392
S393
S394
S395
S396
S397
S398
S399
S400
S401
S402
S403
S404
S405
S406
S407
S408
S409
S410
S411
S412
S413
S414
S415
S416
S417
S418
S419
S420
S421
S422
S423
S424
S425
S426
S427
S428
S429
S430
S431
S432
S433
S434
S435
S436
S437
S438
S439
S440
S441
S442
S443
S444
S445
S446
S447
S448
S449
S450
S451
S452
S453
S454
S455
S456
S457
S458
S459
S460
S461
S462
S463
S464
S465
S466
S467
S468
S469
S470
S471
S472
S473
S474
S475
S476
S477
S478
S479
S480
S481
S482
S483
S484
S485
S486
S487
S488
S489
S490
S491
S492
S493
S494
S495
S496
S497
S498
S499
S500
S501
S502
S503
S504
S505
S506
S507
S508
S509
S510
S511
S512
S513
S514
S515
S516
S517
S518
S519
S520
S521
S522
S523
S524
S525
S526
S527
S528
S529
S530
S531
S532
S533
S534
S535
S536
S537
S538
S539
S540
S541
S542
S543
S544
S545
S546
S547
S548
S549
S550
S551
S552
S553
S554
S555
S556
S557
S558
S559
S560
S561
S562
S563
S564
S565
S566
S567
S568
S569
S570
S571
S572
S573
S574
S575
S576
S577
S578
S579
S580
S581
S582
S583
S584
S585
S586
S587
S588
S589
S590
S591
S592
S593
S594
S595
S596
S597
S598
S599
S600
S601
S602
S603
S604
S605
S606
S607
S608
S609
S610
S611
S612
S613
S614
S615
S616
S617
S618
S619
S620
S621
S622
S623
S624
S625
S626
S627
S628
S629
S630
S631
S632
S633
S634
S635
S636
S637
S638
S639
S640
S641
S642
S643
S644
S645
S646
S647
S648
S649
S650
S651
S652
S653
S654
S655
S656
S657
S658
S659
S660
S661
S662
S663
S664
S665
S666
S667
S668
S669
S670
S671
S672
S673
S674
S675
S676
S677
S678
S679
S680
S681
S682
S683
S684
S685
S686
S687
S688
S689
S690
S691
S692
S693
S694
S695
S696
S697
S698
S699
S700
S701
S702
S703
S704
S705
S706
S707
S708
S709
S710
S711
S712
S713
S714
S715
S716
S717
S718
S719
S720
S721
S722
S723
S724
S725
S726
S727
S728
S729
S730
S731
S732
S733
S734
S735
S736
S737
S738
S739
S740
S741
S742
S743
S744
S745
S746
S747
S748
S749
S750
S751
S752
S753
S754
S755
S756
S757
S758
S759
S760
S761
S762
S763
S764
S765
S766
S767
S768
S769
S770
S771
S772
S773
S774
S775
S776
S777
S778
S779
S780
S781
S782
S783
S784
S785
S786
S787
S788
S789
S790
S791
S792
S793
S794
S795
S796
S797
S798
S799
S800
S801
S802
S803
S804
S805
S806
S807
S808
S809
S810
S811
S812
S813
S814
S815
S816
S817
S818
S819
S820
S821
S822
S823
S824
S825
S826
S827
S828
S829
S830
S831
S832
S833
S834
S835
S836
S837
S838
S839
S840
S841
S842
S843
S844
S845
S846
S847
S848
S849
S850
S851
S852
S853
S854
S855
S856
S857
S858
S859
S860
S861
S862
S863
S864
S865
S866
S867
S868
S869
S870
S871
S872
S873
S874
S875
S876
S877
S878
S879
S880
S881
S882
S883
S884
S885
S886
S887
S888
S889
S890
S891
S892
S893
S894
S895
S896
S897
S898
S899
S900
S901
S902
S903
S904
S905
S906
S907
S908
S909
S910
S911
S912
S913
S914
S915
S916
S917
S918
S919
S920
S921
S922
S923
S924
S925
S926
S927
S928
S929
S930
S931
S932
S933
S934
S935
S936
S937
S938
S939
S940
S941
S942
S943
S944
S945
S946
S947
S948
S949
S950
S951
S952
S953
S954
S955
S956
S957
S958
S959
S960
S961
S962
S963
S964
S965
S966
S967
S968
S969
S970
S971
S972
S973
S974
S975
S976
S977
S978
S979
S980
S981
S982
S983
S984
S985
S986
S987
S988
S989
S990
S991
S992
S993
S994
S995
S996
S997
S998
S999
S1000
RECEIVER

Fig. 24

material and on the geometrical dimensions of the ferrite rods. Five windings can interchangeably be connected in parallel or in series. Fig. 24 shows the connection employed.

Similarly to the transmitter antenna circuit, also the receiving antenna is adjusted to resonance by series connection with switch capacitors. This type has an advantage over parallel circuits since the entire input circuit of the amplifier can be kept low-resistance. The sensitivity to atmospherics and noise can be reduced in this way. The receiving aerial V is simpler. It consists of only one 65 cm long ferrite rod. The cross-coil winding of 3000 turns is also placed in the middle of the rod. The antenna is tuned as described above, owing to its small size, the aerial can be shielded electrostatically and can therefore be calibrated with particular accuracy.

Receiving aerial VI: The low-permeability ferrite core is replaced by a high-permeability iron core with μ_{tor} = 80,000. The laminated core is 100 cm long. At the measuring frequencies used so far (10 and 3 kcps) this design is not superior to the types IV and V. At low frequencies, however, it is supposed to be paramount.

Technical data:

EA IV maximum inductance = 8 H, R = 5 ohms
number of turns 5 x 1600 (Fig. III)

EA V inductance = 2 H, 3000 turns, R = 135 ohms (Fig. V)

EA VI inductance L = 2.2 H, 2 x 1000 turns, R = 56 ohms

μ_{tor} = 80,000, length = 100 cm, cross section = 8 cm^2

Besides these types, also large stationary aerials of various designs were installed. They shall be discussed elsewhere.

The selective amplifier (circuit diagram Fig. 24):
The signal voltage supplied by the aerial rods at long-distance measurements is of the order of μv and even less. To be able to measure precisely these low voltages a special input amplifier with a signal-to-noise ratio as high as possible had to be designed. After thorough investigations into low-background transistor amplifiers a specially chosen transistor of the type BCY 20 supplied by the Siemens company was employed in emitter connection in the input stage. The signal is then amplified again by another low-background input stage transistor AC 107. The input signal can be weakened in steps of 10 db each by means of a calibrated divider. It is then fed into a multistage selective amplifier. The individual stages were d.c.-coupled to avoid undesired phase shifts. The temperature dependence is low as silicon transistors have been used. The temperature of the place of measurement and its environment is constant. The selective network which is a further development of the shunted T member was designed in our laboratory and has proved useful so far. The selective stage is followed by a buffer stage to eliminate feedback. A low-resistance output is reached by a transistor operated in collector connection. From here the signal comes

into the transistor voltmeter for measuring problems on the one hand, and on the other for audio tests into a mixer stage which adds a multivibrator signal. The resultant beat frequency can be led into an amplifier for a loudspeaker. This arrangement is to make audible those signals of known very-long-wave transmitters as GBR and NAA that are above the threshold of audibility. Because of the high requirements concerning constant amplification it was necessary to stabilize the operating voltage, which was supplied by two 9-v batteries, by means of Zener diodes. In this way amplification is independent of the decrease in battery voltage (18 - 15 v). The instrument which is built into the apparatus serves to control the battery but can also be used to indicate the measuring signal.

Technical data of the receiver:

amplification 80,000 $\pm$ 3 db at 15°C
background voltage at the input 0.1 μv
band width about 5%
frequency range 20 cps to 20 kcps
frequency variation 1 : 2
input resistance 5000 ohms
output resistance (measuring output) 1000 ohms
dimensions 15 by 11 by 27 cm.

Specification for receiver (Fig. 24)

no.	R	C	transistors
1	680 kΩ		
2	10 "	3 x 500 pF	Tr 1. BCY20
3	1.2 "		Tr 2. AC107
4	5.6 "	400 pF	Tr 3. BCY20
5	68 "	1 nF	Tr 4. "
6	47 "	10 µF	Tr 5. "
7	470 "	100 "	Tr 6. OC71
8	33 "	5 "	Tr 7. "
9	5.6 "	10 "	Tr 8. AC107
10	15 "	10 "	Tr 9. "
11	1.5 "	100 "	Tr 10. OC71
12	8.2 "		Tr 11. "
13	15 "	variable	GL 1. BA102
14	10 "		Gl 2. OA70
15	680 "	100 µF	SZ 1. OAZ203
16	15 "	100 "	SZ 2. OAZ202
17	220 Ω	25 "	
18	1.2 kΩ	20 nF	potentiometers
19	4.7 "	100 µF	
20	22 "	25 "	P 1. 1 MΩ
21	3.3 "	2 nF	P 2. 10 kΩ
22	47 "	2 "	P 3. 100 kΩ
23	2.7 "	5 µF	P 4. 250 Ω
24	680 Ω	0.47 "	P 5. 5 kΩ
25	6.8 kΩ	40 nF	P 6. 10 kΩ
26	47 "	20 "	P 7. 25 kΩ
27	22 "	40 "	
28	470 "	20 "	
29	12 "	10 µF	
30	10 "	5 "	
31	680 Ω	100 "	
32	500 "	100 "	
33	15 kΩ	100 "	
34	6.8 "	1 "	
35	150 Ω		

The antenna EA IV, the selective amplifier, the transistor millivoltmeter, and the audio amplifier were arranged into one common transport casing for the measurements in the mines. This complete receiving station which in a mine can easily be handled by two persons is shown in Fig. III. For measurements on difficult terrain, very narrow tunnels or shafts the receiver unit was decomposed into two easily portable units. Fig. V shows this measuring arrangement: Antenna EA V, selective receiver, and millivoltmeter.

Calibration of the receiving antenna:

The antenna was calibrated in the same way as described in the last year's annual report. The aerial was placed into a uniform field of known intensity. The voltage induced was measured, i.e., the voltage measured at the output of the selective amplifier was extrapolated to the input. In this way one obtains the relationship between measured voltage and magnetic field strength in Wb/m^2. This determination must be repeated for all the frequencies in question because several parameters vary with frequency in a way very difficult to determine.

When approaching the problem mathematically we find the following:

The voltage induced in a coil is

$$U_{ind} = -L \frac{d\Phi}{dt} \tag{1}$$

Applying this equation to the antennas used by us we have

(2) $$U_{ind} = -L \cdot i\omega \cdot F \vec{B} \cdot e^{i\omega t}$$

and the required amount is

(3) $$|U_{ind}| = L \cdot \omega F \cdot |\vec{B}|; \quad F = f\cos\varphi$$ (cf. formula (31), §2).

The receiving unit does not indicate $|U_{ind}|$ but the output voltage U_a of the selective receiver. The relation between these two quantities is

(4) $$U_a = \alpha \cdot V \cdot |U_{ind}| = \alpha V L \omega F |\vec{B}|$$

α is the factor by which the input voltage of the receiver is greater than the voltage induced in the coil of the antenna. The quantity α and the amplification V of the receiver depend on the frequency ω and are conveniently ascertained by a calibrating measurement.

Fig. 25 shows Eq. (4) logarithmically: Calibration diagrams for the antennas LA IV, V, VI for both 3 and 10 kcps.

The spacing between two parallel straight lines is determined by the quantity $\alpha V \omega L F$ (L = self induction of the aerial coil, F = area). The angle between each line and the abscissa is 45°.

$|\vec{B}|$ is a definite value for each place of reception. If the indicated voltage U_a is to increase either the amplification V or the sensitivity of the antenna have to be raised. The increment in V is limited by the rising background noise and by the instabilities. The sensitivity of the antenna is essentially determined by its area and by its inductance. The product F·L, however, cannot be

increased arbitrarily for the increasing ohmic resistance, the winding capacitances and other losses reduce the Q-factor of the coil. Therefore we have to look for a compromise when designing the antenna.

The dependence of the quality Q on the frequency ω ($Q = \omega_0 L/R$) entails the fact that the antenna delivers an optimum signal voltage to the receiver only in a relatively narrow frequency band. For the frequency bands studied the aerial had to be exchanged or switched over each time. Eq. (4) shows the linear relationship between the magnetic field strength and the voltage measured. As shown in Fig. 25, the calibration curves are shifted parallel according to the frequency, aerial used (or amplification factor V). It is therefore enough in evaluating the measurements to give a number of conversion factors that are independent of frequency for each antenna.

To an output voltage U_a of 1 volt correspond

	3 kcps	10 kcps	
EA IV:	2.32	$0.73 \cdot 10^{-12}$ [Wb/m^2]	at the place of reception
EA V:	6.8	$2.42 \cdot 10^{-12}$ [Wb/m^2]	
EA VI:	3.25	$2.63 \cdot 10^{-12}$ [Wb/m^2]	

To control and/or correct the described calibration of the receiver the following measurements were made: A certain definite magnetic field could be produced by means of a large single-layer cylindric coil in the direction of its axis. The magnetic induction is

$$(5) \qquad |B| = \mu_o \frac{0.4\pi \cdot I \cdot n}{l\sqrt{1 + (\frac{2R}{l})^2}} \left[\frac{Wb}{m^2}\right]$$

The calibration coil was 390 turns wound on an 18.5-cm long ferrite rod, with an inductance of 145 μH. Its size as compared to that of the cylindric coil is so small that the field in the range of the coil can be regarded uniform. Tuning to resonance was avoided to eliminate the effect of the Q-factor whose dependence on frequency cannot be neglected. The voltage measured on the calibration coil must follow the law of induction and be strictly proportional to the frequency. In our above considerations this was not the case because of the dependences $Q(\omega)$ and $V(\omega)$.

Block diagram of the measuring arrangement

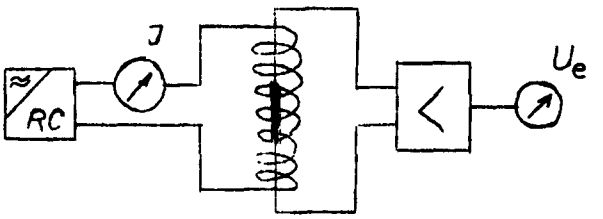

The calibration values measured are

f = 10 kcps $\qquad U_e = 1\ \mu v \longleftrightarrow 5.6 \cdot 10^{-12} \left[Wb/m^2\right]$

f = 3 kcps $\qquad U_e = 1\ \mu v \longleftrightarrow 18 \cdot 10^{-12} \left[Wb/m^2\right]$

All the other antennas can also be calibrated by comparing them with this calibration coil. The calibration factors found in this way depart only little from those that have been known before.

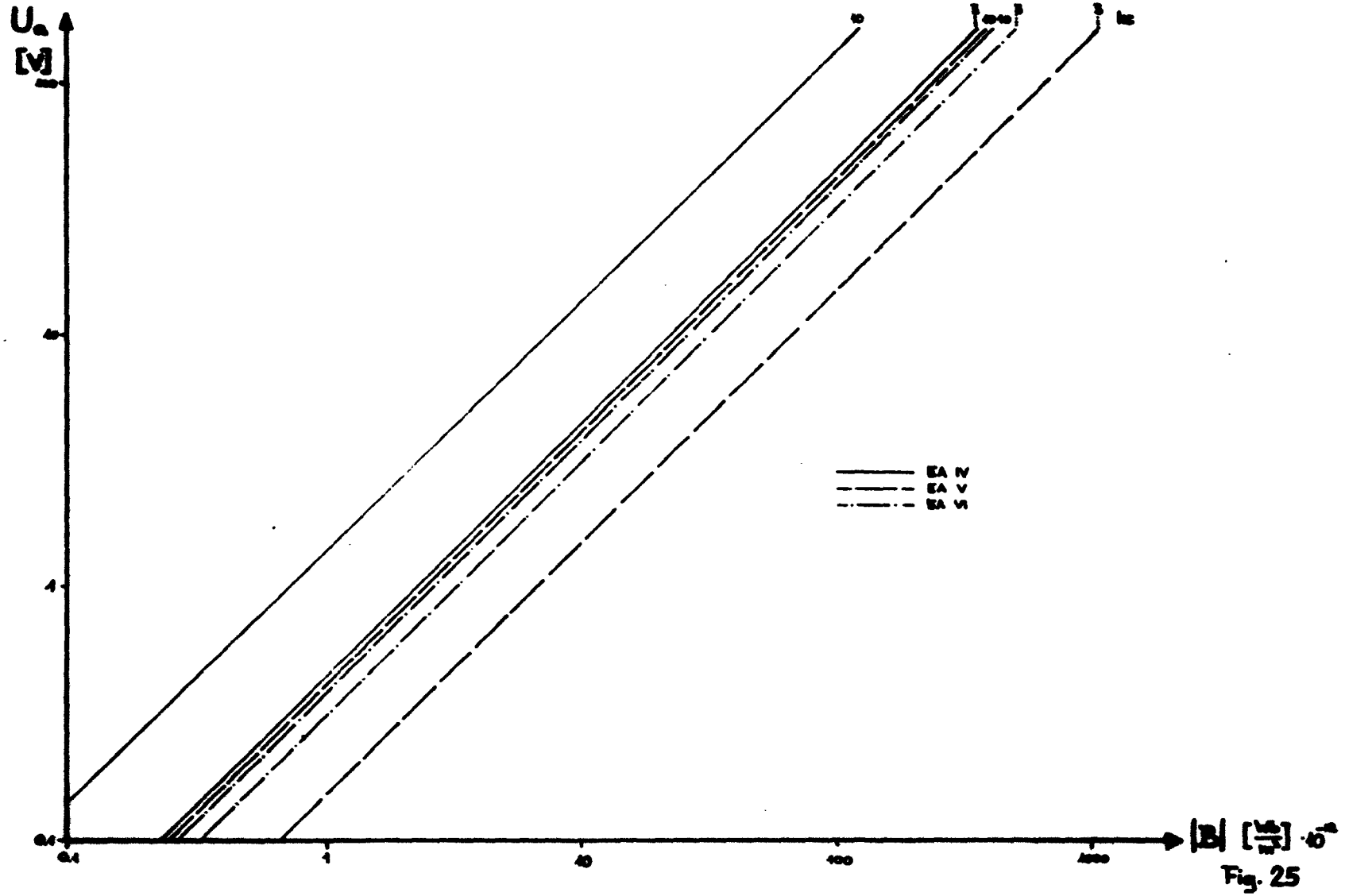

Fig. 25

§ 4. Experimental work in the mine

Unlike the laboratory measurements, the underground measurements involve considerable difficulties. Even the transport to and from the sites of measurement is rendered difficult by narrow and partly very wet galleries. The measuring equipment must be carefully packed to protect it from moisture and also from hard shocks. In the lower bench (main gallery) it is sometimes possible to travel longer distances on the mine railway. The measuring location, however, usually is in abandoned mine regions for the individual measuring sites should be as far as possible from rails, electrical lines and pneumatic pipelines. Therefore, the whole equipment has to be carried in each reconnaissance. The measuring sites often can be reached only creeping because of narrow tunnels. Such a place is shown in Fig. IX.

But not only electrical lines and iron parts have to be avoided when choosing the measuring site. Dislocations, fissures, and larger cavities as e.g. pits produce unclear conditions. As all the theoretical calculations are based on the assumption of a homogeneous medium only such sections can be used for measurements in which the geological structure is known as thoroughly as possible. An ore-lined mountain range was purposely examined only in a few cases, as for instance in Lafatsch. Despite of all care differences in the measurements occur now and then. Their cause is assumed to be a variable electric conductivity. The

departures of the individual curves from the results of the measurements in the figures that shall be discussed later can be explained by this. The communication between receiver and transmitter, orders to turn the aerials, that are necessary for easy and quick measurements were given through a field telephone. As was proven the cable laid for this purpose has no measurable effect on the receiver. Yet a longer distance which was bridged by light signals was left between the telephone and the receiver.

For every measurement of reception one has to know not only the distance and the magnetic field strength but also the exact orientation of the transmitting and receiving aerials. The departures from the North-South direction were ascertained with compass and map. We could, however, not avoid an angular deflection caused by various effects as e.g. inaccurate maps, magnetic influence on the high-sensitivity geological compass, and insufficient possibilities of adjusting the transmitting and receiving aerials in the terrain. The angle ϑ could be set with an accuracy of $\pm 5^{\circ}$, the angle ψ to $\pm 10^{\circ}$. The resultant errors have been corrected by least squares calculus.

The improved transmitting and receiving stations entail one difficulty, namely that of finding two sites of measurement in one mine that are at a sufficiently long distance from one another. The longest distances used so far in measurements are about 1200 meters in the Schwaz mine. In the St. Gertraudi and Lafatsch mines it was not possible

to find two sites at a distance greater than 1 km, not even if the geological structure of the rock between them may be completely inhomogeneous. Measurements between the individual mines are planned for the future with the large transmitter that is being constructed.

§ 5. Results of the measurements

The majority of the measurements in the Lafatsch, Schwaz, and St. Gertraudi mines was made to study the dependence of the magnetic field strength on the distance for fixed angles ϑ and ψ, and also to study the magnetic field strength at a constant distance r as a function of ϑ and ψ.

Lafatsch mine

The first surveying measurements in this mine have already been described in our last year's report. In 1962, particular attention was paid to the inhomogeneities caused by ore deposits (Pb and Zn). Figs. 26 and 27 show the horizontal and vertical projections of the mine area. The transmitter locations are indicated by S_1 and S_2. The locations of the receiver for field strength measurements are indicated by the succession of small letters. The first measurement was made on the sixth bed (Fig. 26). The transmitter location S_1 lies in dolomite rock. At a distance of 85 m from the transmitter a 20 m thick ore vein lies between the points m and p. The ore then abuts on dead limestone.

Measuring table:

LAFATSCH

f = 10 kcps SA VI; I = 0.8 a
transmitter location S_2

points/m		$\lvert B\rvert \cdot \left[\frac{Wb}{m^2}\right] \cdot 10^{-12}$
r	50	125
s	73	53
l	148	5
t	204	2.35
m	212	2.2
q,v	238	1.6
n	266	1.3
p	285	1.05
w	310	0.89
o	321	0.85
x	373	0.62

f = 3 kcps SA VI; I = 2 a
transmitter location S_2

points/m		$\lvert B\rvert \cdot \left[\frac{Wb}{m^2}\right] \cdot 10^{-12}$
r	50	250
s	73	110
l	148	12
t	204	4.5
m	212	4.2
v,q	238	2.8
n	266	2.3
p	285	2.2
w	310	1.8
o	321	1.6
x	373	1.3

The conductivity and the further theoretical conclusions deduced from these values have been discussed in § 8. The experimental curve is shown in Fig. 20. The second measurement which was made in the direction of an ore deposit has an entirely different course. The transmitter location in this case was S_1. The receiver was then placed in the floors below. In the map on Fig. 26, the individual bottoms are indicated by broken lines. In this measurement, particular attention was paid to the precise orientation of both the transmitting and receiving aerials. These had

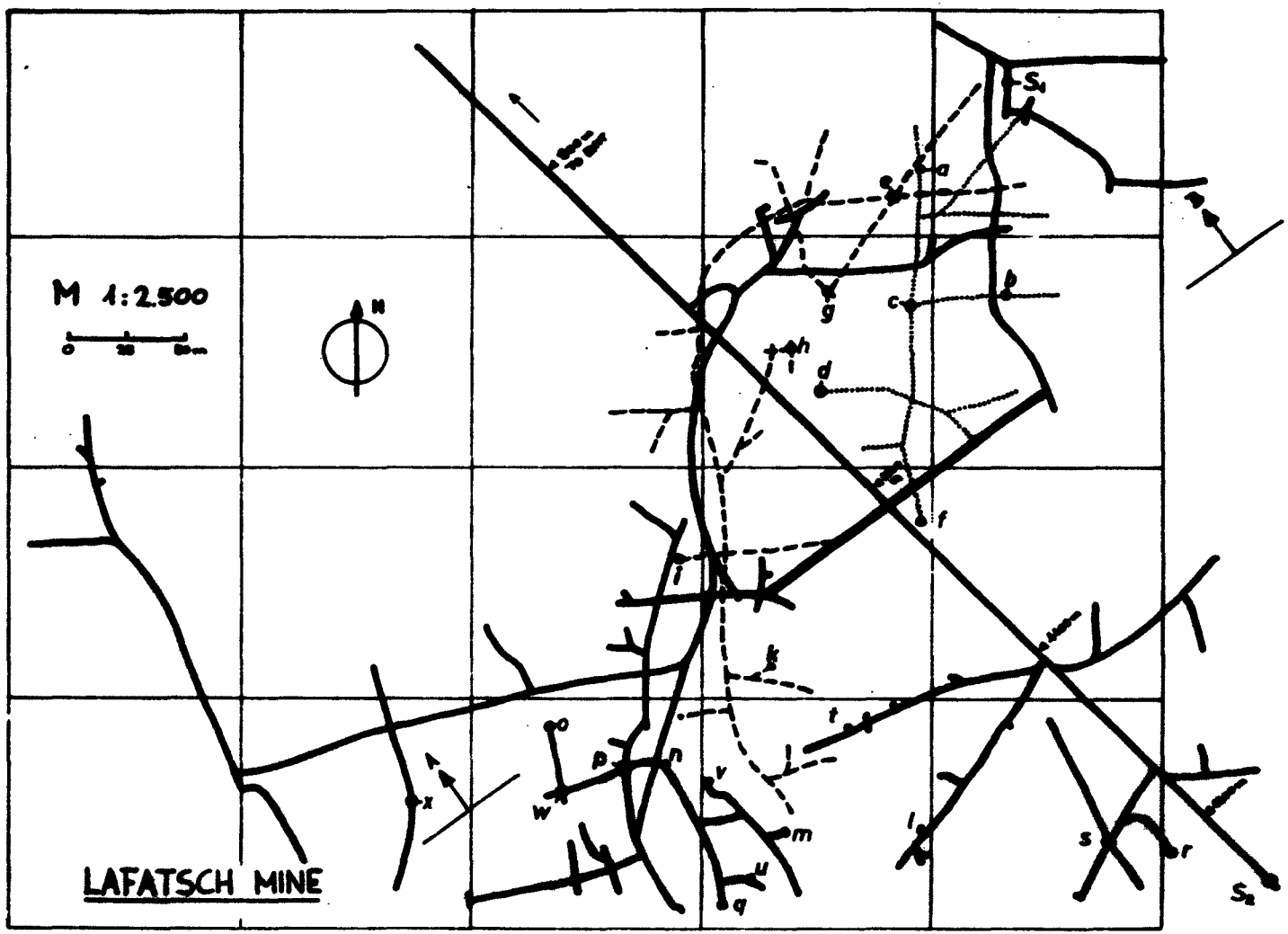

Fig. 26

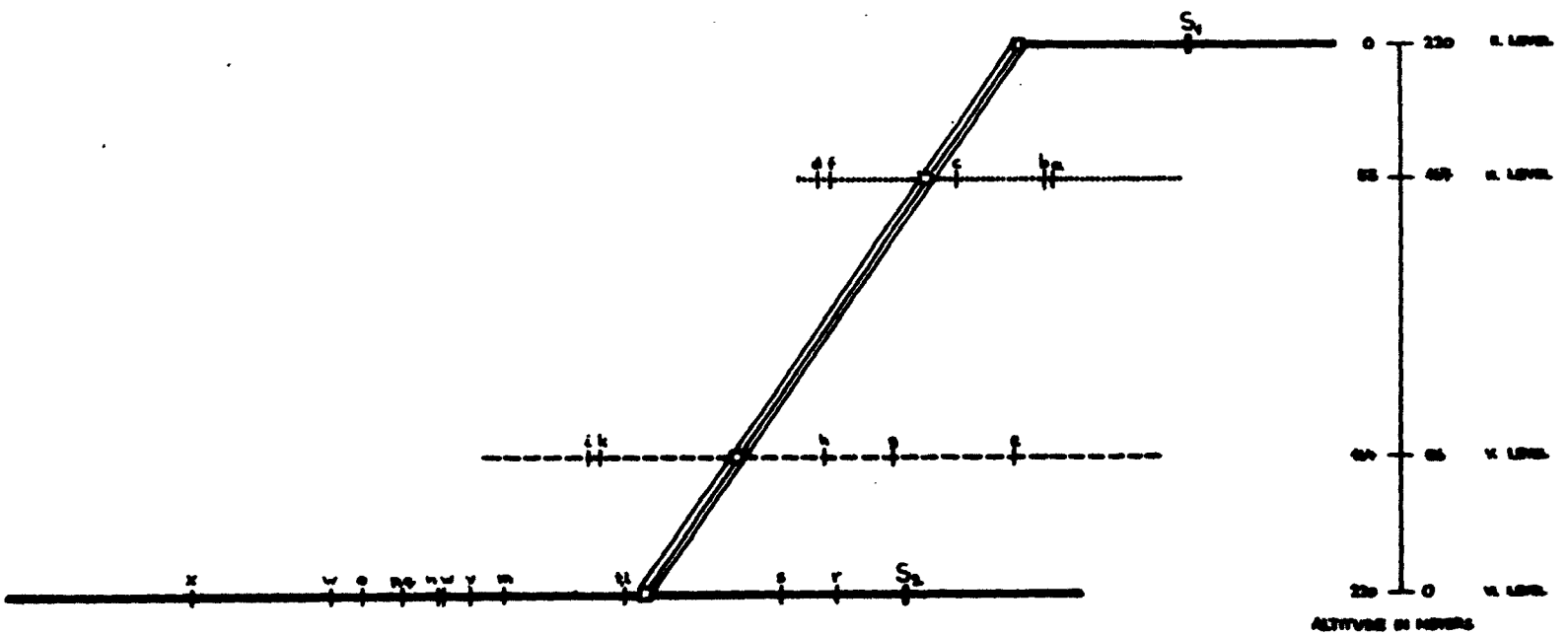

LAFATSCH MINE

PROFIL A-B

M 1:2.500

0 25 50 m

Fig. 27

to be turned not only horizontally but also vertically. The ore-bearing rock extends at a steep angle from the point S_1 in the second course to the region of the points n - q in the sixth course.

Measuring table:

LAFATSCH

f = 3 kcps SA VI I = 2 a

transmitter location S_1

points/m	$\lvert B \rvert \left[\frac{Wb}{m^2}\right] \cdot 10^{-12}$	points/m	$\lvert B \rvert \left[\frac{Wb}{m^2}\right] \cdot 10^{-12}$
a 82	77	j 332	1.4
b 116	28	k 374	1
c 125	20	l 398	0.8
d 170	7.7	m,n 410	0.7
e 186	7	o 412	0.7
f,g 210	4.6	p 414	0.8
h 230	4.1	q 445	0.55
i 304	3.1		

For small values of r these two curves of the first and second measurements depart only slightly from each other. As was discussed already in the theoretical part, conductivity has an effect only at longer distances which in this case is from some 200 m on. The short distances in these measurements in the Lafatsch mine proved to be unfavorable. It was not possible to find more appropriate ranges for measurement.

Schwaz mine

Very suitable galleries were found in particular for the long-distance measurements. As can be seen from the mine chart in Fig. 28, the distance between the points S_1 and 4 is approximately 1300 m. To bridge this distance it was necessary to design a new and larger transmitting aerial (SA VII). A frame coil, 3.80 by 4.5 m, was hoisted on a pole and mounted so that it was possible to rotate it through 180° (Fig. IV). The area of the aerial is several times as large as that of the frames used so far. The electric resistance could be kept within the limits of a few ohms by using thicker wire. The number of turns is 36 and can always be increased.

The experimental curve in Fig. 18 was obtained with this arrangement.

Measuring table:

SCHWAZ

f = 10 kcps SA III, I = 2.1 a

$\vartheta = 0°$, $\psi = 0$

m	$\lvert B\rvert \left[\frac{Wb}{m^2}\right] \cdot 10^{-12}$
30	280
49	140
79	31
110	15
116	10.5
146	4.8
194	2.3
243	1.15
293	0.76
342	0.36
389	0.25
435	0.18
478	0.12

SCHWAZ

transmitter frame SA VII at S_1, f = 3 kcps, I = 1 a

$\vartheta = 0$, $\psi = 0$

points/m	$\lvert B\rvert \left[\frac{Wb}{m^2}\right] \cdot 10^{-12}$
200	38
2 316	2.8
10 405	1.5
620	0.38
740	0.21
850	0.13
910	0.095
3 1000	0.07
1042	0.07
1180	0.042
4 1275	0.035

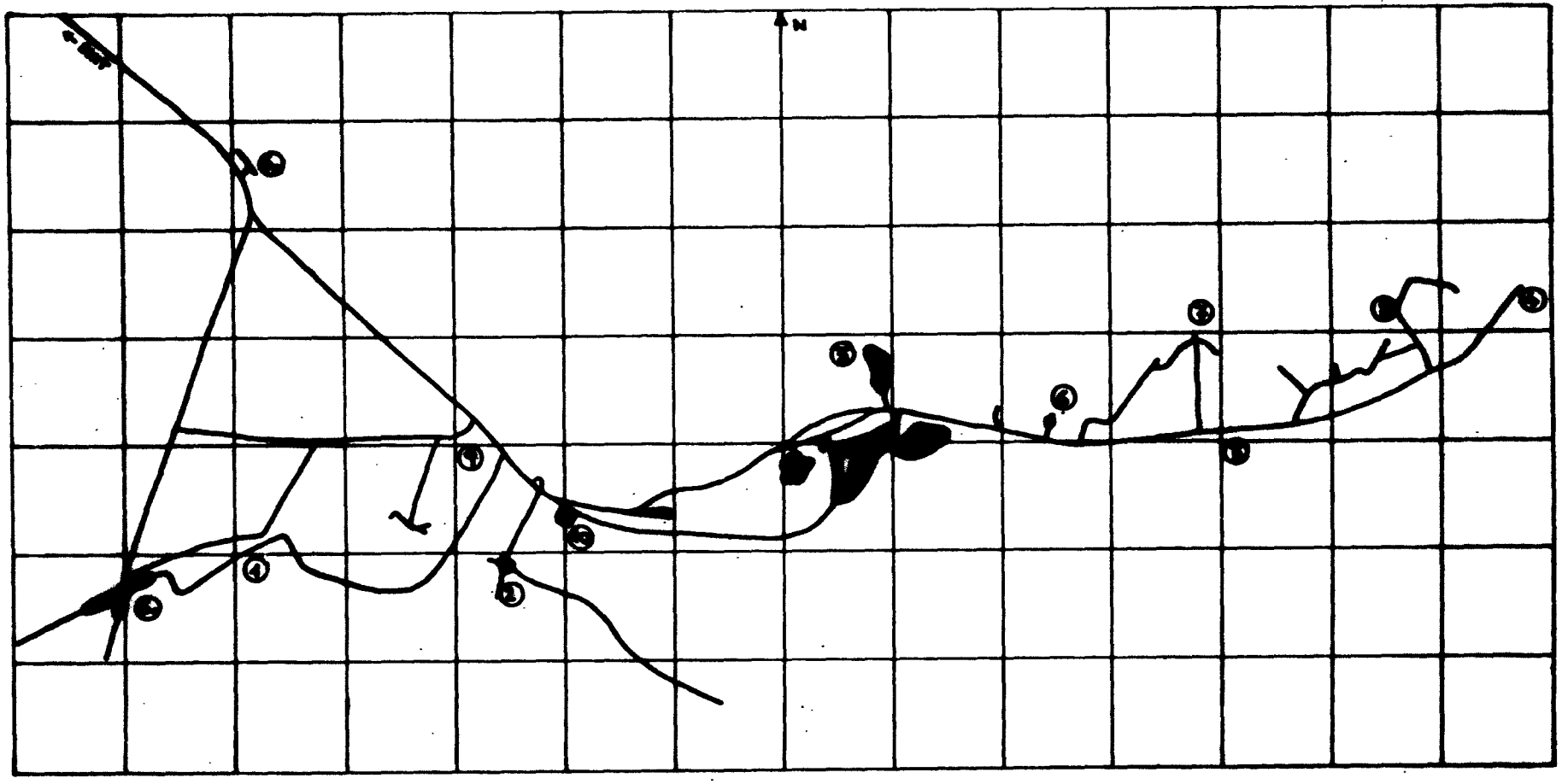

SCHWAZ MINE

SECTION

M 1:5000

Fig. 28

Another section for measurement was between the points S_2 and 8. On the one hand the large cavities at 5 could be avoided, but on the other there is different rock (a slate wedge) in between. Yet the course of the curve as shown in Fig. 18 is approximately the same.

Measuring table

SCHWAZ

transmitter frame at S_2

f = 3 kcps, I = 1.75 a

$\vartheta = 0$, $\psi = 0$

points/m		$\lvert B \rvert \left[\frac{Wb}{m^2}\right] \cdot 10^{-12}$
5	580	0.2
6	760	0.085
7	870	0.035
8	1040	0.014

SCHWAZ

f = 3 kcps, SA III, I = 3 a

$\vartheta = 0$, $\psi = 0$

m	$\lvert B \rvert \left[\frac{Wb}{m^2}\right] \cdot 10^{-12}$
30	300
49	180
79	40
110	20
116	17
146	7.8
194	3.2
243	2.4
293	1.3
342	0.8
389	0.6
435	0.45
478	0.3

Besides these measurements also the dependence $H(\vartheta, \psi)$ was studied as mentioned before. These programs were performed

as follows:

The transmitting aerial (point S_1) was directed so that $\vartheta = 0$. At a distance r the receiving aerial was slowly rotated and the voltages pertaining to ψ: 0°, 30°, 60°,... were read. After one full revolution of the receiving aerial through 360°, the same measurement was repeated for $\vartheta = 30^\circ$. The resultant graphs are given in Figs. 4, 5, 6. The ϑ values are at the periphery, the point with the greatest radius vector on each curve pertails to $\psi = 0^\circ$. By measuring the field strength at $\vartheta = 0^\circ$ and $\vartheta = 90^\circ$ we could also ascertain the ratio $\left|\frac{Hr}{H\vartheta}\right|$ from which we could draw conclusions on the conductivity. Such measurements were made in a large number of galleries. The considerable stray indicates that large differences in conductivity may occur also in highly uniform rock.

St. Gertraudi mine (mine chart Fig. 29):

The Schwaz measurements were repeated. The transmitting aerial was a frame of the same kind as that used in Schwaz. Its location is indicated by S. The section of measurement goes to the points a, b, c. Two series of measurements are evaluated in Fig. 19. The one was made with the transmitting aerial directed to the most distant, the other with the transmitting aerial directed to the nearest site of measurement. In this way the angle ϑ varies from one site of measurement to the other whereas $\psi = 0^\circ$ is conserved.

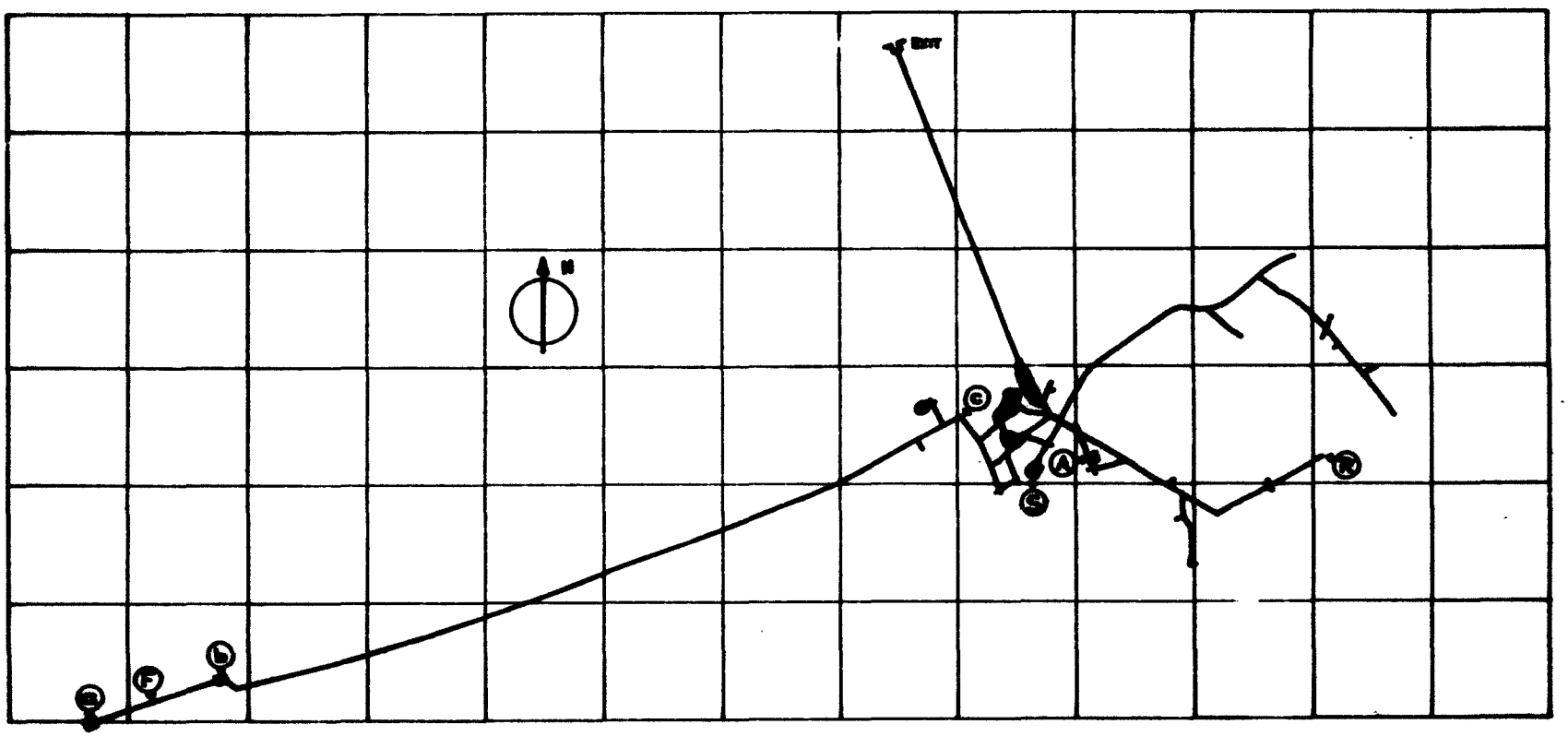

ST. GERTRAUDI MINE

M 1:5000

0 50 100 m

Fig. 29

Measuring table:

ST. GERTRAUDI

f = 10 kcps, SA III, I = 2.2 a $\vartheta = 0°$, $\psi = 0°$

m	$\lvert B\rvert \left[\frac{Wb}{m^2}\right] \cdot 10^{-12}$	m	$\lvert B\rvert \left[\frac{Wb}{m^2}\right] \cdot 10^{-12}$
28	380	216	1.5
48	71	240	1.3
71	22	264	0.9
94	11.8	288	0.74
119	6	313	0.58
142	4.1	337	0.45
167	2.65	362	0.33
191	2		

series I f = 3 kcps

m	ϑ	$\lvert B\rvert \left[\frac{Wb}{m^2}\right] \cdot 10^{-12}$
110	30°	100
150	18°	41
200	11°	20
240	7.5°	11.5
290	5.5°	6.5
340	4°	4
390	3°	3
440	2°	1.6
490	1°	1.5
540	0.5°	1.3
590	0°	1
640	-0.5°	0.75
690	-0.5°	0.6
710	-0.5°	0.5
820	-0.5°	0.3

St. Gertraudi

large transmitter frame at S

f = 3 kcps, I = 1.75 a

series II

m	ϑ	$\lvert B\rvert \left[\frac{Wb}{m^2}\right] \cdot 10^{-12}$
70	0°	220
150	27°	49
240	37°	10
340	41°	3.8
490	44°	1.2
640	45°	0.75
820	45°	0.3

The curves for the field strengths shown so far have been plotted for a frequency of 3 kcps. Fig. 21 shows one curve each taken in the three mines at a frequency of 10 kcps. The distances in these measurements were not greater than 400 m as smaller aerials were employed. Moreover, it was found that at frequencies of around 10 kcps particularly strong interferences occur with the measurements which at low frequencies make it impossible to perform precise measurements.

§ 6. Reception tests with commercial very-long-wave transmitters in the mine

As stated in several intermediate reports quite a number of very-long-wave stations in the range of frequencies around 15 kcps could be received very clearly in the mine. During the first time the arrangement described in § 3 was used as a receiver. However, it was suited only for preliminary probing measurements. First, we tried out which stations could be heard at all. Reception was very good from the GBR station, followed by FUB and others that were somewhat weaker (NAA, EB, UMS, NIT). The stations NAA and GBR could be heard both night and day whereas a number of other stations could be received only in the evening or during the night.

To get this result we had to listen to the frequency band between 10 and 20 kcps for 24 hours.

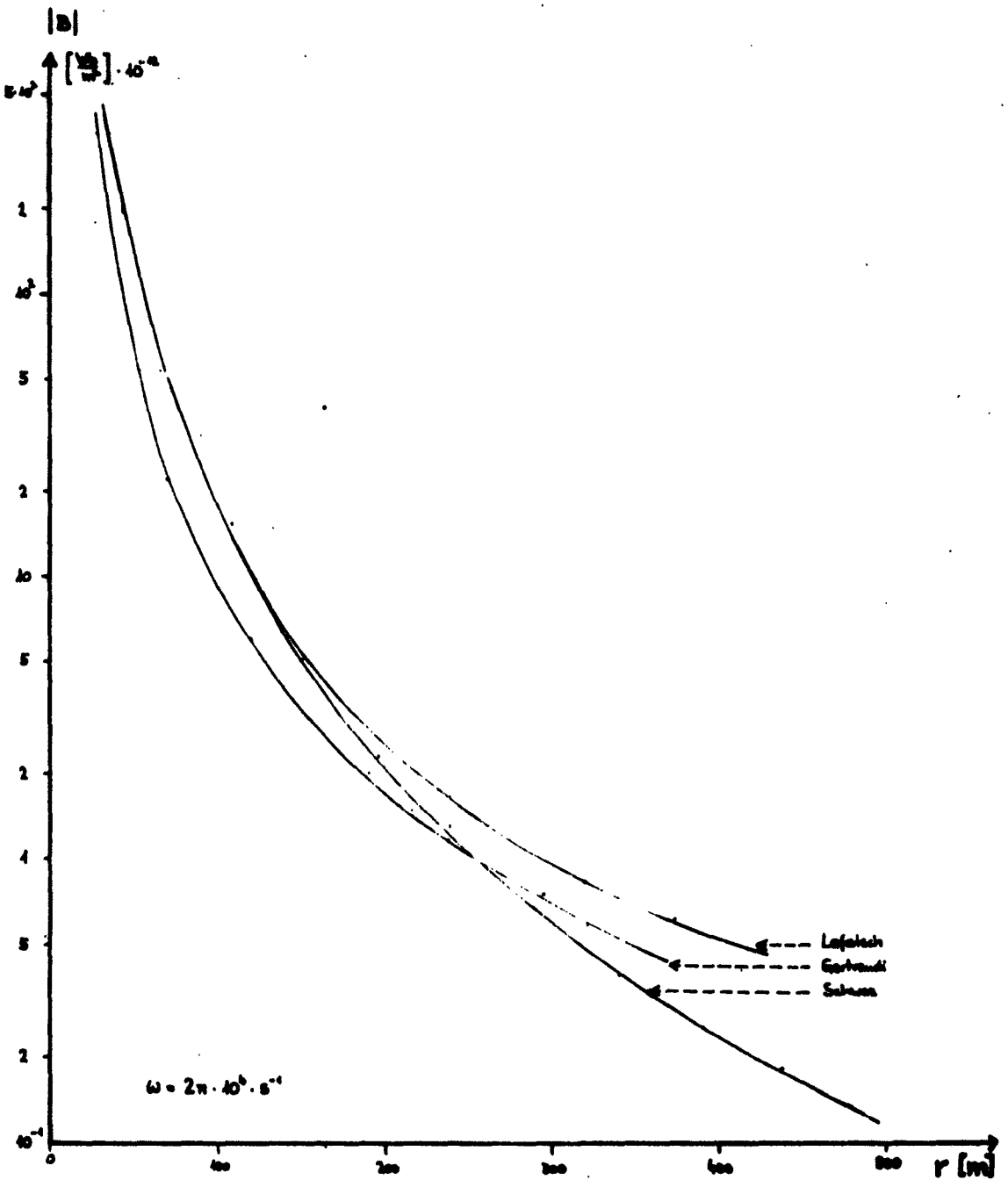
|B|
1
2
5
2
10
5
2
4
5
2
0
400
2000
3000
4000
5000
r [m]
Lafaisch
Gartenstadt
Schauen
ω = 2π · 10⁵ · s⁻¹

Fig. 21

According to the measuring site in the mine, the receiving aerials were either the ferrite aerials described before or large frame aerials constructed for particularly this purpose. One of these is in Schwaz (Fig. 28) at the point 10, the height of rock above this place is some 1000 m. The frame has the size 5 by 20 m and has two turns. It is either connected aperiodically to the receiver or tuned to the receiving frequency.

A second, larger frame is in the Kleinkogel range in St. Gertraudi. A vertical loop of 100 by 40 m was set up there. Using the two shafts a and b (Fig. 29) and the tunnels F which connect them on top and below it was possible to set up such a large antenna. The latter is a two-turn loop also in this case. A second 40 m long aerial was set up vertically in St. Gertraudi and used for receiving purposes. A low-background nuvistor amplifier was designed to reduce the damping of the ferrite aerial and of the large loop aerial. Its wiring diagram is shown in Fig. 32. It is a two-stage battery apparatus. Its smoothly adaptable feedback is adjustable with the potentiometer P.

First of all we had to check what relationship there is between reception in the mine and surface reception. Comparative measurements showed that the signals on the surface were somewhat stronger but that the noise level was a multiple of the useful signal level. This can be explained largely by the fact that these measurements were made in summer when owing to the atmospheric electricity the noise

level is much higher than in winter. Moreover, the band width of the amplifier used by us is relatively great. It amounts to some 5% so that also disturbing pulses of more distant frequencies had an effect. Repeating the measurements under the surface we found that the signals from the transmitter were attenuated but slightly. More than 1 km of rock reduced the signal intensity by about 60%. The attenuation of the atmospherics was considerably greater.

The next step was to prepare the long-term registration of the GBR or NAA stations. It was intended to follow the variation of the field strength above and under the surface over a long period. For this purpose we first had to find a suitable receiver station. A receiver, an integrating circuit, and a recording unit were necessary. Fig. VIII shows the mains-fed device during a test run in the St. Gertraudi mine. The LA IV receiving aerial was used. The receiver can be seen in the middle of the picture. This apparatus is a very-long-wave receiver for the frequency range of 4 - 150 kcps manufactured by the Siemens company and completely modified in our laboratory. Its sensitivity is about 10 μv, its band width is very low so that also transmitters that are close to one another can be separated.

The circuit diagram of the receiver is shown in Fig. 33: On the left side is the two-stage voltage amplifier (ECC 83), adjoining the ring modulator (G11) with the oscillator (ECC 82), followed by the two-stage selective output amplifier (ECF 80). The 1-kcps output signal can either be heard

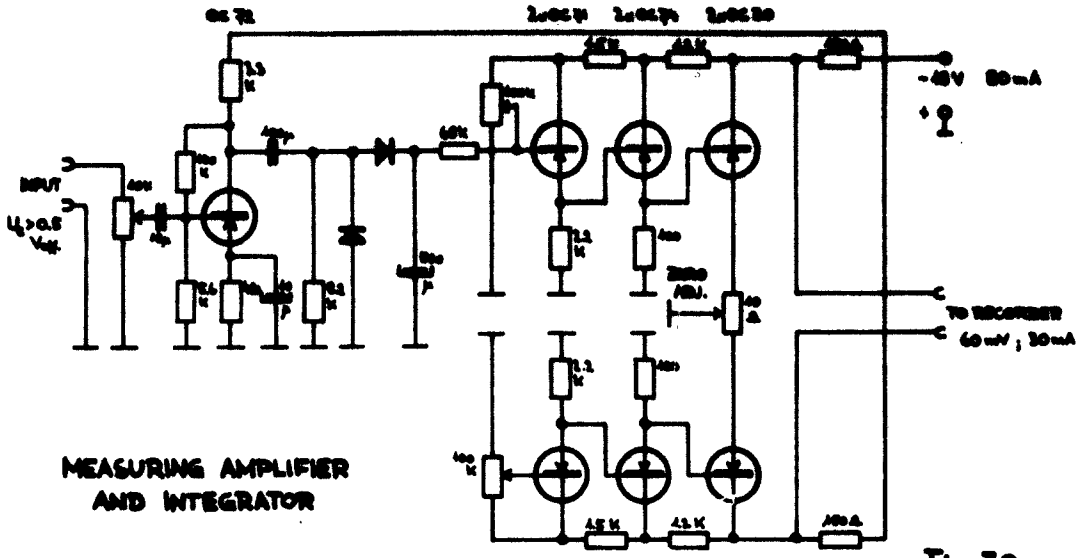

MEASURING AMPLIFIER
AND INTEGRATOR

Fig. 30

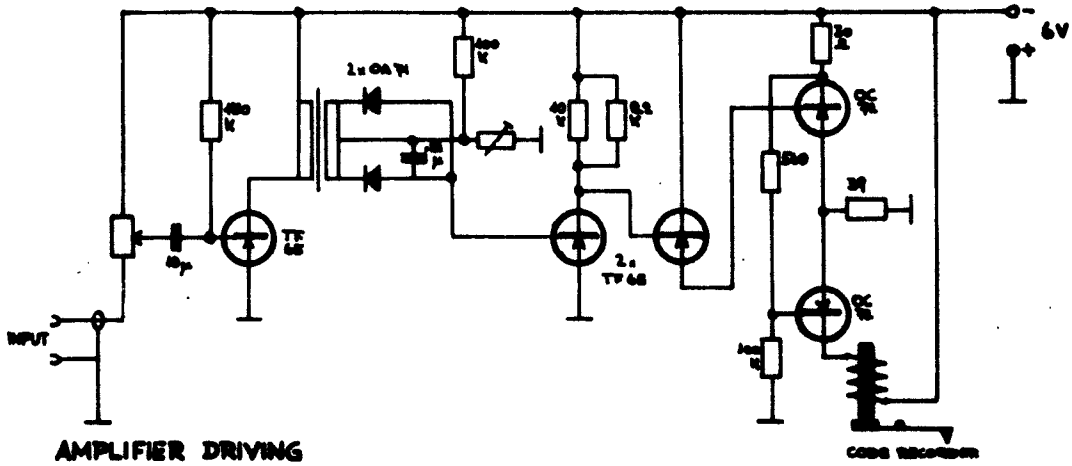

AMPLIFIER DRIVING
CODE RECORDER

Fig. 31

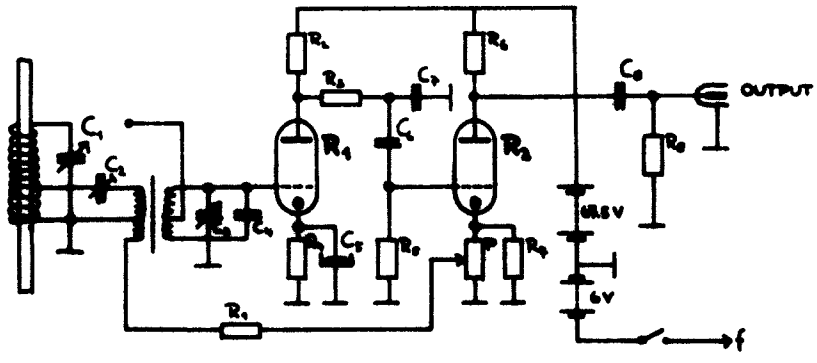

ANTENNA PREAMPLIFIER
$R_1 = R_2$ = NUVISTORS 7586

Fig. 32

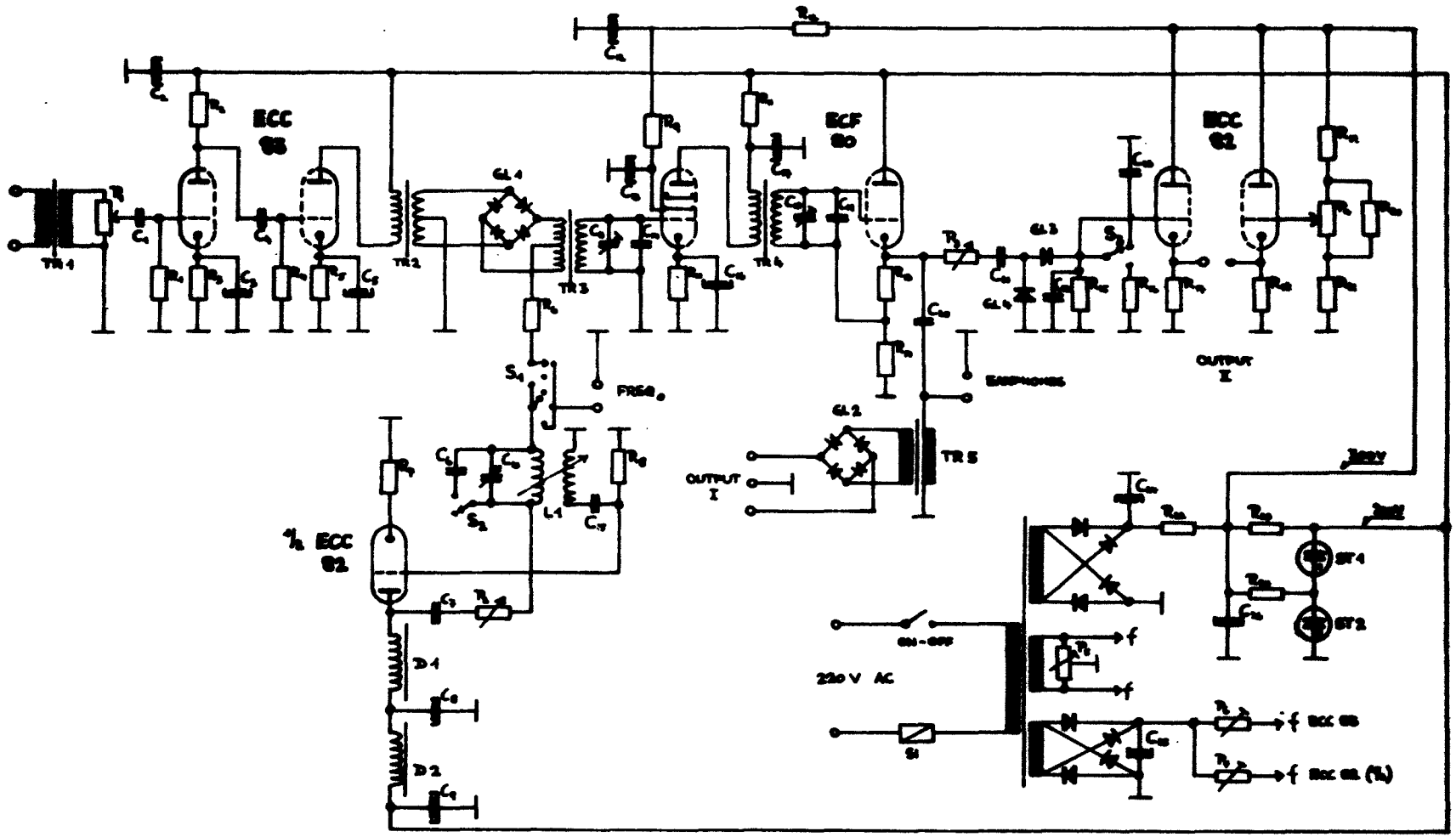

EXPERIMENTAL VLF RECEIVER

Fig. 33

through earphones or be fed into an integrating stage (Gl 3, Gl 4) whose rise and integration times are adjustable. The symmetric output stage (ECC 82) controls a slow graphical recorder via the terminals of output II. Another output over TR 5 and the rectifier bridge GL 2 serves for the control of a rapid recorder (output I). As the stations in question usually transmit morse signals, the problem of recording their field strength is much more difficult than it may seem at first. It has not yet been solved to satisfaction. Work in this respect is being carried on. Besides the slow recorder we used also a rapid recorder whose registrations were very valuable. Short noise peaks could be recorded accurately by means of it. The recorder can be seen in the top right-hand corner of Fig. VII; below is the required amplification unit. Another means for the identification of unknown transmitters was a Morse printer which made it possible to record the received code signals on a paper tape. In this way one can evaluate the signals later without having to listen all the time. The electronic control of this recorder can be seen in Fig. 31. A battery-supplied recording station was set up parallel to the apparatus described. This was necessary to be sure no electromagnetic waves are led through the power mains into the inner mine. Long-term measurements could be made at the deepest spots of the mine by means of this apparatus. It was found then that the supposition made before was wrong. Fig. VII shows this apparatus during an informative measurement in the St. Gertraudi mine. The receiver (left in the picture) was

not yet finished at that time. The recorder is provided with a clockwork. The integrator and the measuring amplifier for the recorder are installed separately. Fig. 30 shows its wiring diagram. A d.c.-amplifier was necessary for the sensitivity of the recorder available was too low to connect it directly to the integrating unit. The picture shows also several auxiliary equipment, as the battery-supplied oscilloscope. a millivoltmeter, and the required power sources. The receiving aerial on its stand is not very clear to see. This aerial is the EA I which has been described before. As mentioned before these measurements are still in their state of beginning. A new highly selective amplifier will soon be put into operation. The results obtained so far must be regarded preliminary. Up to now we cannot draw any definite conclusions as to the mechanism of propagation of electromagnetic waves from the transmitter to the receiver. Such measurements are being prepared.

§ 7. On the determination of ϵ and σ

In the year under review we have worked to design a suitable apparatus for measuring ϵ and σ. Results on preliminary probing measurements of ϵ have been given in our last report. When it is possible to prepare the rock samples in a proper way, i.e. to saw them in pieces, to grind them, and to bring them into contact, these measurements should not be too difficult. The thin (2 - 5 mm) plan

parallel section consumes much time and still gives a large percentage of reject. Things are much more difficult in determining the loss factor, i.e. in measuring the conductivity of the rock in the entire VLF region. The kind of measuring electrodes abutting the rock sample plays such an important part that sufficiently accurate and reproducible measurements have not been possible up to now. The measuring arrangement used is shown in Fig. X. It consists of an RC generator which produced the measuring voltage of the desired frequency, of the measuring bridge, and of the selective thermionic voltmeter which is used as a zero indicator. The rock sample is left in the picture. 4 cm deep holes were drilled into the rock (here it is a dolomite sample from St. Gertraudi) at certain spacings. Contact tests were made with mercury, slightly acid cotton or aluminum foil pressed into the hole. Subsequently, the resistance is determined as a function of the spacing between the individual measuring electrodes. The accuracy of the measuring bridge in this measurement is several times greater than the errors caused by insufficient contacts. Good results were obtained when metal powder was used as a contact in the borehole.

Further work in this field shall enable us above all to determine the conductivity of an arbitrary section of rock in the mine and thus to gain insight into the natural conditions. However, the relevant theoretical problems have not yet been solved. They would make it possible to

find the conductivity of an extensive spatial conductor by measuring its electrical resistance. This work is regarded particularly important since it would offer a control for the determination of conductivity by measuring the attenuation of an electromagnetic wave.

Figures:

Fig. I Transmitter station, RC generator, power amplifier, electronic switch, accumulator

Fig. II flexible transmitting aerial SA VI with transmitter (Hall salt mine)

Fig. III receiving unit: ferrite aerial EA IV, receiver, millivoltmeter, audio amplifier

Fig. IV large rotary frame aerial SA VII and transmitter (Schwaz mine)

Fig. V small receiver station with aerial EA V

Fig. VI measuring team with receiver (Hall salt mine)

Fig. VII battery-operated apparatus for recording field strength (St. Gertraudi mine)

Fig. VIII mains-fed apparatus for recording field strength and noise level

Fig. IX transport of receiver unit in an abandoned mine region

Fig. X laboratory for geoelectrical measurements on rock samples

List of coworkers

team for

theoretical problems	experimental problems
direction: Univ. Prof. Dr. F. Cap	direction: Dr. W. Bitterlich
Dr. R. Hommel	O. Gröbner
I. Steinacker	O. Wörz
N. Nessler	

Other coworkers: T. Elster, W. Gradl, computation team consisting of 10 students

Mining experts: managing director Dipl. Ing. Mlaker

managing director Schwarz

Contractor: Dr. W. Bitterlich

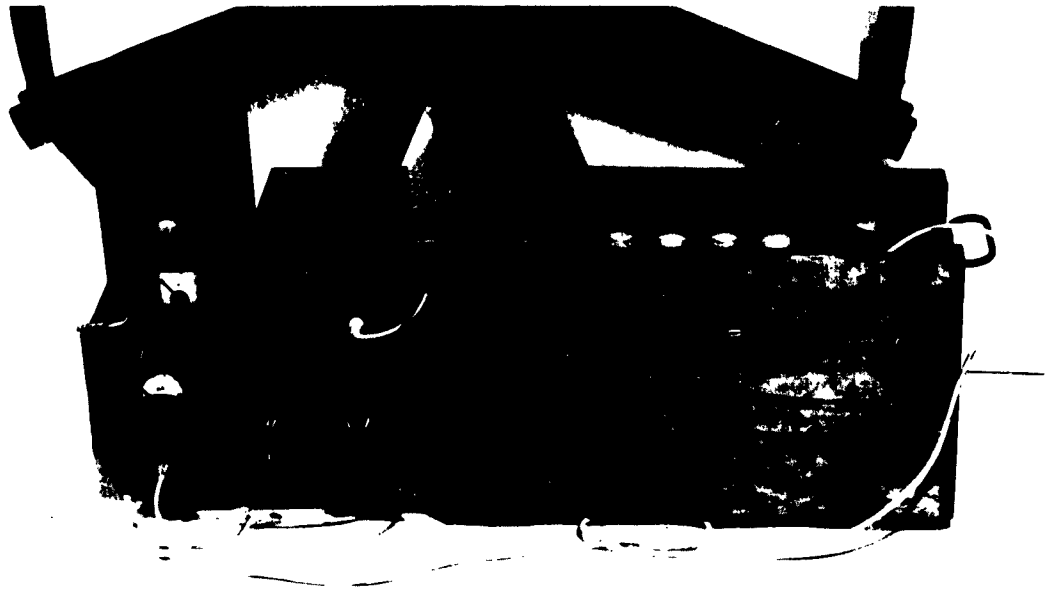

Fig. I

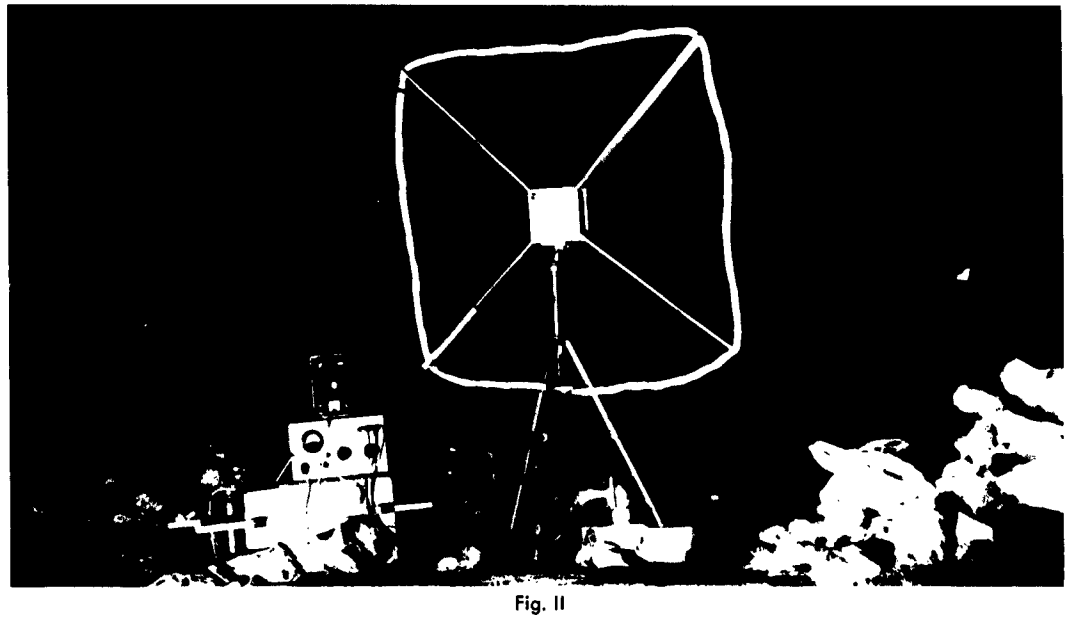

Fig. II

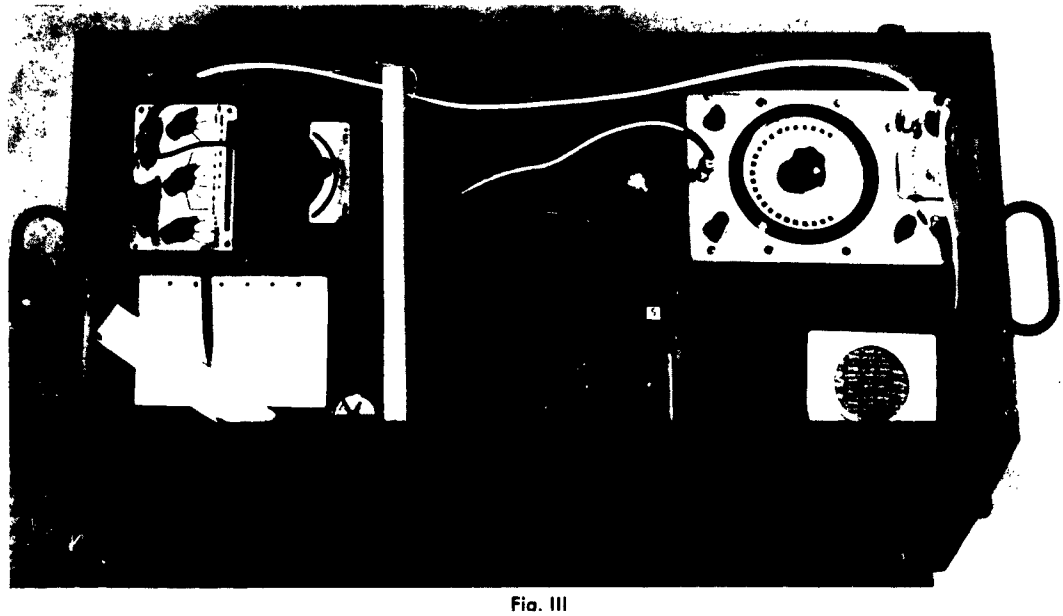

Fig. III

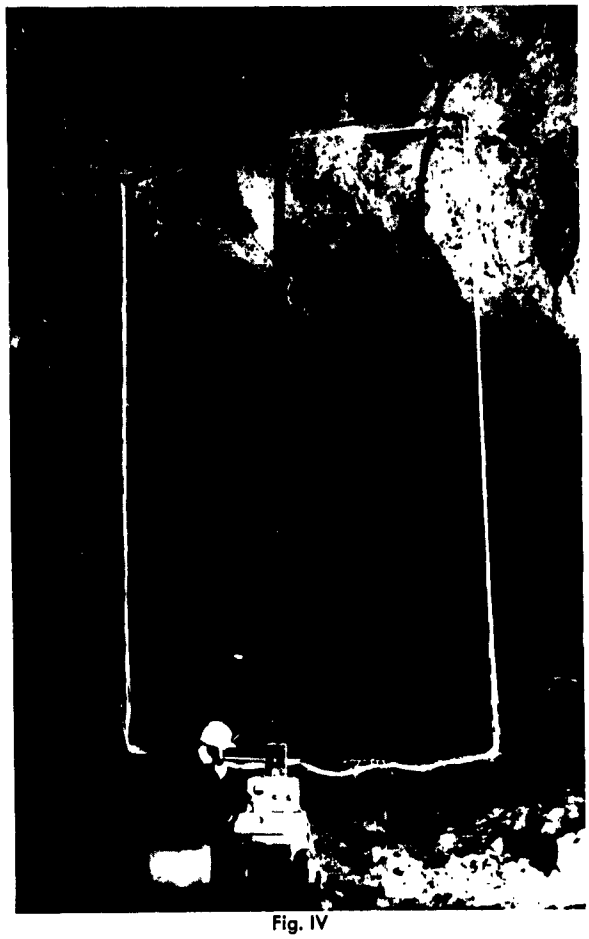

Fig. IV

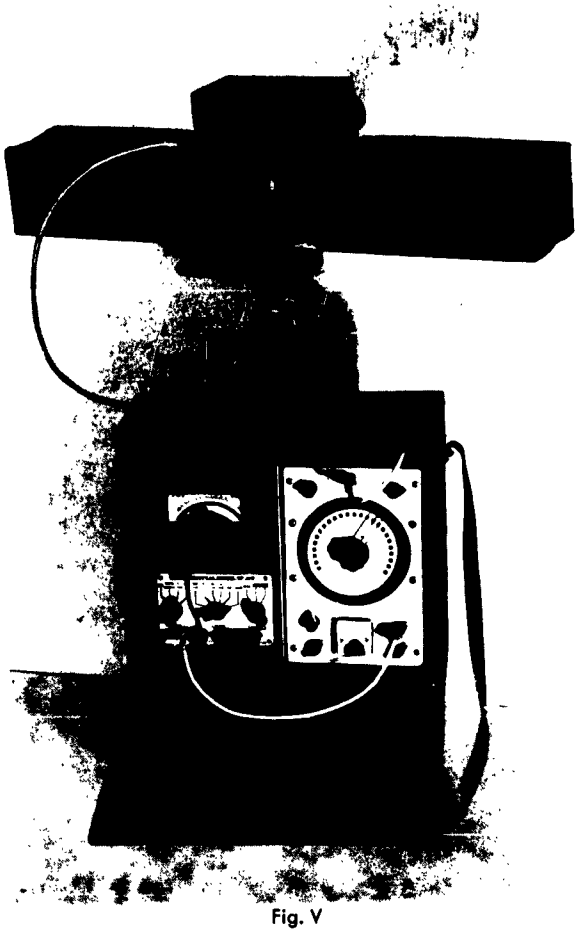

Fig. V

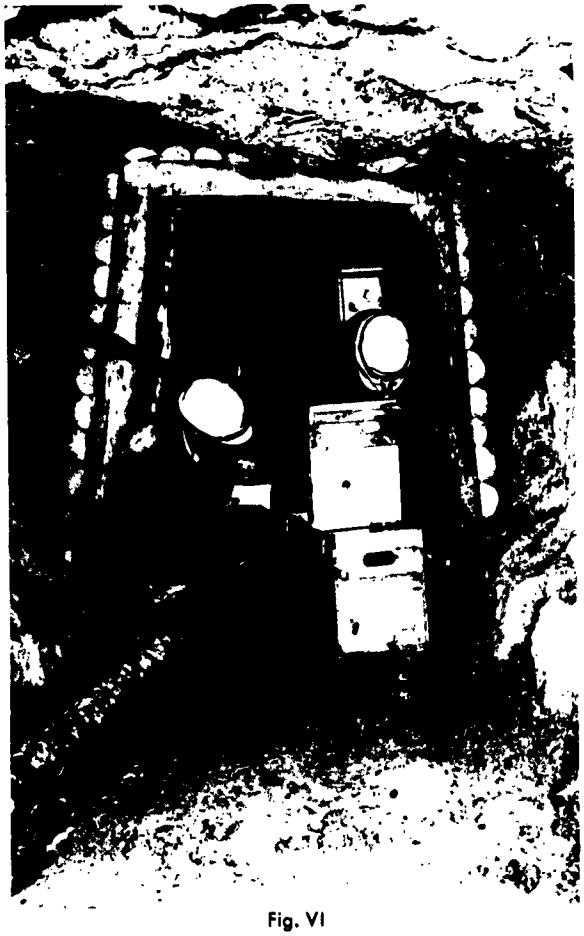

Fig. VI

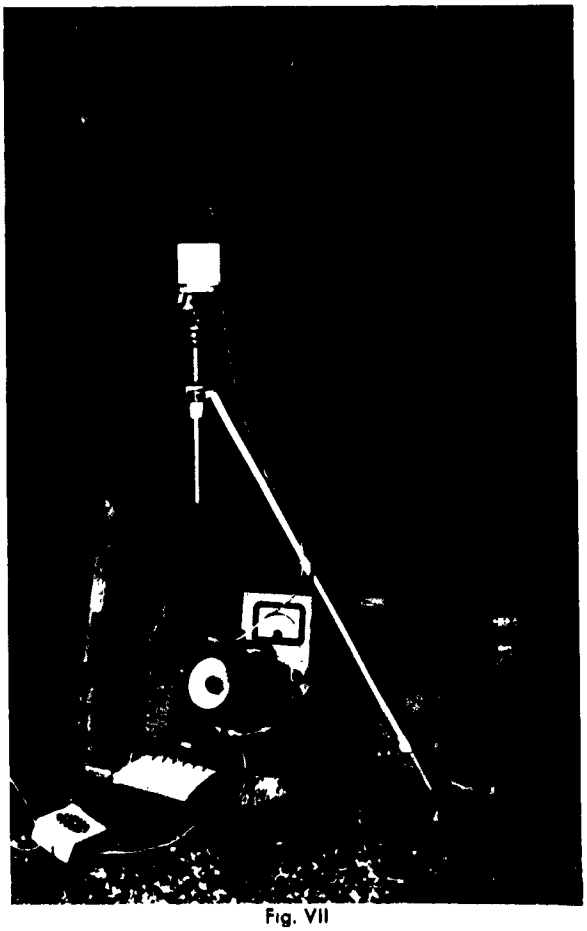

Fig. VII

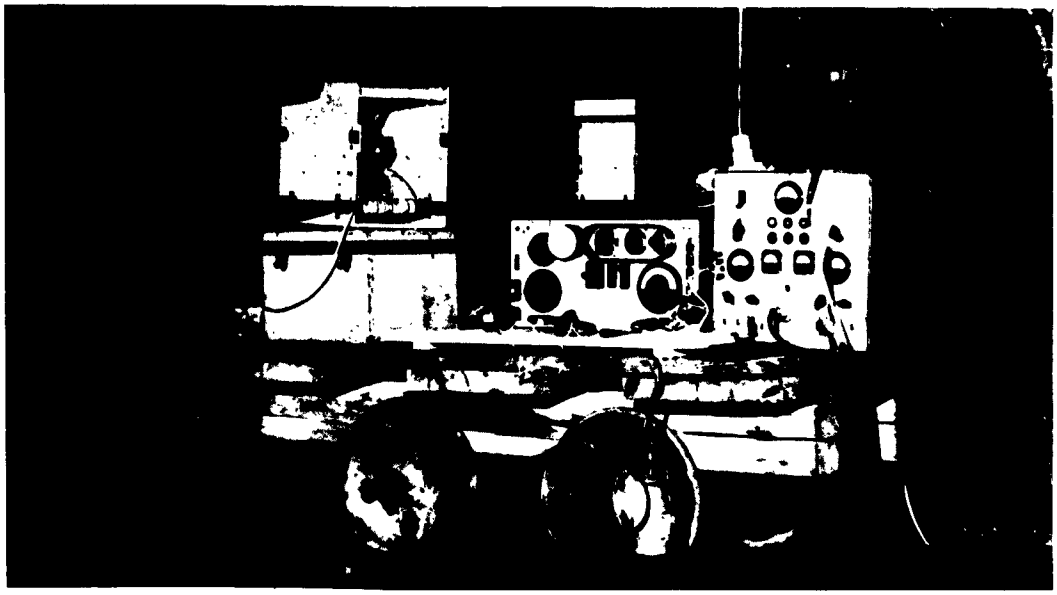

Fig. VIII

Fig. IX

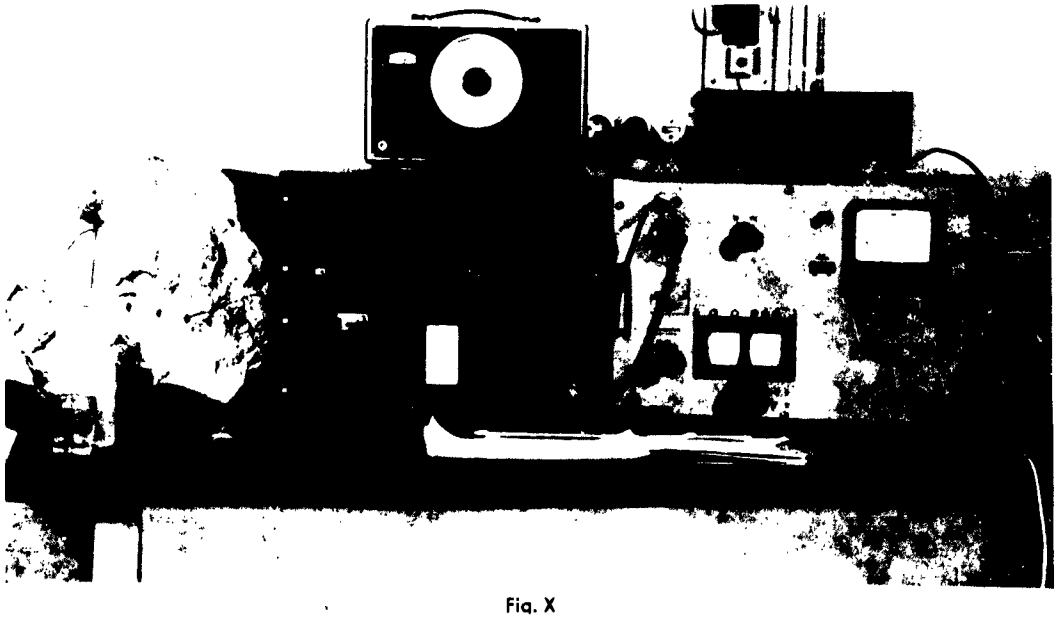

Fig. X